Journal of the National Academy of Forensic Engineers®

http://www.nafe.org

ISSN: 2379-3252

DOI: 10.51501/jotnafe.v42i2

Vol. 42 No. 2 December 2025

National Academy of Forensic Engineers®

Journal Staff

Technical Review Process

The Technical Review Committee Chair chooses the reviewers for each Journal manuscript from amongst the members and affiliates of the NAFE according to their competence and the subject of the paper, and then arbitrates (as necessary) during the review process. External reviewers may also be utilized when necessary. This confidential process concludes with the acceptance of the finished paper for publication or its rejection/withdrawal. The name(s) of authors are included with their published works. However, unpublished drafts together with the names and comments of reviewers are entirely confidential during the review process and are excised upon publication of the finished paper.

National Academy of Forensic Engineers®

Board of Directors

President
Michael Aitken, PE, DFE
Senior Member

President-Elect
Tonja Koob Marking, PhD, PE, DFE
Senior Member

Senior Vice President
Daniel Couture, PEng, DFE
Senior Member

Vice President
Ben Railsback, PE, DFE
Fellow

Treasurer
Bruce Wiers, PE, DFE
Senior Member

Secretary
Shawn Ray, PE, DFE
Senior Member

Past Presidents
Steven Pietropaolo, PE, DFE
Senior Member

Joseph Leane, PE, DFE
Fellow

Samuel Sudler, PE, DFE
Senior Member

Directors at Large
Greg Boso, PE, DFE
Member

Paul Tucker, PE, DFE
Senior Member

Executive Director
Amanda Hendley

Journal of the National Academy of Forensic Engineers®

Editorial Board

Submitting Proposed Papers to NAFE for Consideration

Please visit the Journal's author page for submission details.

We are looking for NAFE members who are interested in giving presentations on technical topics that will further the advancement and understanding of forensic engineering at one of the academy's biannual meetings and then developing those presentations into written manuscripts/papers, which will go through a single-blind peer review process before publication. Only papers presented at a NAFE regular technical seminar and that have received oral critique at the seminar will be accepted for review and publication. We recommend that you review the About the Journal page for the journal's section policies as well as the Author Guidelines listed on the Submissions page. Authors need to register with the Journal prior to submitting, or (if already registered) they can simply log in and begin the process. The first step is for potential authors to submit a 150-word maximum abstract for consideration at an upcoming conference into the online journal management system.

Copies of the Journal

The Journal of the National Academy of Forensic Engineers® contains papers that have been accepted by NAFE. Members and Affiliates receive a PDF download of the Journal as part of their annual dues. All Journal papers may be individually downloaded from the NAFE website. There is no charge to NAFE Members & Affiliates. A limited supply of Volume 33 and earlier hardcopy Journals (black & white) are available. The costs are as follows: $15.00 for NAFE Members and Affiliates; $30.00 for members of the NSPE not included in NAFE membership; $45.00 for all others. Requests should be sent to NAFE Headquarters, 1266 W Paces Ferry Rd NW #141, Atlanta, GA 30327 or call (770) 268-0802.

Comments by Readers

Comments by readers are invited, and, if deemed appropriate, will be published. Send to: Ellen Parson, Journal Managing Editor, 3780 SW Boulder Dr., Lee's Summit, MO 64082. Comments can also be sent via email to journal@nafe.org.

Material published in this Journal, including all interpretations and conclusions contained in papers, articles, and presentations, are those of the specific author or authors and do not necessarily represent the view of the National Academy of Forensic Engineers® (NAFE) or its members.

 ISSN: 2379-3252

Table of Contents

ø Paper presented at the NAFE seminar held in July 2024 in Ann Arbor.
ʊ Paper presented at the NAFE seminar held in January 2025 in Santa Fe.
‡ Paper presented at the NAFE seminar held in July 2025 in Ottawa.

Discerning Wind-Related Damage to Residential Roofs

By Ziad Azzi, PhD, PE, DFE (NAFE #1343M), Krishna Sai Vutukuru, PhD, PE, and Manuel Matus, PhD

Abstract

Hurricane season brings a significant rise in wind-related insurance claims, as powerful storms lead to property damage (particularly to roofs). Distinguishing between wind- and nonwind-related damage, as well as pre-existing issues with roofing components, is critical to ensuring fair, efficient, and timely resolutions. This study presents an in-depth analysis of wind-related damage to two common roof covering materials: asphalt composition shingles and clay/concrete tiles. A series of detailed studies coupled with data from field inspections is utilized to differentiate wind-induced damage to roofs from issues stemming from wear and tear, material aging, installation deficiencies, and simulated wind damage (among other environmental and mechanical factors). Damage patterns, damage location, and material behavior from field observations coupled with wind flow around bluff-bodies (such as residential structures) are examined to highlight how the unique properties of each roof (including its location, height, shape, and slope) influence its response to wind-induced pressures during extreme wind events. These insights enhance damage identification, including cause, origin, and duration of roof covering failures, as well as support informed decision-making for roof inspectors.

Keywords

Hurricane season, insurance claims, inspections, tile roofs, shingle roofs, wind damage, forensic engineering, residential roofs, weather-related roof damage

Introduction

Within the discipline of forensic engineering, civil and structural engineers are routinely engaged to perform evaluations of roofing systems in relation to alleged storm-related damage. Their objective and technically substantiated assessments are frequently integral to resolving matters that involve insurance disputes and legal proceedings. The expertise of these professionals is typically grounded in a combination of formal education, practical experience, and specialized training, qualifying them as expert witnesses in this domain.

Accurately distinguishing wind damage from other causes of damage on the roofs is essential for streamlining the insurance claims procedure and improving efficiency. Misclassification and improper damage attribution often lead to delays, disputes, and litigation, making the whole process expensive to both insurers and the insureds.

Advanced assessment methods, such as those discussed, help streamline the process, ensuring that the claims with actual wind damage are handled promptly. Enhanced damage identification, including cause, origin, and duration of roof covering failures, supports informed decision-making for roof inspectors.

The objective of this manuscript is fourfold: (1) to provide foundational background on roofing systems, with emphasis on the most commonly utilized roof covering materials; (2) to examine typical wind-induced damage patterns through the lens of fundamental wind science and wind engineering principles, highlighting how such damage is largely dependent on roof geometry, building height, configuration, and site exposure (among others); (3) to present illustrative case studies from field inspections conducted after major storm events, distinguishing between wind-related and nonwind-related damage to shingles and tiles; and (4) to summarize key guidelines for the assessment of wind damage in residential roofing systems by roof inspectors.

Ziad Azzi, PhD, PE, 5335 NW 87 Ave., Ste. 109, #381, Doral, FL 33178, (305) 874-7399, ziad@ddaforensics.com

Background Information

A tropical cyclone is a rotating system of low atmospheric pressure characterized by organized thunderstorm activity and the absence of frontal boundaries, which typically separate air masses of different densities. When the system's maximum sustained wind speeds are below 39 miles per hour (mph), it is classified as a tropical depression. Once these sustained winds increase to at least 39 mph, the system becomes a tropical storm[1,2]. If the storm intensifies further — and wind speeds reach or exceed 74 mph — it is designated as a hurricane.

Hurricanes are categorized using the Saffir-Simpson Hurricane Wind Scale, which ranks storms from Category 1 to Category 5 based on their maximum sustained wind speed (higher categories indicate a greater threat of structural and environmental damage). These powerful storms generally develop in the Atlantic basin, encompassing the Atlantic Ocean, Caribbean Sea, and Gulf of Mexico as well as in the eastern, and, less commonly, central regions of the North Pacific Ocean[1,2]. Note that the Saffir–Simpson Hurricane Wind Scale classifies hurricanes according to their maximum sustained wind speeds, measured over a one-minute period at a height of 33 feet (or 10 meters) above open water (or unobstructed terrain).

Over the past half-century, windstorms have accounted for roughly 70% of all insured losses attributed to natural disasters[3]. Nearly 39% of the U.S. population resides in coastal counties vulnerable to hurricanes and severe thunderstorms, and data show that this number is growing[4,5]. Although advancements in building codes have significantly improved structural resilience against wind forces in recent decades, substantial damage continues to occur primarily to the external building envelope[6], particularly roofing components such as roof sheathing, tiles, shingles, and metal roofs on residential structures, among other components[7,8,9,10].

In residential houses in the United States, two commonly used roof coverings are asphalt composition shingles and clay or concrete tiles.

Typically, asphalt shingles are favored for their affordability and variety of design choices[11,12]. These systems are made up of overlapping strips composed of asphalt-saturated organic or fiberglass mats, which act as a protective, water-repellent layer over the structural roof deck. Most asphalt shingles have been manufactured with a heat-activated sealant strip (typically asphalt-based) located on either the top or underside of each shingle. When the roof warms above the sealant's softening temperature, the adhesive bonds the shingles in place, helping to prevent uplift at the edges during high winds and allowing wind pressure to be distributed down to the underlying shingle layer[13,14].

On the other hand, clay and concrete tiles are commonly selected in roofing applications due to their strength, long service life, and aesthetic nature. Tiles are particularly valued for their ability to endure extreme weather, including strong winds, intense rainfall, and fire exposure. Such roofing components are most commonly installed using mechanical fasteners (such as screws or nails), mortar- or cement-set, or adhered to the roof deck using a foam application. It is worthwhile to note that in certain locations across the United States, the installation details of roofing components may be governed by the local jurisdiction of that geographical area. This manuscript will only tackle the most common roof covering components, including shingles and tiles.

During severe wind events, damage is typically caused by intense wind-induced uplift or suction forces concentrated at roof corners, edges, and ridge lines, also referred to as high suction pressure zones[15,16]. Elevated suction pressures develop at the roof corners of low-rise buildings due to conical vortex formation[17,18,19]. Consequently, roofing elements like tiles or pavers and rooftop equipment may become detached, transforming into hazardous windborne debris. Additionally, the detachment of roofing materials and rooftop appurtenances exposes structures to rainwater penetration and consequent interior damage[16,20,21,22,23,24,25,26]. Moreover, past research in wind engineering has clearly demonstrated that the aerodynamic behavior and overall wind performance of low-rise buildings are heavily influenced by roof design, roof shape, and roof pitch, among other characteristics[27,28,29].

Typical Wind Damage Patterns

Wind-related damage to residential roofs is largely influenced by wind speed, wind duration, wind direction, and the amount of turbulence inherent in the oncoming wind. The most common damage patterns include wind-induced uplift, windborne debris impact, and progressive failure. The damage caused by wind-induced uplift is classified under direct wind effects, and the damage caused by windborne debris is classified under indirect wind effects. Uplift (or suction) occurs when the wind pressure on the roof covering exceeds the wind resistance of the roof covering, leading to detachment of shingles or tiles. Debris impact can cause punctures or fractures. Progressive

failure refers to the cascading effect — where initial damage weakens the roof covering and exposes the underlayment, making it more susceptible to further wind forces from one particular windstorm event and subsequent moisture intrusion.

Studies have shown that asphalt composition shingle roofs are particularly vulnerable to wind-induced damage due to their layered structure[30]. This structure consists of individual overlapping shingles that are installed in successive courses, where each course partially covers the one beneath it. While this arrangement facilitates water shedding and is effective for waterproofing under normal conditions, it also creates multiple points of uplift vulnerability. Wind forces can exploit the edges and gaps between these layers, particularly at the leading edges of the shingles, initiating progressive detachment or lifting and exposing underlying layers to moisture intrusion. Additionally, once one shingle is displaced, it can compromise the sealing of adjacent shingles, leading to a cascading failure across the roof surface[12,13].

While heavier and more resistant to uplift, concrete and clay tile roofs can suffer from breakage due to windborne debris. The American Society of Civil Engineering (ASCE) building code, *Minimum Design Loads and Associated Criteria for Buildings and Other Structures* (ASCE 7-22)[31], provides updated design guidelines for wind load calculations on buildings and structures. One of the key aspects of ASCE 7-22 is the identification of high-pressure zones, particularly at roof edges, corners, and ridges. These areas experience intensified wind forces due to flow separation and vortex formation leading to turbulence.

Figure 1 shows the peak pressure distributions (or contour plots) for three roof configurations: gable, hip, and flat as well as the locations of the high-pressure zones for each configuration, courtesy of Tokyo Polytechnic University (TPU)[32,33]. Note that the peak pressure coefficients (which are directly proportional to the peak pressures) are negative, indicating the wind forces are pulling away from the surface of the roof (or exerting uplift or suction pressures).

This graphic demonstrates that a typical wind damage pattern is generally located near the roof edges, corners, and ridges (or hip lines in case of hip roof configuration) before the wind can cause uplift to other areas, such as the field of the roof. While this is true for shingle and tile roofs, flat or low-slope roofs are typically covered with membranes, which may call for stricter guidelines or attachment methods for membranes located in zones of high-suction pressures. Additionally, during a high wind event, severe winds are typically recorded from a particular direction. Although the predominant wind direction might sometimes shift during rotational storms such as hurricanes, the roof inspector should first consider the predominant windward slope direction for wind damage assessment. As such, the above criteria can help the inspectors understand and segregate wind-related damage from other types of damage noted on the roofs.

On the other hand, wind flow characteristics around a building are significantly affected by terrain exposure and

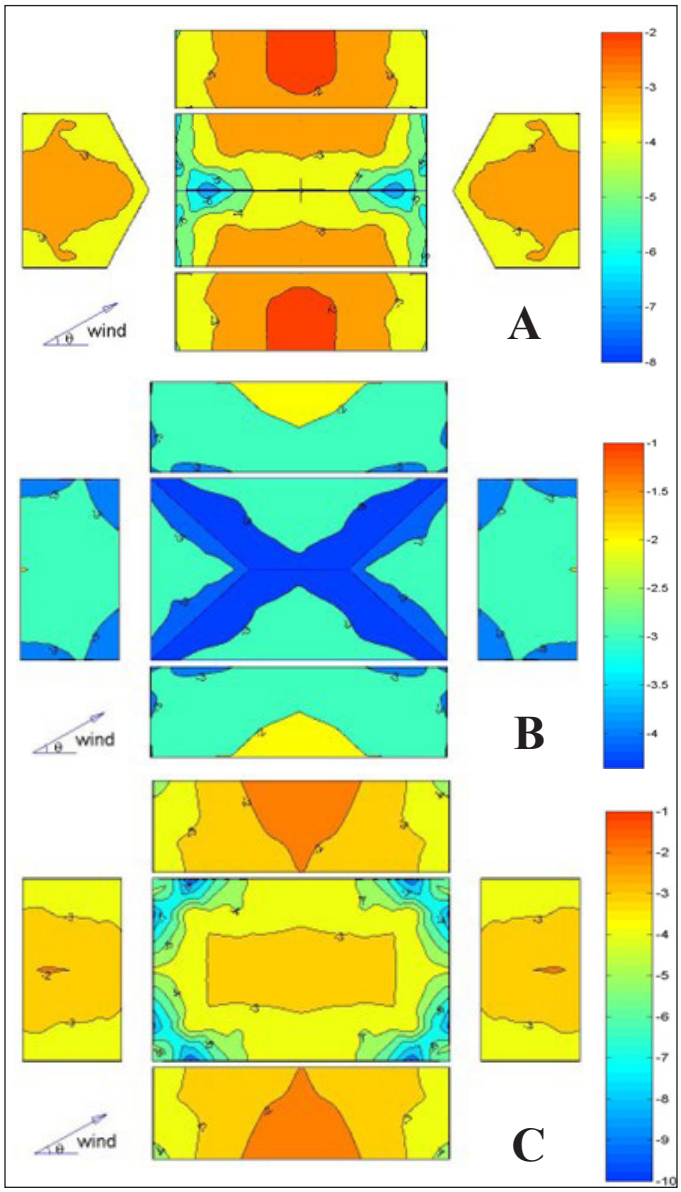

Figure 1
Contour plots of critical peak pressure coefficients for:
a) gable roof, b) hip roof, and c) flat roof.
Courtesy of Tokyo Polytechnic University (TPU)[32,33]

building height. ASCE 7-22 classifies terrain into three exposures — mainly B, C, and D — where:

- Exposure B represents urban or suburban areas with numerous obstructions.
- Exposure C includes open terrain with scattered obstructions.
- Exposure D pertains to coastal regions with unobstructed wind flow.

Buildings in Exposure D experience the highest wind loads due to minimal surface roughness (such as structures directly facing the ocean), and buildings in Exposure B experience the lowest wind loads due to numerous obstructions to the wind flow (such as structures located farther inland). Additionally, building height plays a crucial role in the distribution of wind pressure. Taller structures encounter increased wind speeds at higher elevations, necessitating stronger roof anchoring systems and stringent design. Hence, in general, a two-story residential building experiences higher wind forces than a one-story residential building in a similar location. Thus, in jurisdictions where no stricter attachment methods are enforced for roofing components located in high-suction pressure zones, it is highly unlikely that a lower roof gets damaged during a windstorm with no wind-related damage to the higher roof of the same structure.

The shape and configuration of a roof determine how wind interacts with its surface, as depicted in **Figure 1**. Gable roofs, for instance, create strong uplift forces at the ridges due to flow separation, making them more vulnerable to wind-induced damage. In contrast, hip roofs tend to distribute wind loads more evenly, reducing the likelihood of localized failure. Flat roofs, on the other hand, are particularly susceptible to vortex-induced suction, which can lead to the detachment of the roof covering at the corners. Roof slope is another critical factor influencing wind pressure distribution. Studies using computational fluid dynamics (CFD) simulations indicate that steeper slopes can reduce uplift forces, while flatter roofs experience higher suction forces[34]. Optimizing roof slope can significantly enhance wind resistance, particularly in hurricane-prone regions.

Aerodynamic mitigation strategies, such as parapets, roof overhangs, and curved roof designs, can significantly reduce wind-induced damage[35,36]. Parapets disrupt wind flow, reducing suction forces on flat roofs, while curved roofs help streamline airflow, minimizing turbulence. Overhangs, however, must be carefully designed, as excessive extension can amplify wind loads rather than mitigate them[18]. In addition, the presence of non-rectangular-shaped buildings also significantly affects the wind loads on the roof.

For instance, protruding sections of a structure may induce tunneling effects that could exacerbate the generation of wind-induced pressures on different roof sections. In addition, re-entrant flows shed from sections located upwind may introduce unconventional pressure distributions on areas of the roof that may deviate from typical wind-induced pressure distributions[37,38,39]. Furthermore, roof openings and ventilation systems can alter wind flow patterns.

Research indicates that buildings with strategically placed openings experience lower wind pressure coefficients than fully enclosed structures[40,41]. This highlights the importance of integrating ventilation designs that enhance wind resistance by reducing suction pressures on the roofs while maintaining structural stability. While the previous methods, strategies, or configurations are mostly related to enhancing the design and performance of roofing components during severe winds, the forensic engineer would greatly benefit from understanding how winds flow around bluff-bodies and irregularities in roof configurations to make an accurate determination in a roof damage case.

Asphalt Shingle Roofs

Asphalt shingles are a widely used roofing material in residential construction. They are made from a base mat that can be organic (such as cellulose fibers) or fiberglass, which is saturated and coated with asphalt to provide it with its waterproof capabilities. The top surface is then embedded with mineral granules, which provide color, protect against ultraviolet (UV) rays, and enhance fire resistance. Asphalt shingles come in a variety of styles, including 3-tab and architectural (dimensional) shingles, allowing homeowners to choose options that suit both aesthetic preferences as well as desired and/or required performance needs.

The history of asphalt shingles dates to 1901, when they were developed as a more affordable and practical alternative to wood shingles and slate tiles. They began to be mass-produced and marketed across the United States by 1911[42]. Initially, organic-based shingles dominated the market; however, by the 1960s, fiberglass-based shingles

were introduced and quickly gained popularity due to their superior durability, lighter weight, and improved resistance to fire and weathering[43]. Throughout the decades, advancements in materials science and manufacturing techniques have significantly improved the performance of asphalt shingles. Modern shingles can feature algae resistance, enhanced wind ratings, and impact-resistant designs. Asphalt shingles remain one of the most popular roofing materials in North America due to their advantageous balance of durability, affordability, and aesthetic flexibility[11].

Although the design of asphalt shingles has improved over the past several decades, the susceptibility to wind-induced damage has not been fully mitigated. Therefore, problems such as design, manufacturing, installation, and durability of asphalt shingles continue to play a crucial role in their performance during extreme weather conditions. In fact, there are numerous research efforts aimed at better understanding the performance of asphalt shingles and their particular modes of failure[12,14,29,44,45].

Types of Shingles

Traditional Shingles

Traditional shingles, commonly referred to as 3-tab asphalt shingles, are composed of a single fiberglass mat layer embedded in asphalt and topped with mineral granules for UV protection. From a materials engineering perspective, their uniform geometry and minimal thickness contribute to their lighter dead load on structural systems (**Figure 2**). However, due to their lower tensile strength and limited dimensional stability, they exhibit reduced resistance to uplift forces, making them more vulnerable in high-wind zones.

In forensic evaluations, traditional shingles are frequently associated with failure modes, such as edge lifting, granular loss, and tab separation, particularly in aging systems or after moderate wind events. Their service life typically ranges from 15 to 20 years, contingent on environmental exposure and installation quality (according to the International Association of Certified Home Inspectors or InterNACHI).

Architectural Shingles

Architectural, or dimensional, shingles consist of multiple laminated layers of asphalt-saturated fiberglass mats, providing increased mass and enhanced mechanical interlock. This multi-layered configuration improves their modulus of elasticity and resistance to wind uplift forces. The irregular geometry and increased thickness contribute to better impact resistance. From a structural engineering standpoint, the higher unit weight imposes a slightly greater dead load but offers improved inertia against fluttering and delamination. These shingles generally exhibit a service life of 25 to 30 years (when adequately maintained). They are better suited for regions with moderate to high wind loads, offering enhanced aesthetic and functional performance (according to the International Association of Certified Home Inspectors or InterNACHI), as shown in **Figure 2**.

You can identify dimensional shingles by their unique look. Unlike 3-tab shingles, these shingles are not cut into identical shapes. Instead, each shingle is manufactured with alternating areas or tabs of single and double layers. This pattern is often referred to as “dragon’s teeth.” Some manufacturers also add a shadow line to some products,

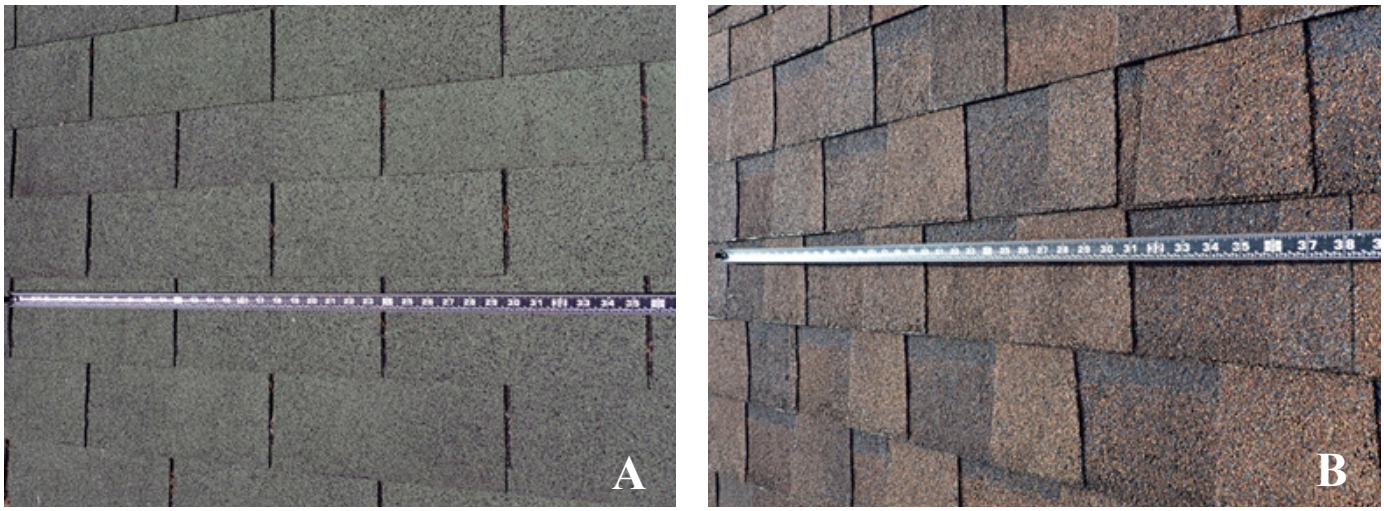

Figure 2
Types of shingles: a) 3-tab, b) architectural.

which is a band of darker granules. The intermittent double-layer tabs, in conjunction with the intermittent shadow band on the single-layer areas, add dimension to the roof — intended to enhance the home's look and style. It is important to note that, from a forensic engineering standpoint, the loss or debonding of the architectural tabs reduces the overall performance of this shingle type.

There are other types of shingles available in the market, such as premium shingles and "hip and ridge shingles." This paper will be limited to field observations gathered from inspections of 3-tab, architectural, and ridge or hip shingles.

Wind-Related Damage

Asphalt shingles are susceptible to damage resulting from a combination of intrinsic material characteristics and extrinsic environmental and structural influences. Intrinsic factors include the physical and mechanical properties of the shingle itself, such as the shingle mat (whether organic or fiberglass-based) chemical composition and aging resistance of the asphalt binder as well as the mineralogical composition and adhesion of surface granules. These elements collectively determine the shingles' resistance to thermal degradation, moisture infiltration, and UV-induced brittleness.

Extrinsic factors, such as improper installation techniques, insufficient sealing, or curing time, and the influence of structural aerodynamics (e.g., uplift pressures from turbulent flow separation at roof edges), significantly impact the shingles' performance under wind-induced loading conditions. While the mechanics of asphalt shingles' damage under high-wind scenarios have been extensively documented[11,12,14,24,29,43,44,45], distinguishing genuine wind-induced failures from damage due to aging, manufacturing defects, or mechanical impacts remains a critical challenge in forensic engineering investigations. Misattribution of wind damage to shingles can lead to incorrect failure diagnoses or disputes in insurance and legal contexts. Therefore, it is essential to understand damage attributable to excessive wind-induced pressures and how it manifests on roof sections.

A previous study was able to identify four primary modes of asphalt shingle failures, which were obtained from field observations performed after Hurricane Frances in 2004[45]. According to the study, the four identified wind-induced damage modes are: 1) creasing (**Figure 3a**); 2) flipping/flapping (**Figure 3b**); 3) tearing/removal (**Figure 3c, Figure 3d** and **Figure 3e**); and 4) abrading from flying or falling debris (**Figure 3f**)[45]. In addition, the study identified factors that can lead to asphalt shingle failure during windstorms, such as degree of weathering, design, quality of manufacture, and quality of installation.

The resistance of asphalt shingles against wind-induced uplift forces is primarily dependent on the sealant strip, which is a strip comprised of bituminous material that acts as a "Velcro" type of attachment between the top and bottom shingle tabs. However, the integrity of the sealant strip is susceptible to age-related deterioration due to exposure to environmental weather conditions (e.g., temperature swings, rain, ice, among others), causing reduction of the bonding capacity between the two asphalt shingle layers, which can lead to complete debonding of the layers. To assess wind-induced damage on asphalt shingles, the material transfer will differentiate between age-related deterioration of the bonding material — where the observations of material transfer between the two asphalt shingle layers would indicate external forces with magnitudes greater than those provided by the bonding force of the sealant strip[12].

Creasing

Shingle creasing refers to the visible lines or ridges often generated because of wind damage. When strong winds lift and flap shingles, they can bend and develop creases, which not only affect the roof's appearance but also indicate potential structural issues of the shingle's internal components (e.g., mat integrity). Creased shingles may lose granules, making them more vulnerable to sun damage, water leaks, and microbial growth.

The creasing of shingles occurs due to excessive wind suction pressures, which generate a lifting force that overcomes the predominant hold-down force provided by the shingle tab sealant plus the shingle self-weight. In a structure under the influence of hurricane wind forces, the highest suction pressures develop on the windward-facing roof slopes and in the roof critical zones identified as roof edges as well as ridges (see **Figure 1** for exact locations of critical zones)[31]. Thus, the creasing of shingles will first develop in windward-facing roof edges/eaves, rakes and hip/ridge lines and then in the roof field. The lack of creased shingles in the most susceptible areas of the windward roof sections, while finding creased shingles in areas less susceptible (e.g., field and leeward roof sections), may indicate that the creasing was caused by external forces unrelated to wind. Note that this statement typically applies when the attachment method of the shingles is uniform across the entire roof area[12,14,45,46].

It must be noted that the capacity of asphalt shingles to counteract the suction pressures induced by wind loading is achieved by the shingles' sealant strip, which bonds the upper layer shingle (bottom edge) with the lower layer shingle (upper edge). The sealant strip is made out of bituminous material, which ages with time, causing a reduction in the wind resistance[44] and making the roof prone to premature wind-induced damage such as creasing.

Figure 3
Wind-related damage: a) creasing, b) flipping/flapping, c) tearing of hip shingles, d) tearing of ridge shingles, e) removal, and f) windborne debris impact (linear pattern).

Flipping/Flapping

Shingle flipping/flapping is a failure mechanism observed in asphalt shingles, characterized by the uplift and permanent deformation of individual shingles due to aerodynamic loading. This phenomenon initiates when the shingle is detached from its asphalt sealant strip, typically as a result of wind-induced pressures exceeding the adhesive bond strength. Once unsealed, the leading edge of the shingle is susceptible to uplift and rotation.

If the imposed deformation exceeds the elastic limit of the shingle assembly (comprising the asphalt coating and the fiberglass or organic mat), the material undergoes localized creasing. This creasing represents a plastic deformation process in which the mat's flexural stiffness is irreversibly compromised, and the asphalt matrix may exhibit both macro and micro fracturing or cohesive failure. The result is a permanent loss of structural and elastic recovery capacity. Once this threshold is exceeded, the shingle is unable to return to its original installed position, thereby losing its functional performance in terms of wind resistance, water shedding, and overall system integrity. Similar to the shingle creasing phenomenon, shingle flipping/flapping will develop in the roof slopes facing the predominant wind direction and should first appear in roof edges/eaves, rakes and hip/ridge lines, before manifesting in the roof field[12,14,45,46].

Tearing/Removal

Wind-induced forces pose a significant challenge to the integrity of roof shingles, often leading to tearing or complete removal of roof covering sections. High wind speeds generate dynamic pressures and suction forces across the roof surface, particularly at edges and corners where airflow separation creates localized low-pressure zones. These forces exert uplift and shear stresses on shingles, exceeding their adhesive and mechanical fastening capacities.

Factors such as material properties, installation quality, and roof geometry further influence susceptibility to damage. Prolonged exposure to cyclic wind loading can weaken adhesive bonds and fatigue shingle tabs, initiating cracks or tears that propagate under subsequent wind events. In extreme wind events, such as hurricanes, intense uplift forces can dislodge entire shingle sections that compromise the roof's protective barrier, especially in the most susceptible areas of the roof, and expose the underlayment to environmental and wind damage. Understanding these mechanisms is critical for developing wind-resistant roofing systems and improving building codes in high-wind regions[12,14,45,46].

Windborne Debris Impact to Shingle Roofs

As defined by ASCE 7-22[31], the *2023 Florida Building Code* (FBC)[47] and the *2024 International Building Code* (IBC)[48], windborne debris refers to objects propelled by high winds during extreme weather events, posing a risk to the building envelope, particularly glazed openings.

Mechanical damage to asphalt shingles resulting from windborne debris is a significant failure mode observed in residential and light commercial roofing systems subjected to severe wind and storm events. This damage mechanism arises when solid objects entrained by high winds impact the shingle surface with sufficient kinetic energy to compromise its protective and structural function. Windborne debris, such as branches, loose construction materials, or gravel, can cause tearing, puncturing, edge lifting, or complete shingle detachment, especially in older or poorly fastened roofing systems. The nature and severity of the damage depend on various factors, including debris shape, mass, and velocity; impact angle; shingle composition; installation quality; and exposure age. Granular loss leaves the underlying bitumen layer exposed to UV radiation and moisture, initiating premature aging and leakage pathways[12,14,45,46].

The Federal Emergency Management Agency (FEMA) has extensively documented such damage patterns through post-disaster assessments, highlighting their widespread occurrence and role in initiating progressive roof system failures. For instance, the FEMA findings after Hurricane Charley in 2005[49] note that windborne debris and hail often work in tandem with uplift forces to weaken the roof covering, especially in cases where shingles are not rated for high-wind or impact resistance. FEMA's analysis emphasizes that improperly installed or inadequately secured shingles are particularly susceptible to damage, even under moderate impact loads. The report further recommends the use of asphalt shingles that meet or exceed Class 4 impact resistance standards as defined by UL 2218[50] and high-wind performance classifications under ASTM D7158[51], particularly in regions designated as high-wind or hail-prone zones[49].

Nonwind-Related Damage

Asphalt shingles are susceptible to a variety of nonwind-related damage mechanisms that compromise the roof system's integrity over time. From a forensic engineering perspective, several contributory factors must be considered in diagnosing shingle failure unrelated to wind uplift forces[46]. Improper installation practices, including misalignment, under-driven or over-driven fasteners, and

inadequate surface preparation, can create stress concentrations and initiate premature distress[12,14,45,30]. Sealant strip failure (whether due to contamination, poor adhesion, insufficient activation, or age) can diminish inter-shingle bonding, making the system more vulnerable to moisture infiltration and material displacement.

Manufacturing inconsistencies, such as variable asphalt saturation, granule loss, or dimensional irregularities, further affect shingle performance and durability. Age-related material degradation, exacerbated by UV radiation and environmental exposure, leads to embrittlement and cracking. Thermal expansion and contraction cycles introduce fatigue stresses, often manifesting as buckling or splitting along the shingle body. Additionally, mechanical damage from foot traffic or tool impact, as well as external abrasions from overhanging vegetation or animal interference, contribute to localized wear and physical compromise. A comprehensive evaluation of these factors is essential in forensic assessments aimed at distinguishing between wind-induced and other failure modes in asphalt shingle roofing systems that are nonwind-related. The most common field observations of nonwind-related damage to asphalt shingles are presented in the following paragraphs.

Shingle Debonding

Shingle debonding, specifically the loss of adhesion along the sealant strip, is a critical issue in asphalt shingle roofing systems and has been widely documented across in-situ assessments and post-storm evaluations. The sealant strip, a thermally activated bitumen-based adhesive located along the leading edge of each shingle, is essential in transferring uplift forces through the roofing assembly[13].

Field investigations have shown that partial or full unsealing of shingles can occur as roofs age, independent of wind loading. A comprehensive survey in Florida revealed that up to 79% of shingle strips on roofs older than six years exhibited signs of unsealing, with the phenomenon notably absent in roofs younger than six years[12,14]. The primary mechanism behind field shingle debonding appears to be internal shear failure of the sealant strip, driven by long-term thermal cycling that imposes repetitive expansion and contraction stresses on the shingle system[45]. Unsealing patterns tend to follow the geometry of shingle installation — that is diagonal patterns for diagonally laid shingles and vertical patterns for vertically laid ones. Additionally, the unsealing patterns are often localized to the extreme end tabs of 3-tab shingles or along specific courses in laminate shingles[12,14] (**Figure 4**).

In contrast, debonding observed at hip and ridge caps frequently stems from either inadequate sealant application during installation or weak initial adhesive bonding, rather than aging-related mechanisms. Typically, field inspections of debonded shingles reveal improper nailing or nailing over the sealant strip, in which fasteners were driven over the sealant strip of the downslope shingles. This phenomenon results in a reduced uplift capacity of the shingles to resist wind forces.

Shingle Mechanical Damage

Mechanical damage to asphalt shingles encompasses a broad spectrum of nonwind-related physical impacts that compromise the integrity, performance, and longevity of roofing systems. As described in previous investigations/assessments[45,30], this type of damage often results from

Figure 4
Shingle diagonal debonding pattern.

incidental contact with overhanging tree limbs, animal activity, foot traffic, or even deliberate actions. Such impacts may lead to localized abrasions, granule displacement, tears, marring, or deformation of individual shingle elements.

Scuffing from foot traffic, displacement under pressure (especially on hot shingles) and flaking due to weak granule adhesion are examples of mechanically induced conditions that expose the asphalt-impregnated base mat, accelerating degradation through UV radiation.

Unlike wind-induced uplift damage, mechanical damage tends to appear in irregular patterns, typically concentrated in walkable areas away from zones of high suction pressures. Intentional or misattributed damage may also be identified by specific patterns, such as the removal of shingle corners rather than complete tab displacement. Marshall et al. (2010)[45] further noted that the presence of torn sealant remnants can indicate that shingles were originally well bonded, requiring significant force for separation (likely caused by forceful attempts to manually simulate wind damage), a key distinction in post-storm forensic evaluations (**Figure 5**). Given the potential for mechanical damage to reduce a roof's water-shedding capability or service life, accurately identifying its source may be valuable for an owner requesting insurance assessments and structural evaluations of roofing systems.

Shingle Cupping and Clawing

Cupping and clawing are deformation patterns in asphalt shingles that affect both the visual appearance and functional performance of steep-slope roofing systems, often leading to misidentification as wind damage. Cupping refers to the upward curling of the shingle corners or the butt edge, producing a concave distortion that can protrude up to 1 inch above the roof surface, while clawing is the downward curling of the shingle corners toward the roof deck[45,46]. These anomalies typically begin within the first few years of service (sometimes as early as 18 months after the shingles have been installed), and said damage is observed in both square-tab and traditional 3-tab fiberglass shingles. Such anomalies result from a combination of factors, including long-term material fatigue, aging of the asphalt binder, thermal cycling, and inadequate attic ventilation[44].

Cupping occurs when the top layers of the shingles shrink more than the lower layers, whereas clawing initiates at the exposed corners and progresses inward. The progression of both distortions is characterized by initial deformation on the shingle tabs edges (**Figure 6**). Although commonly dismissed as aesthetic issues, these forms of deformation may signal underlying structural degradation and increase susceptibility to cracking or wind uplift over time. Differentiating them from true wind-induced failures, such as creasing or tearing, is essential for accurate roofing evaluations and insurance assessments[45,46].

Shingle Blistering and Granular Loss

Blistering and granular loss are common asphalt shingle anomalies (both of which are nonwind-related), and can compromise the long-term performance of residential roofing systems.

Granular loss refers to the shedding of the protective granule layer from the shingle surface, which exposes the underlying asphalt-impregnated base mat to UV radiation and mechanical damage, thereby accelerating deterioration and potentially shortening the roof's service life[30]. While hail and windborne debris impacts can cause acute and localized granule displacement (meeting the definition of "damage" due to reduced water-shedding capability), granular loss can also result from non-impact-related mechanisms such as aging, scuffing from foot traffic, marring, flaking, and general mechanical abrasion[50].

Blistering, on the other hand, is a material defect caused by gas pockets within the base mat that rise to the surface and release, displacing granules in small, scattered patterns. This condition typically manifests in areas of poor ventilation of the attic below the damaged shingles and is distinguished from hail impact by the size and distribution of the affected areas. Unlike hail damage, which is round and localized, blistering produces smaller and more random granule loss that can be mistaken for impact damage (**Figure 5**). Differentiating between these forms of deterioration is crucial during forensic assessments to ensure accurate attribution of cause and to avoid misclassification in roofing evaluations[30].

Shingle Splitting

Shingle splitting is a failure mode that results from long-term thermal cycling and material fatigue, typically manifesting as cracks or splits in asphalt shingles. According to previous studies[12,14], splitting often occurs at the end joint of the shingle course below, with cracks emanating from this point due to internal tensile failures in the fiberglass reinforcement mat. This type of failure is exacerbated by the repeated expansion and contraction of the shingle material caused by fluctuating temperatures over its service life. Over time, the tensile strength of the

reinforcement mat may degrade to the point where the mat can no longer withstand thermal stresses, leading to splitting.

Koonts (1990)[52] further attributes this failure to insufficient tensile strength of the mat, which, when combined with the shear forces acting on the sealant strip, results in

Figure 5
Nonwind-related damage: a) debonding, b) tree abrasion, c) animal activity, d) blistering, e) granular loss, and f) alligatoring.

cracking. These splits are typically observed more frequently in aged shingles, with studies showing that the likelihood of such failures increases as the roof ages, particularly after six years of service[12,14].

Shingle splitting can take several forms, including horizontal, vertical, random, and in-line cracking. Horizontal splitting occurs between the two lines of restraint, with one part of the shingle fastened to the roof deck and the other edge secured by the sealant strip. Vertical splitting typically occurs when the top shingles shrink over the butted joints of the underlying shingles, with splits extending vertically upslope in racked installations and in curved patterns in diagonally installed shingles[45]. A couple of examples of shingle thermal splitting are provided in **Figure 6**.

Severe splitting of aged shingles is typically referred to as "alligatoring," since the cracked and wrinkled appearance of the shingles surface resembles the hide of an alligator (**Figure 5**). Random cracking does not follow any distinct pattern, often starting as surface crazing and eventually leading to complete splits as the shingle ages, while in-line cracking occurs directly above joints in the sheathing panels, depending on the movement of the roof decking[46]. These cracks can significantly compromise the roof's structural integrity, increasing the risk of water infiltration and wind damage, making shingle splitting a critical concern for designers and contractors.

Concrete/Clay Tile Roofs

Globally recognized for its timeless design and resilience, tile roofing stands apart with a heritage unmatched by any other roofing material. Although tiles have played a vital role in architecture for thousands of years, the modern era has seen a remarkable surge in innovation and industry development[53,54]. As such, concrete and clay tiles are among the most prevalent types of roofing materials.

Concrete tiles are typically made from a blend of

Figure 6
Nonwind-related damage: a) clawing, b) cupping (or curling), c) random thermal splitting, and d) horizontal thermal splitting.

Portland cement, sand, and water in varying ratios. This mixture is then shaped under high pressure using individual molds. Often, the tile surface is treated with cement-based materials and enhanced with synthetic oxides to create a glossy finish, or colored by adding pigments directly to the mix. The final surface can be either smooth or textured. Once molded, the tiles are placed in controlled environments with regulated temperature and humidity to undergo hydration and achieve the necessary strength prior to distribution. Among concrete tiles, the most widely used designs in the roofing industry are the high-profile S-curved tiles and the flat-style varieties, both represented in **Figure 7**[55].

Conversely, clay tiles are derived from natural materials such as clay, shale, or similar earth-based substances. These tiles are shaped and then hardened through a high-temperature firing process. In the United States, S-shaped clay tiles are the most popular configuration, also illustrated in **Figure 7**[41]. Despite the aesthetic and historical appeal of clay tiles, concrete tiles are often favored due to their superior durability, strength, and resilience against long-term weathering effects[56].

Concrete tiles are produced in a range of sizes, profiles, and colors. They are generally thicker at the top and bottom, with strengthening ribs between those points. The upper part of the tile, which rests on a wooden batten, is known as the "head lug," while the "nose lug" refers to the section that overlaps with the course of tiles below it (**Figure 7**). Modern flat and curved tiles often feature interlocking systems with ribs and grooves along their edges. These interlocks enhance structural alignment, ensure consistent spacing and mitigate moisture intrusion beyond the tile. The interlocking strip is usually about 1 inch wide and half the tile's thickness on either side[55].

Wind-Related Damage

The impact of wind forces on roofs with permeable coverings, such as tiles, is influenced by several factors,

Figure 7
a) S-shaped concrete tile, b) flat concrete tile, c) S-shaped clay tile, d) head and nose lugs in flat tiles.

including the overall roof profile (e.g., configuration and slope), the design details of the roof covering elements, and the degree of roof porosity. Tile systems are generally known for their strong resistance to environmental stressors, yet extreme weather conditions can still affect them to varying extents. During high wind events, damage to tile roofs becomes clearly visible. Common signs include displaced tiles, tiles entirely blown off the roof (indicating direct wind damage), and fractured tiles caused by impact with windborne debris (signifying indirect wind damage). This section will focus on direct and indirect wind damage to tile roofs.

Tile Uplift

As previously noted in the discussion on common wind damage patterns, hip, ridge, and perimeter tiles are particularly vulnerable to wind-related damage. This increased susceptibility arises because these tiles are situated in regions (previously referred to as "high suction pressure zones") where wind flow separation and conical vortex formation generate intense, localized suction forces or uplift pressures. While field tiles may also experience the effects of these conical vortices, the strength of the vortices and the resulting negative pressures tend to diminish as wind moves away from the roof corners and edges[19,57,58,59,60,61,62].

Some roof manufacturers, especially in recent times, have included additional fasteners in these zones to increase wind resistance in these zones. Further studies have shown that most roof damage tends to occur on the windward side, where tiles are subjected to higher net uplift forces. This is because both external and internal pressures (with internal pressure forming in the gap between the tiles and the roof deck) align in the same direction, increasing the overall forces on these tiles. In contrast, tiles on the leeward side benefit from a reduction in stress, as the internal and external forces act in opposite directions, providing a degree of relief[63,64,65,66] (**Figure 8**).

According to the *2023 Florida Building Code* (FBC)[47], to dislodge a tile, the overturning moment produced by wind-induced suction must exceed the resisting moment, which is determined by factors such as the tile's weight, attachment method to the roof deck, tile size, tile profile, and other related parameters. As previously noted, clay and concrete tiles are typically secured to the roof with fasteners or adhesives such as foam or mortar in high wind zones such as coastal Florida. However, in certain regions as well as in the case of the hip and ridge zones, tiles are installed using mortar.

Field investigations and past reconnaissance have shown that mortar attachments are often inadequate to withstand the high uplift pressures experienced during hurricanes, particularly in storm-prone areas. This is mainly because mortar tends not to bond effectively with the tiles unless the tiles are pre-wetted — a practice indicative of less effective construction[53]. Consequently, when subjected to extreme wind forces, tiles either detach from the mortar or tear the underlayment, leading to significant roof damage[54] (**Figure 8**).

Windborne Debris Impact to Tile Roofs

Roof tiles are highly susceptible to damage from windborne debris during high-wind events such as hurricanes, where debris may originate from various sources, including broken tree limbs, dislodged rooftop equipment, cladding components, or even other roof coverings like tiles and pavers. As established by Kordi and Kopp[67], the likelihood of roof tiles becoming airborne and contributing to further damage is closely tied to their orientation relative to the oncoming wind.

When the angle of exposure aligns with favorable aerodynamic conditions, tiles can be uplifted and transformed into projectiles, traveling downwind and potentially compromising the roof coverings of both the originating structure and neighboring buildings. Their study[67] found that tile flight velocities typically range between 30% and 60% of the mean roof-height gust speed at the moment of failure. This underscores the significance of initial aerodynamic conditions in the behavior of roof-covering components as debris.

Beyond the hazards posed by flying tiles, the impact of such debris on intact roofing systems can be severe. According to a previous research investigation, projectile impacts on tiled roofs often result in localized cracking or shattering of the impacted tiles (**Figure 8**). However, the damage extends beyond the point of impact; loss of tiles due to projectile strikes can lead to breaches in the roof covering that promote wind infiltration beneath adjacent tiles, thereby escalating the overall damage through progressive failure[68]. Comparative testing between concrete and clay tiles revealed key performance differences: concrete tiles exhibited 39% greater resistance to impact forces than clay tiles[67]. Moreover, concrete tiles tended to break in larger, more localized pieces, particularly when bonded with mortar, absorbing the impact energy. In contrast, clay tiles tended to shatter extensively, creating larger areas of failure around the impact zone[68].

Figure 8
Wind-related damage: a) uplifting of hip cap tiles, b) uplifting of ridge cap tiles, c) impact with windborne debris, d) fractures from impact with windborne debris (black arrows indicate oncoming wind direction on the date of loss).

Damage to concrete roof tiles induced by windborne debris displays distinct failure mechanisms and fracture characteristics when compared to mechanical damage from nonwind-related sources. Windborne debris impacts are typically high-velocity and irregular, arising during extreme wind events such as hurricanes. These impacts frequently result in localized, brittle failures manifesting as transverse cracking, edge fragmentation, or surface spalling with the most damage observed on roof slopes oriented toward the prevailing wind direction (**Figure 8**).

Such damage can undermine the aerodynamic performance of the roof system, potentially triggering progressive dislodgement of adjacent tiles[68]. The severity and pattern of failure are influenced by multiple factors, including the tile's orientation relative to the wind, the quality of its underlying support, and the method of installation, among others.

Nonwind-Related Damage

While known for their aesthetic appeal and long-term durability, clay and concrete tile roofing systems are nonetheless susceptible to various nonwind-related degradation mechanisms that can compromise performance and reduce service life. From a forensic engineering perspective, identifying and differentiating these modes of failure from wind-induced damage is essential for accurate post-event assessments and insurance determinations[69,70,71]. The most common field observations of nonwind-related damage to the roofing tiles are presented below.

Improper Tile Installation

Tile roofs are particularly vulnerable to damage resulting from improper installation practices. Common errors include insufficient fastening (e.g., using incorrect nails or omitting required fasteners), poor alignment, and improper mortar bedding or foam adhesive application[72,73]. These

deficiencies introduce localized stress concentrations, reduce mechanical interlock, and create voids or misalignments that may lead to premature tile cracking or slippage under normal thermal or mechanical loads[69] (**Figure 9**).

Additionally, improper installation includes nail heads that are installed flush with the tile surface restraining the tiles from any movement. Such practices lead to premature linear cracking of the tiles at the nail penetration location. Improper installation also renders the tiles susceptible to flutter/chatter during repeated windstorm events, which loosens the fasteners further, abrade the underlayment and exposes the roof underlayment to moisture intrusion. The loosening of these fasteners aggravates the tile

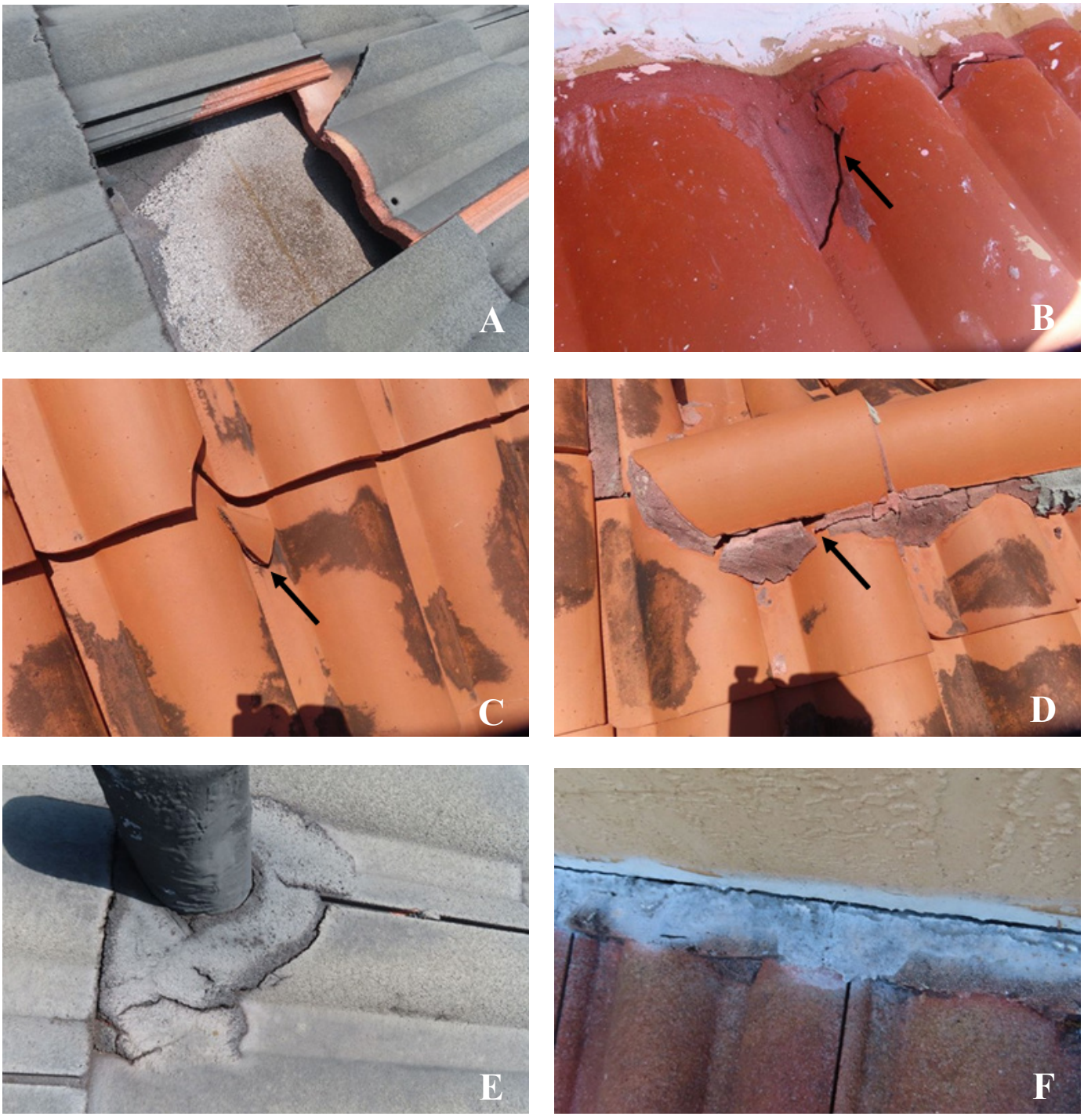

Figure 9
Nonwind-related damage: a) downward shifted tile due to missing fastener, b) improperly sized tile and poor alignment, c) corner chipped tile, d) premature cracking and chipping of mortar, e) cracked mortar around a plumbing vent, f) cracked mortar at roof-to-wall interface.

movement and furthers deterioration. It is important to note that the fluttering/chattering of tiles is commonly observed in steeper roofs and such tiles are recommended to be installed with wind clips along with a construction-grade sealant as a precaution to prevent instability and movement of the tiles from excessive pressures, especially in the high suction pressure zones[48].

Material Quality Control and Defects in Tiles

Tile manufacturing and material inconsistencies, such as a lack of quality control to ensure dimensional regularities, porosity, and proper mix proportions of mortar, can lead to premature deterioration and subsequent cracking. Concrete tiles with improper quality control are more susceptible to thermal degradation[74]. Clay tiles with dimensional variances are more susceptible to edge/corner chipping and fatigue cracking during the expected useful life of the roof[75]. The absence of gouges or holes at or near the intersection of the fractures may be a further indication that the cracking is not the result of impact with windborne debris. The brittleness of clay tiles and the shrinkage of cement in concrete tiles contribute to cracks or corner chips under cyclical loading[71]. The inadequate quality control of the mortar mix, insufficient curing time, or improper curing of the mix lead to premature cracking of the mortar (**Figure 9**).

Nonwind-Related Impact Damage to Tiles

Impact damage is a leading cause of nonwind-related failure in tiled roofing systems. This includes localized cracking from foot traffic, impacts from overhanging branches, and tool or ladder contact during maintenance activities. Such cracks are typically irregular and located in walkways, valley intersections, or under satellite dish mounts[69,76]. Concrete tiles, though more resilient than clay, are still susceptible to cracking or chipping at unsupported corners when subjected to concentrated loads emanating from foot traffic and mechanical impact[70] (**Figure 10**).

Footfall damage to roof tiles is typically evidenced by a linear nature of the cracks and lack of radial cracks emanating from point of impact to broken tile surfaces. Broken tile pieces typically remain in place or are slightly displaced downward, depending on the age of the fracture itself. As such, broken tile fragments that remained in place are evidence that the cracking was not caused by wind, as strong wind would have removed the cracked portion from its original position.

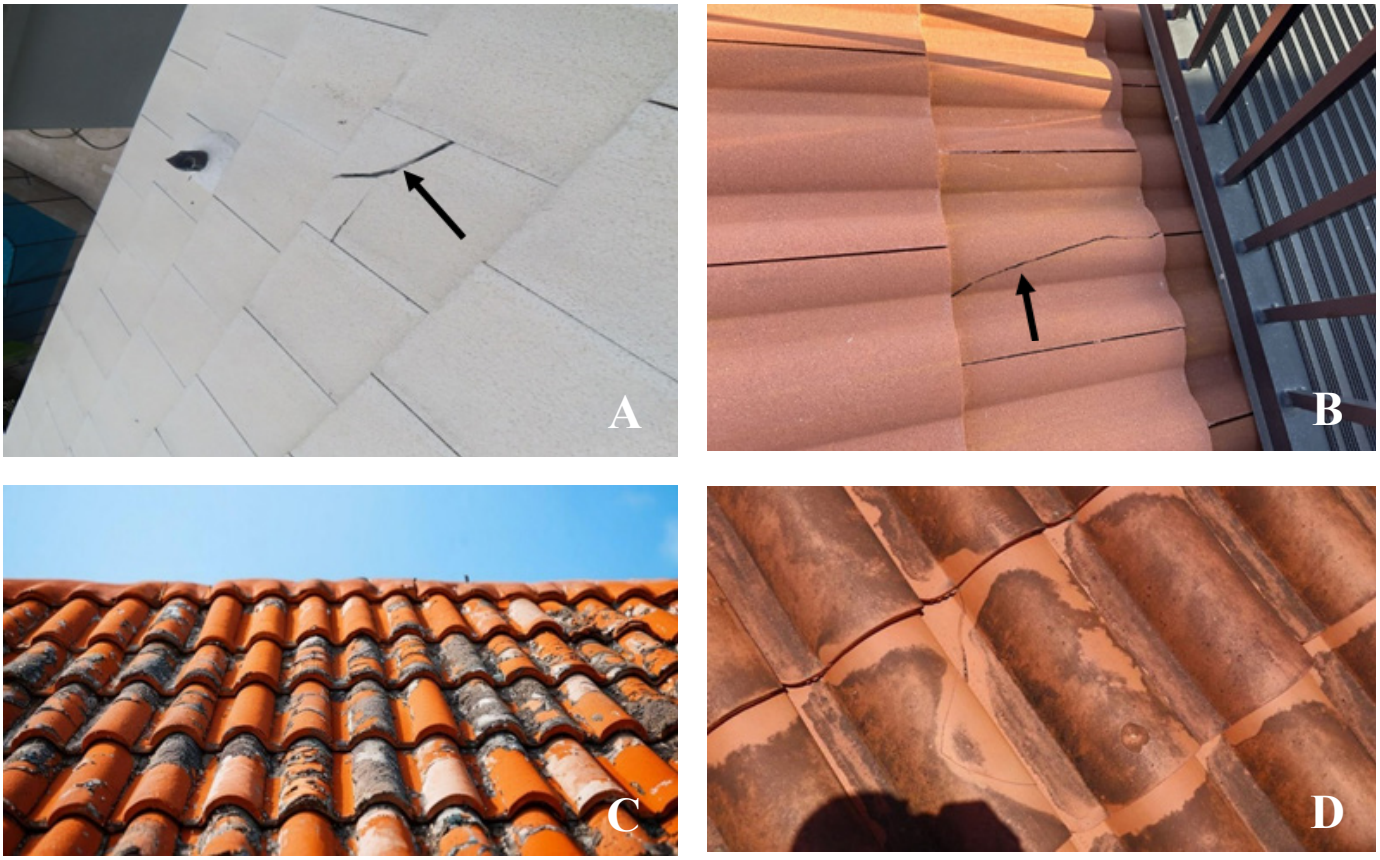

Figure 10
Nonwind-related damage: a) footfall damage, b) fractured tile due to foot traffic, c) algae accumulation, d) mildew growth.

Biological and Environmental Effects in Tiles

Moss, algae, and lichen growth can degrade both clay and concrete tile surfaces. These organisms retain moisture against the tile, encouraging efflorescence and biological etching over time. Root systems from lichens and mosses can expand existing microcracks and lead to mechanical tile displacement[77,78]. Furthermore, animal activity, such as droppings, often damages the surface of the tile, resulting in gradual deterioration and discoloration of tiles[71] (**Figure 10**).

Conclusion

Based on extensive experience evaluating hundreds of roofs for potential wind damage, and understanding of windstorm events, wind flow around structures, and bluff-bodies in the built environment, the following general guidelines are recommended for evaluating wind damage:

- A crucial first step involves reviewing wind speeds, including both sustained winds and gusts, during and around a particular storm event. This helps determine whether wind speeds were sufficient to cause uplift and failure of roofing components. This step also includes obtaining the duration for which the wind speed was sustained to determine the amount of time the structure was exposed to windstorms.

- Wind direction also plays a prominent role, as higher damage is typically observed on windward-facing roof slopes. Wind damage consistently occurs in high-pressure zones, as outlined in the ASCE 7-22 standard as previously discussed. Therefore, the initial indications of wind damage are often located at the edges, corners, ridge lines, and hip lines of a roof. For recent construction, a higher emphasis is placed on adding more fastening mechanisms in the high-suction pressure zones and hence, it is recommended to review the manufacturer specifications whenever applicable. For shingle roofs, this damage often manifests as compromised sealant strips, creasing, tearing, folding, or missing shingles. For tile roofs, typical damage includes broken, missing, uplifted or displaced tiles.

- Damage caused by windborne debris during storms can be classified based on the randomized nature of debris impacts, the damage patterns noted on the roof covering, and the location of these impacts. In cases of indirect wind damage caused by windborne debris, a thorough evaluation of collateral evidence (including oncoming wind direction on or around the date of loss) and a holistic understanding of potential damage to other vulnerable elements such as mechanical equipment, garage doors or roof top equipment are critical.

- Installation deficiencies, manufacturing imperfections, age-related deterioration, and nonwind-related damage patterns should be considered. Such deficiencies include debonding, splitting, cupping and clawing, granular loss, and mechanical damage to shingle roofs, footfall damage, biological growth, and thermal chipping and cracking to tile roofs among other forms of damage.

Forensic experts, equipped with insights into how roofing materials respond to impact forces and practical experience examining storm damage, are exceptionally positioned to evaluate storm-induced damage to residential roofing systems, including both shingle and tile roofs. The authors' forensic engineering experience indicates that engineers must adopt a holistic approach when evaluating a roof for wind damage. Each failure mechanism discussed in this paper must be considered in light of the roof's history and either included or excluded based on the observed physical evidence at the time of the inspection.

Acknowledgements

The authors greatly acknowledge the internal support provided by DDA Forensics and the engineering team. The contents of this paper reflect the views of the authors, who are responsible for the facts and the accuracy of the information presented herein.

References

1. B. Norcross, Hurricane Almanac: The Essential Guide to Storms Past, Present, and Future, St. Martin's Press, 2007.

2. K. Emanuel, Divine Wind: The History and Science of Hurricanes, Oxford University Press, 2005.

3. J. Holmes, Wind Loading of Structures, 4th Ed., Taylor & Francis, 2021.

4. NOAA, "Population Trends from 1970 to 2020," National Oceanic and Atmospheric Administration, National Coastal Population Report, 2023.

5. Z. Azzi, H. Al Sayegh, O. Metwally and M. Eissa, "Review of Nondestructive Testing (NDT) Techniques for Timber Structures," Infrastructures, vol. 10, no. 28, 2025.

6. K. Vutukuru, M. Moravej, A. Elawady and A. Chowdhury, "Holistic Testing to Determine Quantitative Wind-Driven Rain Intrusion for Shuttered and impact Resistant Windows," Journal of Wind Engineering and Industrial Aerodynamics, vol. 206, 2020.

7. MDC-BCCO, "Post Hurricane Wilma Progress Assessment," Miami-Dade County Building Code Compliance Office, Miami, FL, 2006.

8. W. Suaris and P. Irwin, "Effect of Roof-Edge Parapets on Mitigating Extreme Roof Suctions," Journal of Wind Engineering and Industrial Aerodynamics, vol. 98, p. 483–491, 2010.

9. Z. Azzi, F. Habte, A. Elawady, A. Chowdhury and M. Moravej, "Aerodynamic Mitigation of Wind Uplift on Low-Rise Building Roof Using Large-Scale Testing," Frontiers in Built Environment, vol. 5, no. 149, 2020.

10. G. Bitsuamlak, W. Warsido, E. Ledesma and A. Chowdhury, "Aerodynamic Mitigation of Roof and Wall Corner Suctions Using Simple Architectural Elements," Journal of Engineering Mechanics, vol. 139, no. 3, pp. 396-408, 2013.

11. M. Noone and W. Blanchard, "Asphalt Shingles — a Century of Success and Improvement," in Tenth Conference on Roofing Technology, Gaithersburg, Maryland, USA, 1993.

12. C. Dixon, F. Masters, D. Prevatt, K. Gurley, T. Brown, J. Peterka and M. Kubena, "The Influence of Unsealing on the Wind Resistance of Asphalt Shingles," Journal of Wind Engineering and Industrial Aerodynamics, vol. 130, pp. 30-40, 2014.

13. J. Peterka, J. Cermak, L. Cochran, B. Cochran, N. Hosoya, R. Derickson, C. Harper, J. Jones and B. Metz, "Wind Uplift Model for Asphalt Shingles," Journal of Architectural Engineering, vol. 3, no. 4.

14. C. Dixon, D. Prevatt, F. Masters and K. Gurley, "The Unsealing of Naturally Aged Asphalt Shingles: An In-Situ Survey," in 1st Residential Building Design & Construction Conference, Bethlehem, PA, USA, 2013.

15. D. Banks, R. Meroney, P. Sarkar, Z. Zhao and F. Wu, "Flow Visualization of Conical Vortices on Flat Roofs with Simultaneous Surface Pressure Measurement," Journal of Wind Engineering and Industrial Aerodynamics, vol. 84, p. 65–85, 2000.

16. B. Bienkiewicz and Y. Sun, "Wind Loading and Resistance of Loose-Laid Systems," Journal of Wind Engineering and Industrial Aerodynamics, vol. 72, no. 1, pp. 401-410, 1997.

17. G. Kopp, C. Mans and D. Surry, "Wind Effects of Parapets on Low Buildings: Part 4. Mitigation of Corner Loads with Alternative Geometry," Journal of Wind Engineering and Industrial Aerodynamics, vol. 93, pp. 873-888, 2005.

18. G. Kopp, D. Surry and C. Mans, "Wind Effects of Parapets on Low Buildings: Part 1. Basic Aerodynamics and Local Loads," Journal of Wind Engineering and Industrial Aerodynamics, vol. 93, pp. 817-841, 2005.

19. R. Hazelwood, "The Interaction of the Two Principal Wind Forces on Roof Tiles," Journal of Wind Engineering and Industrial Aerodynamics, vol. 8, pp. 39-48, 1981.

20. C. Feng, A. Chowdhury, A. Elawady, D. Chen, Z. Azzi and K. Vutukuru, "Experimental Assessment of Wind Loads on Roof-to-Wall Connections for Residential Buildings," Frontiers in Built Environment, vol. 6, 2020.

21. K. Alawode, K. Vutukuru, A. Elawady and A. Chowdhury, "Review of Wind Loading on Roof to Wall Connections in Low-Rise Light Wood-Frame Residential Buildings," Journal of Wind Engineering and Industrial Aerodynamics, vol. 236, 2023.

22. H. Kawai and H. Nishimura, “Field Measurement on Wind Force on Roof Tiles, Texas Tech University, Lubbock, Texas,” in Proceedings of the 11th International Conference on Wind Engineering, Texas Tech University, Lubbock, Texas, USA, 2003.

23. A. Robertson, R. Hoxey, N. Rideout and P. Freathy, "Full-scale study of wind loads on roof tiles and felt underlay and comparisons with design data," Journal of Wind Engineering and Industrial Aerodynamics, vol. 10, no. 6, pp. 495-510, 2007.

24. B. Visscher and G. Kopp, "Trajectories of roof sheathing panels under high winds," Journal of Wind Engineering and Industrial Aerodynamics, vol. 95, pp. 697-713, 2007.

25. Z. Azzi, F. Habte, K. S. Vutukuru, A. G. Chowdhury and M. Moravej, "Effects of roof geometric details on aerodynamic performance of standing seam metal roofs," Engineering Structures, vol. 225, no. 111303, 2020.

26. H. Al Sayegh, A. Chowdhury, I. Zisis, A. Elawady, J. Estephan and A. Tolera, "Full-scale experimental investigation of wind loading on ballasted photovoltaic arrays mounted on flat roofs," Journal of Wind Engineering and Industrial Aerodynamics, vol. 256, 2025.

27. P. Krishna, "Wind loads on low rise buildings - A review," Journal of Wind Engineering and Industrial Aerodynamics, vol. 54/55, pp. 383-396, 1995.

28. T. Stathopoulos, "Wind loads on low-rise buildings: a review of the state of the art," Engineering Structures, vol. 6, no. 2, pp. 119-135, 1984.

29. A. Tolera, K. Mostafa, A. Chowdhury, I. Zisis and P. Irwin, "Study of wind loads on asphalt shingles using full-scale experimentation," Journal of Wind Engineering and Industrial Aerodynamics, vol. 225, 2022.

30. L. Sharara, J. Jordan and R. Kimble, "Residential Roofing Evaluation," in Fifth Forensic Engineering Congress, Washington, D.C., USA, 2009.

31. ASCE/SEI-7, Minimum Design Loads and Associated Criteria for Buildings and Other Structures, Reston, VA, USA: American Society of Civil Engineers (ASCE), 2022.

32. Y. Quan, Y. Tamura, M. Matsui, S. Cao and A. Yoshida, "TPU Aerodynamic database for low-rise buildings," in Proceedings of the 12th International Conference on Wind Engineering (ICWE12), Cairns, Australia, 2007.

33. Y. Tamura, “Wind and Tall Buildings,” in Keynote Lecture: the 5th Europe-African Regional Conference on Wind Engineering (EACWE5), Florence, Italy, 2009.

34. D. Prasad, T. Uliate and M. Rafiuddin Ahmed, “Wind Loads on Low-Rise Building Models with Different Roof Configurations,” International Journal of Fluid Mechanics Research, vol. 36, pp. 231-242, 2009.

35. T. Ho, D. Surry, D. Moorish and G. Kopp, “The UWO Contribution to the NIST Aerodynamic Database for Wind Loads on Low Buildings: Part 1. Archiving Format and Basic Aerodynamic Data,” Journal of Wind Engineering and Industrial Aerodynamics, vol. 93, no. No.1, pp. 1-30, 2005.

36. S. Wagaman, K. Rainwater, K. Mehta and R. Ramsey, “Full-Scale Flow Visualization Over a Low-Rise Building,” Journal of Wind Engineering and Industrial Aerodynamics, vol. 90, no. No.1, pp. 1-8, 2002.

37. D. Hrishikesh, I. Zisis and M. Matus, “Effects of Roof Shape on Wind Vulnerability of Roof Sheathing Panels,” Journal of Structural Safety, vol. 100, 2023.

38. O. Metwally, H. Ibrahim, A. Elawady, I. Zisis and A. Chowdhury, “Wind Load Impact on Tall Building Facades: Damage Observations During Severe Wind Events and Wind Tunnel Testing,” Frontiers in Built Environment, vol. 10, 2025.

39. M. Eissa, O. Metwally, K. Alawode, A. Elawady and G. Lori, “Performance of High-Rise Building Façades under Wind Loading: A State-of-the-Art Review,” Journal of Building Engineering, vol. 113, 2025.

40. L. Marslan, K. Nguyen, Y. Zhang, Y. Huang, Y. Abu-Zidan, T. Gunawardena and P. Mendis, "Improving Aerodynamic Performance of Tall Buildings Using Façade Openings at Service Floors," Journal of Wind Engineering and Industrial Aerodynamics, vol. 225, 2022.

41. NIST, "Generic Clay Roofing Tile," National Institute of Standards and Technology, 2005.

42. H. Snoke, "Asphalt-Prepared Roll Roofings and Shingles," National Bureau of Standards, Report BMS70, 1941.

43. W. Cullen, "Research and Performance Experience of Asphalt Shingles," in 10th Conference on Roofing Technology, Gaithersburg, MD, USA, 1993.

44. F. Masters, "Phase II Report: Investigation of the Wind Resistance of Asphalt Shingle Roof Coverings," Oak Ridge National Library, 2013.

45. T. Marshall, S. Morrison, R. Herzog and J. Green, "Wind Effects on Asphalt Shingles," Haag Engineering Co., Irving, TX, USA, 2010.

46. R. Ribble, D. Summers, R. Olson and J. Goodman, "From Generation to Generation: Issues and Problems Facing the Steep Slope Roofing Industry," in 10th Conference on Roofing Technology, Gaithersburg, MD, USA, 1993.

47. FBC, Florida Building Code, 8th Edition, Florida Building Commission, International Code Council, Inc., 2023.

48. IBC, 2024 International Building Code, International Code Council, Inc., 2024.

49. FEMA, "Hurricane Charley in Florida - Observations, Recommendations, and Technical Guidance," Federal Emergency Management Agency, FEMA 488, 2005.

50. IIBHS, "Relative Impact Resistance of Asphalt Shingles," Insurance Institute for Business & Home Safety, 2014.

51. ASTM-D7158-20, "Standard Test Method for Wind Resistance of Asphalt Shingles (Uplift Force/Uplift Resistance Method)," American Society for Testing and Materials International, 2020.

52. J. Koontz, "Shingle Splitting Problem," Western Roofing Magazine, 1990.

53. R. Fulmer, "Tile Roof Systems: Analysis and Inspection Techniques for Roof Consultants," International Institute of Building Enclosure Consultants (IIBEC), 2006.

54. T. Marshall, "Roof Damage Issues in Hurricanes," Haag Engineering Company, 2004.

55. T. Marshall, "Curved Corner Fractures in Concrete Tile," Haag Engineering Company, 1990.

56. V. Durão, J. Silvestre, R. Mateus and J. de Brito, "Comparative Assessment of Roof Tiles' Environmental Performance from Cradle to Cradle," in World Sustainable Built Environment 2024, 2024.

57. C. Geurts, "Wind Loads on Permeable Roof Covering Products," in Fourth Colloquium on Bluff Body Aerodynamics and Applications, Bochum, Germany, 2000.

58. P. Huang, A. Mirmiran, A. Chowdhury, C. Abishdid and T. Wang, "Performance of Roof Tiles under Simulated Hurricane Impact," ASCE Journal of Architectural Engineering, vol. 15, no. 1, pp. 26-34, 2009.

59. C. Kramer and H. Gerhardt, "Wind Loads on Permeable Roofing Systems," Journal of Wind Engineering and Industrial Aerodynamics, vol. 13, no. 1, pp. 347-358, 1983.

60. H. Okada, J. Katagiri and T. Ohkuma, "Study on Method for Evaluating Wind Performance of Tiled Roof," in Proceedings of the 7th Asia-Pacific Conference on Wind Engineering, Taiwan, 2009.

61. A. Robertson, R. Hoxey, N. Rideout and P. Freathy, "Full-Scale Study of Wind Loads on Roof Tiles and Felt Underlay and Comparisons with Design Data," Wind and Structures, vol. 10, no. 6, pp. 495-510, 2007.

62. F. Habte, M. Mooneghi, T. Baheru, I. Zisis, A. Chowdhury, F. Masters and P. Irwin, "Wind Loading on Ridge, Hip and Perimeter Roof Tiles: A Full-Scale Experimental Study," Journal of Wind Engineering and Industrial Aerodynamics, vol. 166, pp. 90-105, 2017.

63. H. Kawai and H. Nishimura, "Field Measurement on Wind Force on Roof Tiles," in Proceedings of the 11th International Conference on Wind Engineering (ICWE11), Lubbock, Texas, USA, 2003.

64. R. Li, "Effects of Architectural Features of Air-Permeable Roof Cladding Materials on Wind-Induced Uplift Loading," ProQuest ETD Collection for FIU. AAI3541803., 2012.

65. A. Tecle, G. Bitsuamlak, N. Suskawang, A. Chowdhury and S. Fuez, "Ridge and Field Tile Aerodynamics for a Low-Rise Building: a Full-Scale Study," Wind and Structures, vol. 16, 2013.

66. T. Baheru, F. Habte, M. Moravej and A. Chowdhury, "Full-Scale Testing to Evaluate Wind Effects on Residential Tiled Roofs," in International Conference on Building Envelope Systems and Technologies (ICBEST), Aachen, Germany, 2014.

67. B. Kordi and G. Kopp, "Effects of Initial Conditions on the Flight of Windborne Plate Debris," Journal of Wind Engineering and Industrial Aerodynamics, vol. 99, no. 5, pp. 601-614, 2011.

68. A. Mirmiran, T. Wang, C. Abishdid, P. Huang, D. Jimenez and C. Younes, "Performance of Tile Roofs Under Hurricane Impact - Phase 2," International Hurricane Research Center (IHRC), 2007.

69. FEMA, "Mitigation Assessment Team Report - Hurricane Irma in Florida," Federal Emergency Management Agency (FEMA) P-2023, 2018.

70. C. Dunlop, Roofing Inspection, Home Reference Book, 2015.

71. S. Petty, Forensic Engineering: Damage Assessments for Residential and Commercial Structures (2nd ed.), CRC Press, 2021.

72. NRCA, Roofing Manual: Steep-Slope Roofing Systems, National Roofing Contractors Association, 2023.

73. FBC, Tile Roofing Installation Manual for Florida, Florida Building Commission (FBC), FRSA/TRI 7th Edition, 2023.

74. A. Neville, Properties of Concrete, 5th Edition, Pearson, 2011.

75. ASTM-C1167-22, Standard Specification for Clay Roof Tiles, ASTM International, 2022.

76. Haag-Engineering, Field Guide to Residential Roof Damage Assessment, Haag Engineering Company, 2020.

77. P. Berdahl, H. Akbari, R. Levinson and W. Miller, "Weathering of Roofing Materials – An Overview," Construction and Building Materials, vol. 22, no. 4, pp. 423-433, 2008.

78. E. Di Giuseppe, "Algal Growth on External Building Envelope," Nearly Zero Energy buildings and Proliferation of Microorganisms, Springer Nature, 2013.

Inside 40 Years of Advances in Failure Analysis of Polymeric Composite Materials

By Geoffrey Clarkson, P.Eng. (NAFE #1143A), Manning Laureate, and Daniel P. Couture, P.Eng., DFE (NAFE #951S)

Abstract

Use of polymeric composite materials is becoming increasingly widespread. Diverse applications include fixed infrastructure, industrial chemical processing, power generation, and aeronautics. Engineers have codified design principles and manufacturing practices so they are accessible to practitioners with general engineering education. In almost all cases, when polymeric composites enter service, none of the design codes, approaches, or construction standards apply, and they cannot be used to determine Fitness For Service. When failures occur, approaches that are normally followed in investigation yield inconclusive results, which often creates a conclusion that: "There was an undetected manufacturing defect." All polymeric composites are non-crystalline, non-linear viscoelastic materials, and their mechanical properties change continuously while in service. This paper describes how damage occurs in these materials, demonstrates how it can be detected, and provides a methodology for addressing these failures.

Keywords

Fiber reinforced polymer, FRP, failures, creep, relaxation, accumulated damage, laminated structures, engineered rubber, fatigue, failure analysis methods, stiffness of composites, forensic engineering

Introduction

This paper begins with a historical review of how these interesting materials evolved through human intervention, starting with rubber, followed by metals, wood laminates, and thermoset polymers. Rubber, a naturally sourced elastomer, needs to be treated with sulfur and heat (vulcanized) to have useful mechanical properties, as discovered by Charles Goodyear in 1839. The original use of fibers to bolster polymer mechanical properties occurred when R.W. Thompson of Scotland used canvas covered on both sides with India rubber in 1845 for bicycle tires. J. Boyd Dunlop improved upon this by making calendered rubber sheets containing cloth for horseless carriage tires, as described in his 1888 patent[1]. Michelin enhanced the technology and began industrial production of "pneumatiques" for air-cushioned support of bicycle wheels on roads. Assembling such disparate materials with totally different sets of properties required much trial and error, but it was revolutionary and accelerated the transportation industry's progress. The rapid adoption of Dunlop's innovations spread beyond transportation during the Industrial Revolution, often leaving scientific understanding to follow empirical application.

Original analysis of rubber and fiber composites using finite-element models was rudimentary — the concepts of matrix and fiber properties, along with their directional variation, created difficult boundary conditions. The techniques of T.J. Dudek at General Tire[2] were based on the continuum mechanics of composite materials summarized by R.M. Jones in 1975[3]. Rubber is a non-linearly viscoelastic material, and is sensitive to external forces and factors, especially temperature.

Cotton fibers twisted into yarn and woven into cloth had inherent variations. Over time, these yarns were replaced with synthetics, such as Nylon 66 and polyester (polyethylene terephthalate), and the life-cycle performance of

Geoffrey Clarkson, P.Eng., RPO Hespeler, 101 Holiday Inn Dr., Cambridge, Ontario, Canada N3C 0E6, (519) 590-3252, g.clarkson@utcomp.com

tires improved. Steel wires for belts on radial tires were often supplemented with polyamide high-strength fibers (Kevlar™ aramids), which augmented the mechanical properties and minimized variations. As the materials changed, the models for engineered rubber composites improved drastically by incorporating the known characteristics of the components into the boundary conditions. Young's modulus (E), Poisson's ratio, elongation to break, and other material properties tie the understanding of the behavior back to fundamentals of polymer physics, and allow real-world feedback to optimize the products for consumers. In the early 1970s, finite-element models of tire behavior[4] emerged from the laboratories connecting field experience with mathematics and mechanics of solids.

In the metal world, the canon of knowledge was developing steadily. In 1679, Robert Hooke observed that certain metals would return to their original length after being loaded (*Ut tensio, sic vis*, or as the extension, so the force), reacting elastically to the addition and then subtraction of forces. Although it was well known since the Middle Ages that metal properties would change with heating, beating, and alloy content[5], the "why" was unclear until the development of the theory of dislocations in 1948. This theory provided a fundamental understanding of how metal grains had interior slip systems that reacted to external forces and stored energy.

The first photograph of an edge dislocation was taken by Sir James Menter and can be seen in Plate 14 of that reference[6]. These geometric crystalline slip systems, when overwhelmed by external forces, allowed the creation of cracks to dissipate energy. With knowledge of what was happening at the microscopic level, the macroscopic level manifestation of the properties could be correctly understood. With the same basic set of knowledge of properties (Young's modulus, shear modulus, and Poisson's ratio), a second rank tensorial representation could be made in mathematics[7]. A second rank tensor is one that takes one vector as input and gives one vector as output, such as the Cauchy stress tensor, such that the expected reaction of a material to stress and strain is modelled successfully. A constitutive equation is typically a phenomenological mathematical model used to describe the relationship between stress and deformation, and can be used to predict behaviors at various applied stress conditions. Equations were developed that could explain the metal's behavior, and, better yet, could be used with explicit criteria (Tresca or von Mises stress limits) to pinpoint when a transition from elastic to yielding would occur.

Such information can be related to design stress characteristics for metal structures and components, which ties the real world to the microscopic world in a useful way for engineers. Best of all, one can work backward from a crack origin to solve for the conditions of initiation of the fracture — and, from this, an understanding of causation — for a failure of a component. In practice, the engineering world does not use yielding directly — traditional designs use the 0.2% offset stress on the stress-strain diagram, and then apply factors of safety. When these techniques are properly applied, a layman need not worry about whether a metal structure can safely take the load. The elastic behavior assumption dominates classic calculations for structures.

Wood-based laminates with glass or carbon fiber reinforcement rose to prominence during the World Wars for airplanes. They continued to be constructed in volume with the rise of the wind-turbine industry. The blades of such electricity-generating stations are wing-shaped and travel rapidly around the hub of the nacelle, enduring cyclic loading. Design code requirements for fatigue testing to qualify for service are restrictive, as prescribed by design codes to simulate service loadings[8]. Models of the behavior encounter the same complications as others, with assumptions necessary to complete the description of the response of the laminates to external stimuli.

An important subset of materials was developed when the epoxies and thermosetting polymers were combined with the fiber glass mats to create formable, light, strong structures: fiber-reinforced polymers (FRPs). Entrepreneurs could take a mold, add gel coat, fiber mat, and chopped fiber, and, before curing with heat, create their own boat, canoe, or motorcycle fairing. Since their introduction in the 1930s, applications now range across household products, amusement parks, marine structures, reinforced concrete, armor, heavy industrial equipment, electrical generation and distribution, spacecraft, and others. Polymers that cure irreversibly are termed thermosets. The design and fabrication of thermosets can be tuned precisely to match service conditions of combined mechanical and chemical environments. Thermosets are used for a wide variety of applications to take advantage of some key properties:

- Superior resistance to corrosion compared to many construction materials
- Lower density than many construction materials

That brings us to today, where we have many applications, but the fundamental understanding has stalled since the original rapid advances. Each family of material type provides a different mix of information for the forensic engineer seeking to understand why a structure or component has failed in service, as shown in **Figure 1**.

This paper describes how standard engineering failure analysis methods must be adapted to yield conclusive results. It then describes how a shift from introducing unconventional knowledge can often reveal what happened in the failure and why.

Practical Designs Based on Experience

As applications were explored, engineers developed design methods based essentially on experimental design and the application of safety factors to provide allowable stresses. As usage of load and resistance factor design (LRFD) evolved, such as for building codes, resistance factors have been developed. These developments continue to provide design and fabrication methods that engineers with conventional education can apply. This has resulted in a growing population of standards and codes that can be used for design and construction.

In the case of FRP materials, the empirical observation that failure can occur at stresses less than the measured ultimate strength of the as-built FRP led to the practical application of safety factors to reduce the maximum applied stress to an allowable level. This mirrors allowable stress design as used for much mechanical design. Resistance factors used for LRFD are a form of safety factor.

	Metals	Rubber FRPs	Wood Laminate FRPs	Thermoset FRPs
Property characterization and measurement	Excellent	Good	Rudimentary	Rudimentary
System characteristics	Isotropic or anisotropic	Orthotropic	Orthotropic	Orthotropic
Developed constitutive equations or deformation models	Excellent reproducibility	Equations are limited to the new condition and do not incorporate changes to the materials from service damage.	Constitutive equations or models are not available for damaged materials.	Poor constitutive equations or models are not available for damaged materials.
Fracture theory maturity	Defined and characterized by dislocation theory	Moderate and covered extensively in published material	Poor. There is no coverage in published material.	Poor. There is no coverage in published material.
Energy absorption or dissipation behavior	Overload and fatigue	Temperature degradation	Delamination by fatigue	Non-linear viscoelastic creep that leads to brittle fracture
Established techniques for examination	Visual; microscopy; metallography; scanning electron microscopy	Visual	Visual; microscopy	At the time of this writing, there are no established standards for visual or microscopy. Ultrasonic and acoustic methods.
Certainty of analysis of causation	Excellent possible match to theory	Results are usually inconclusive because no standard is available.	Results are usually inconclusive because no standard is available.	Results are usually inconclusive because no standard is available.

Figure 1
Matrix of the family of materials.

Nomenclature

In this paper, the following variables are used:

A = Extensional stiffness matrix (3x3).
B = Coupling stiffness matrix (3x3).
D = Bending (flexural) stiffness matrix (3x3).
ε = Strain tensor (3x1).
E_0 = Young's modulus at start.
E_g = Young's modulus of elasticity for glass.
E_p = Young's modulus of elasticity for polymer.
$E\tau$ = Young's modulus at time τ.
Ex = Young's modulus of elasticity in x-direction.
Ey = Young's modulus of elasticity in y-direction.
K = Curvature tensor (3x1).
M = Moment resultant tensor (3x1).
N = Stress resultant tensor (3x1).
Φ_E = Coefficient for general loading condition.
Φ_i = Coefficient for loading condition i.
r = Exponent applied to exposure time for general loading condition.
r_i = Exponent applied to exposure time for condition i.
τ_i = Time of application of condition i.
t_g = thickness of glass.
t_p = thickness of polymer.
t_t = total thickness.
v_{ab} = Poisson's ratio in b-direction from strain in a-direction.
v_g = volume fraction of glass.
v_p = volume fraction of polymer.

Design Basis for Composite Structures

Engineers spend much of their formal education understanding the fundamental principles of the design of any structure. In many cases, structural, load-bearing materials are considered to have constant Young's modulus, Poisson's ratio, and to be linearly elastic so that Hooke's Law can be used to describe their stress-strain response to applied loading.

When these conditions are met, structural analysis of any material can follow systematic approaches from several references and textbooks that deal with linear elastic materials. Virtually all design and construction standards and codes expect and dictate linear elastic behavior. Occasionally, interest arises in analyzing structures composed of different materials joined together, each of which is distinct and identifiable. The engineering properties of these materials are an amalgam of the properties of their individual components. Known as composite materials, examples include tires, car windshields, and fiber-reinforced polymers.

When different materials are combined, such as in the layers of shatterproof glass, the behavior of each component material can be modeled, and engineering properties of the mixture can be calculated (or measured by testing). A model of the layers of glass and polymer in a shatterproof car windshield is shown **Figure 2** and calculations in Equations (1) to (3).

The calculations will be based on unit width and unit depth of the material mixture. Glass sheet and polymer sheet used for each layer is isotropic, with equal mechanical properties in all directions. Equation (1) determines the Young's elastic modulus in the x-z plane[9].

$$E_x = E_z = \frac{\sum t_g E_g + \sum t_p E_p}{t_t} \qquad (1)$$

This elastic modulus applies to plane stress in the x-z plane. If bending moments are applied to the plate, the elastic modulus needs to incorporate the distribution of the constituent materials. This will result in a different elastic modulus value, normally referred to as the flexural modulus. Equations (2) and (3) show the calculation of the flexural modulus for the laminated plate in **Figure 2**. Equation

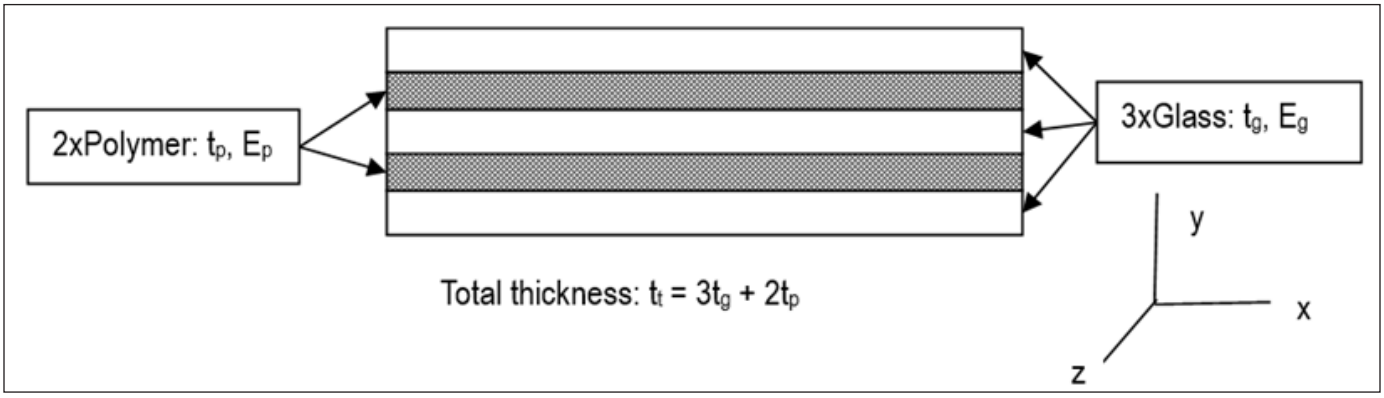

Figure 2
Model of laminated shatterproof glass.

(2)[9] determines the location of the neutral axis from the bottom surface of the laminate in **Figure 2**.

$$h_n = \frac{\left(\frac{9t_g}{2}+3t_p\right)E_g+(3t_g+2t_p)E_p}{t_t E_x} \quad (2)$$

And Equation (3) determines the elastic modulus for out-of-plane loading, which typically produces bending moments. This is commonly known as the flexural modulus.

$$E_f = \frac{\left(3t_g^3+2t_g\left(\frac{3}{2}t_g+t_p-h_n\right)^2\right)E_g+(2t_p^3+2t_g\left(\frac{t_g+t_p}{2}\right)^2)E_p}{t_t^3} \quad (3)$$

The differences between Equations (1) and (3) show clearly that the tensile properties can be substantially different from the bending properties of laminated composites, with bending properties highly dependent on the distribution through the thickness of the constituent materials.

In general, design of equipment using composite materials is dominated by in-plane tensile or compressive loads. When elastic instability or buckling occurs, empirical testing has shown that both tensile and flexural modulus contribute. Design for in-plane stress commonly uses allowable stress design where the tensile strength of a particular composite is determined by destructive testing, and a factor of safety is applied to provide the allowable stress for design. When designing to ensure elastic stability, the factor of safety is usually applied to the expected collapse load of the member, such as from compression or applied external pressure. Note that the factor of safety used for the two situations is not usually the same value.

Now consider the situation where the composite material shown in **Figure 2** is comprised of glass and polymer mixed more intimately together, such as small-diameter glass fibers surrounded by polymer that is bonded to the glass. In these cases, the properties of a layer become a function of the combined component properties. This forms the basis for micromechanics lamination theory, meaning a layer comprised of this mixture is treated as an orthotropic, homogeneous material with a unique elastic modulus in each direction and a single Poisson's ratio for each direction. The volume fraction of the component materials is used for this calculation. For the example shown in **Figure 2**, the volume fractions are given by Equations (4) and (5).

$$v_g = \frac{\sum t_g}{t_t} \quad (4)$$

$$v_p = \frac{\sum t_p}{t_t} \quad (5)$$

NASA played a key role in developing methodologies for modeling laminated composite material. This started with a lamination theory that determines the mechanical properties of layers and laminates[10] using the rule of mixtures. These models take advantage of approximately linear elastic material mixture response at a given state of reinforcement and polymer condition. The initial model does not include provision for changes to material properties as a result of damage. The models also include some important boundary conditions: no slippage at the interfaces of laminae; and no slippage at the coupling of reinforcement and polymer. It can also be general enough to incorporate bending and in-plane stresses. This modeling works well for allowable stress design of components and is used by codes such as RTP-1[11]. Equation (6) shows examples along the orthogonal material directions of the component in plane stress.

$$\begin{bmatrix} N \\ M \end{bmatrix} = \begin{bmatrix} A & B \\ B & D \end{bmatrix} \begin{bmatrix} \varepsilon \\ K \end{bmatrix} \quad (6)$$

where A_{ij}, B_{ij}, and D_{ij} incorporate elastic modulus and Poisson's ratio of the constituent materials and the fraction occupied by each. Note that the methods described to this point do not provide any values for the strength of the material — only stresses and stiffness result.

These models look very similar to the generalized equations that may be used for any linear, elastic material, such as metal alloys. They have been in regular use for polymeric composite design since the 1970s.

Experience with applications of components made using composites found that lifetime reliability of components was increased by applying simple factors of safety[11,12]. For Allowable Stress Design methods, the factor of safety is applied to the measured strength of the composite to determine allowable stress for design. For membrane stresses, it is common for this factor of safety to be 10. When the design must include elastic instability, stress is no longer a key element; therefore, the factor of safety is applied to increase the collapse load (often the buckling point). The factor of safety commonly used for elastic instability is 5. For load and resistance factor design (LRFD), a typical resistance factor applied to the 5th percentile tensile strength is 0.55, and elastic instability conditions are generally avoided.

Some design methods use allowable strain as the basis of the design. This approach places a limit on maximum strain values that may be used for design. In this method, a factor of safety — sometimes the same as that used for

allowable stress design — is applied to the minimum elongation at failure of the constituent materials. Some codes, such as RTP-1, use arbitrary values that amount to about 5% of the minimum constituent elongation at failure.

More advanced calculations may be used to model the behavior of individual layers with their own unique anisotropic properties. Typically, each layer is modeled as a 2D material with five independent uniaxial strengths. These are aligned and orthogonal to the principal direction of reinforcement — tensile and compressive in each principal direction and shear with respect to pure shear in the principal directions. This is described by Daniel et. al[14]. The basic principle is to determine the actual material strains that will cause failure of either the polymer or the reinforcement. Versions of this process include the "Tsai-Wu Interaction Criterion"[9] or "Quadratic Interaction Criterion"[11]. It is particularly important to note that these processes do not include or recognize yielding, nor do they include provision for changes to failure strain of composite constituents as a result of damage.

Damage Accumulation in Practical Terms

As FRP composites were included as an option for sophisticated uses like aircraft and space vehicles, the need arose for both explicit engineering analysis and for definitions of failure incorporating an understanding of damage accumulation. This analysis provided the foundation for calculating the time until failure. This was especially important to allow planning for replacement or obsolescence, particularly for complex or inaccessible structures.

It is normal for designers and engineers to use some method to predict future properties and the expected lifetime of structures. For metal alloys, this often includes consideration of corrosion rates and the effect of service conditions on the structure. For reinforced polymers, the mechanical properties, such as elastic modulus and strength of the individual structural constituents, usually change because of most service conditions: stress, applied strain, chemical attack, corrosion, etc. These changes accompany irreversible damage accumulation within the structure. For components that will be inaccessible or where tolerance of failures is low, it is desirable to have a model that will predict damage development, as addressed by Dillard, et al[13].

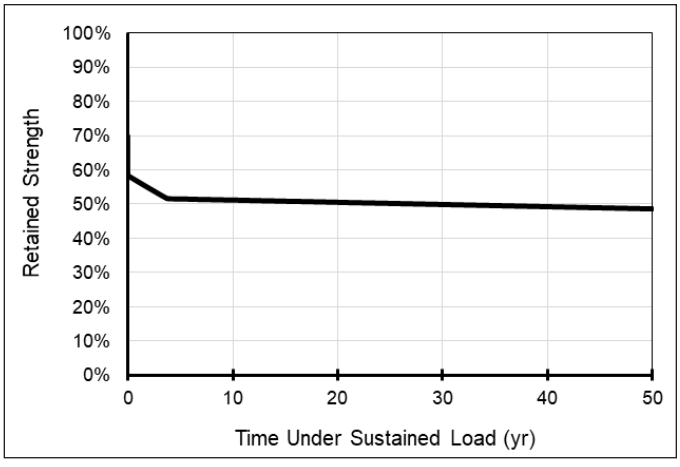

Figure 3
Change in strength of glass reinforcement. (Source: Owens Corning)

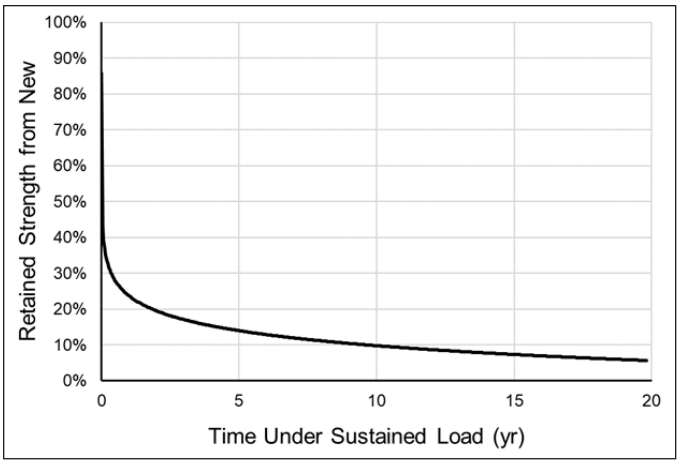

Figure 4
Change in strength of thermosetting polymer
(Source: Ashland literature)

Figures 3 and **4** show typical strength vs. time in service for glass reinforcement and thermosetting polymer subjected to mechanical stress only. The reader can see from both curves that the change in strength is non-linear and shows continuous reduction from its maximum of 100% for load application time of about 1 microsecond. These are non-linear viscoelastic materials.

The curve shows a logarithmic path where the full, original strength of 100% occurs for about 1 microsecond of sustained load at full strength. When the sustained loads are reduced, the glass fibers will support the load for longer times. In general, this change in strength for the glass is based primarily on a reduction in the strain at failure of the glass, while the elastic Young's modulus remains somewhat constant. The curve shown is for glass in air. When exposed to other substances via cracks that form in the polymer, or diffusion, the retained strength of the glass after five years can range from 84% of the air values for tap water to less than 12% of the air values for weak acid. One could consider the "air" values to represent the expected behavior of glass reinforcement that is embedded

in an undamaged polymer or elastomer.

Findley et. al[14] provides a model to describe changes that occur in properties, such as elastic modulus, as a function of time, generally of the form given in Equation (7).

$$E_\tau = E_0 + \Phi_E \tau^r \quad (7)$$

Where:

E_τ = Property at time, τ.
E_0 = Property at starting time.
Φ_E = Coefficient corresponding to applied conditions.
r = Exponent corresponding to the applied conditions.

It should be expected that, if the conditions applied are not static — and thus have some variation with time — the more general form of the model will incorporate the product of changes from each applied condition, similar to Equation (8).

$$E_\tau = E_0 + \prod \Phi_i \tau_i^{r_i} \quad (8)$$

Findley et. al. discuss that determining the coefficients Φ_E and r for a non-linear viscoelastic material requires experimentation, probably consisting of at least 30 trials for each combination of condition and material. There are currently no standardized methods for these tests, nor any published record of this experimentation or any of the relevant coefficients. Dillard et. al. chose to adopt the Findley approach for characterization of damage, but the limited availability of coefficients and the amount of variation encountered in test specimens still limit this to an academic exercise, with virtually no published data to allow informed use of damage accumulation models.

Other models are discussed by Greaves[8] for damage accumulations, including the Palmgren-Miner rule, which is linear, and other non-linear models. All of these require specific destructive test data on the FRP being considered to develop the damage model. Furthermore, most models are focused on the strength of layers as a mixture. All models described here to date essentially incorporate time (or its Laplace inverse of frequency) as a key part of the equations.

Polymer manufacturers use changes in flexural modulus[15] of FRP coupons that are exposed to operating environments as the primary means to assess the suitability of a polymer for use in that environment. Generally, a chemical attack is more aggressive than simple stress exposure in damaging polymers. Consider Equation (3), when the physical dimensions are unchanged and the Young's modulus of the glass (E_g) remains constant, a change in flexural modulus is directly related to change in the Young's modulus of the polymer. This same effect is also documented for cases of purely mechanical loading in Appendix D[12] and by Clarkson[16].

Clarkson[17] also decoupled the changes in polymer elastic modulus with reductions in strain at failure from time. This shows that the accumulated damage in FRP from service exposure can be determined using the retained elastic modulus of the FRP, irrespective of exposure time. Non-destructive methods to determine the retained flexural modulus, and thus, the total damage accumulation, are described by Clarkson[16].

Figure 5 shows the retained elongation at failure and retained polymer strength for the source data[18]. The reduced tensile strength from damage also requires less energy input for fracture. It is important to note at this stage that the reduced Young's modulus of the polymer also corresponds to a reduction in shear modulus and shear strength. The reductions will have a direct impact on the interfacial bonding of reinforcement to the polymer and thereby alter the distribution of loads through the polymer and protection of reinforcement from any chemical species.

For most materials, when fractures form, it is common to look at the crack formation and track the crack tip through the material as it "pries" deeper. Nuismer summarizes this, at least within an individual layer[19].

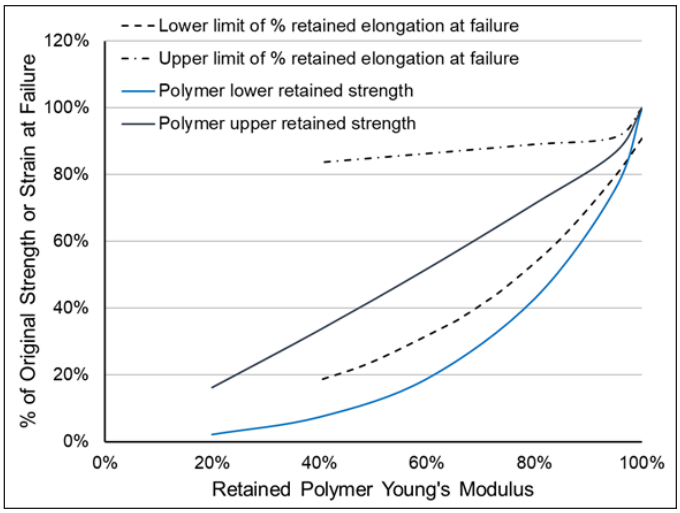

Figure 5
Polymer damage decoupled from time.

The initial energy release rate for a branch crack propagating at an arbitrary angle from an existing crack tip is obtained in a simple fashion and in closed form by using a continuity assumption. It is then postulated that the branch crack propagates in the direction which causes the energy release rate to be a maximum and that initiation occurs when the release rate reaches a critical value. It is shown that these postulates yield results identical to the maximum stress theory, since the direction in which the maximum circumferential stress occurs is also the direction causing the maximum energy release rate.

When the stress to cause cracks is low, as implied in **Figure 5**, cracking can progress easily. In the case of most FRP structures, when a crack tip that formed in damaged polymer encounters polymer that is less damaged, it is arrested and diverted until damage accumulates in the "blocking" polymer. This is illustrated in **Figure 6**, where cracking is shown to change directions within the FRP. The photo is taken from a cutout from equipment that had been in service for several years. For the situation shown in **Figure 6**, the FRP is under hoop stress only, with some chemical exposure on the blackened material on the cracked side. The cracks in the damaged polymer can accelerate damage to the undamaged polymer and reinforcement by providing easy pathways for exposure to chemicals from the service environment.

In fact, the strain at failure of polymers has been shown by Clarkson[18] to correlate to the retained Young's modulus of the polymer. To date, no data are published that addresses the changes that occur to Poisson's ratio with damage, but there is clear evidence that this occurs, also supported by some studies since polymers can degrade to a powder with Poisson's ratio of 0.

Figure 6
Crack progression in composite laminate.

Composites using thermoplastic polymers that include a very low population of cross-links connecting the long-chain molecules might yield and will often undergo measurable creep changes as damage accumulates. When the polymer is cross-linked, such as in thermosets and most rubbers, when applied strain exceeds the failure strain of the material in its current condition, brittle fracture occurs.

Failure Analysis Approach for FRPs

The spectrum of FRP failures can range from visible blemishes to the collapse of a component. In general, we should expect that a failure corresponds to a condition where the component can no longer function. In some cases, failure analysis is intended to determine if it is possible to continue in service for some time. In others, a carcass must be analyzed to determine the cause. Investigation and analysis of failures have been found to work well universally when following a basic, systematic approach that requires detailed information. Many FRP components, such as holding tanks and wind turbine blades, are large compared to humans. When they fail, there is a considerable set of tasks to complete to understand what has happened.

Figure 7 provides a sequential list of the important elements for a large-scale reconstruction of a service failure. Besides the elements that are familiar to most forensic engineers, there are notes for items also recommended for consideration when the material of construction is FRP and other reinforced polymers. These additional items may also be applied to other visco-elastic materials.

The principal task is to locate the most probable origin. Defects involved in a failure are likely to be obliterated by the failure. The best approach to determine if a defect was implicated is to evaluate all of the data available to see if the presence of a defect is required to explain the failure initiation.

The considerations listed in **Figure 7** serve to address this.

The answers to these questions provide data that can be evaluated to reveal the cause of the failure. Many times, another question that arises is whether the new component complied with the design specification or criteria. The discussion above shows that damage accumulation is inevitable for any FRP component that is exposed to service conditions, so failure may be independent of the original design and manufacture.

Figures 8 and **9** provide an example of a large-scale component examination, which attempted to locate the origin of the wind-turbine blade fracture. There had been an allegation that a blemish was seen on the pressure side of the blade near its root a few months prior to an unexpected disassembly event that brought down the steel tower.

Element	Element of Reconstruction	Specific Considerations for FRP
1	Collect components from the site, and conduct a total station survey or LIDAR scan of the area to preserve spatial information, taking into consideration ASTM E1188 *Standard Practice for Collection and Preservation of Information and Physical Items* by a technical investigator.	
2	Index, catalog, and identify component remnants.	
3	Review original structural drawings and/or obtain an exemplar component.	Drawings are often not complete. Materials of construction may not be documented to provide exemplar component. Determine retained flexural modulus as close to the fractures as possible. Remove specimens of relatively intact materials and deconstruct to allow modeling of the as-built structure.
4	Categorize each piece to determine its original spatial orientation and its fracture mode.	FRP fractures are normally brittle. Spatial orientation of pieces is critically important combined with an effective stress distribution model combined with Young's modulus of damaged composites to identify strains. Recalculate the Young's modulus to incorporate retained flexural modulus distribution.
5	Use fracture mechanics principles to work backward to the origin of the sequence.	Determine the likely elastic strain distribution in the structure and determine the most probable origin.
6	Consider the potential primary mechanism of failure.	
7	Eliminate secondary and tertiary fractures from consideration.	
8	Concentrate on the primary mechanism and the area of origin, to confirm the fracture mode.	Determine if the data available on accumulated material damage supports the conditions at the origin to result in failure or if a defect or increase in assumed loads must be incorporated to meet the conditions for failure.
9	Use a model to better understand the pre-fracture force patterns.	
10	Validate the hypothesis of causation by comparing the evidence and the model, with a designed experiment on similar structures.	Ability to do this may depend on ability to duplicate the structure.

Figure 7
Large scale service failure reconstruction elements.

Figure 8
Parts of a wind-turbine blade set down for inspection and cataloging.

Figure 9
Wind-turbine blade fracture surface.

As described above, compliance with the design specification or criteria can be approximated by determining the details of the FRP construction from the carcass. However, its current properties, as determined by standardized tests, are unlikely to accurately reflect the new properties. Sometimes, additional testing is required from intact materials to determine things like porosity.

From Element 3 of **Figure 7**, the retained flexural modulus of the carcass material can often be determined using non-destructive acoustic and ultrasonic methods[18]. To ensure that the actual construction of the FRP is used in the analysis, specimens of the material from the failed component should be deconstructed, and lamination analysis methods, as described in Equations (1), (2), (3), and (4) and as described in [9] or [10], can be used with the Tsai-Wu or Quadratic Interaction methods to determine the approximate new strength.

Even when details of the original design are unavailable, it is still possible to compare the as-built information with the conditions that existed at failure. This requires additional testing of the failed FRP to determine the actual sequence of reinforcements with the volume fractions of all constituents. This information is then generally used with the "as-new" properties of the constituent materials to construct the stiffness, coupling, and bending matrices for use in the original tensor equation using the applied conditions at the time of failure, thus allowing some assessment of the "original" composite material.

As described previously for damage accumulation, there is little information about properties of "as damaged" materials used here, and properties of new materials are readily available. In addition, damage to the reinforcement from the operating environment also depends heavily on changes in its protection from the polymer as it is damaged.

This approach may help identify whether failures are driven by components that do not comply with relevant construction standards or specifications, but it seldom shows that failures could occur for anything beyond extreme loads that exceed the design safety factors of 5 to 10 applied to new material values. In almost every case where this is requested, the component was often found to still comply with all tests that measure against the original design and thus offers no conclusion on the cause of the failure.

Incorporating the Accumulated Damage Concept

The discussion to this point describes how damage accumulation occurs and how it should be incorporated into failure analysis.

Attenuation-based ultrasonics described by Clarkson[17] has been shown to distinguish between damage accumulation adjacent to fractures from areas that have not fractured. Detailed data from a large structure would allow a sufficiently detailed material model to explain a failure.

Some additional testing may provide supporting qualitative data. This additional testing includes: microscopic examination of the fractured zone using a microscope, where with enough magnification, evidence of reinforcement damage such as notches in the fibers from leaching may be observed; energy dispersive X-ray (EDX) to detect elements or chemicals that may be part of the chemical environment that existed in the composite; and visible features that may support hypotheses. This information may be used to supplement the accurate model of the composite.

Summary of Insights

Although not all the techniques available in the metal world are readily available for the analysis of FRP failures, the general approach to a failure investigation still applies with some additional considerations to be included. Gathering information about the context is important and will set the stage for a coherent analysis of causation. The complexity of FRP failures (especially large-scale ones) means that the origin of a fracture may not be explicitly identified. However, techniques that evaluate the damage accumulation and level of change of the properties of the FRP may provide insight into how and when the structure loses its integrity. Forensic engineers are advised to approach each case by considering these factors, so that the investigation will successfully identify the cause of failure. Employment of non-destructive methods may keep the structure owner ahead of the situation and mitigate costly incidents in industrial equipment.

References

1. E. M. Morton, Introduction to Rubber Technology, Toronto: Van Nostrand Reinhold Company, 1959.

2. T. J. Dudek, "Mechanical Properties of Cord/Rubber Composites" in *1981 International Rubber Conference*, Harrogate, EN, 1981.

3. R. Jones, Mechanics of Composite Materials, New York: McGraw Hill, 1975.

4. R. Kennedy, "A Look Back at the First Two Decades of Tire Finite Element Analysis — Laying the Foundation," Tire Science and Technology 10.2346/TST-24-001, 2024.

5. G. Agricola, De Re Metallica (translated by Herbert Hoover et al), Vienna: Dover Publications, 1556.

6. J. Gordon, The New Science of Strong Materials or Why You Don't Fall Through the Floor, New York: Pelican, 1976.

7. C. N. Reid, Deformation Geometry for Materials Scientists, Permagon Press, 1973.

8. P. Greaves, "Fatigue Analysis and Testing of Wind Turbine Blades," Durham, 2013.

9. L. M. Daniel and O. Ishai, Engineering Mechanics of Composite Materials, New York: Oxford University, Press, 1994.

10. A. Nettles, Basic Mechanics of Laminated Composite Plates, Marshall Space Flight Center: NASA, 1994.

11. ASME, ASME RTP-1 Reinforced Thermoset Plastic Corrosion-Resistant Equipment, New York: ASME.

12. ISO, EN 13121 GRP Tanks and Vessels for use above ground, BSI.

13. D. Dillard, D. Morris and H. Brinson, "Creep and Creep Rupture of Laminated Graphite/Epoxy Composites," Virginia Polytechnic Institute, Hicksburg, VA, 1981.

14. W. N. Findley, J. S. Lai and K. Onaran, Creep and Relaxation of Nonlinear Viscoelastic Materials, New York: Dover Publications, 1976.

15. ASTM, "ASTM C-581, Standard Practice for Determining Chemical Resistance of Thermosetting Resins Used in Fiber-Reinforced Structures Intended for Liquid Service," ASTM, West Conshocken.

16. G. E. Clarkson, "Baseline Values for Non-Destructive Structural Evaluation of Glass Reinforced Composites," Orlando, 2014.

17. G. Clarkson, "Toward Objective Evaluation of FRP Corrosion Barrier Condition," in AMPP Corrosion 2022, San Antonio, 2022.

18. G. Clarkson, Assessment of Existing Fiber Reinforced Polymer Equipment for Structural Damage, 2nd Ed., New York: Welding Research Council, 2023.

19. R. Nuismer, "An Energy Release Rate Criterion for Mixed Mode Fracture," International Journal of Fracture, vol. 11, no. 2, pp. 245-50, 1975.

20. B. W. R. Edward and A. Humphreys, "Properties Analysis of Laminates," in Composites Handbook, Metals Park, OH, ASM, 1987, pp. 218-224.

Analysis of a UTV Axle Fracture Associated with Rollover

By Stephen A. Batzer, PhD, PE (NAFE #677F)

Abstract

An analysis of the fracture mechanism of a rear axle shaft of an off-road side-by-side utility vehicle (UTV) is presented in this paper. Two minors were recreating; they were riding a UTV within the fenced confines of the family farm. While driving on a dirt trail at a substantial velocity, the UTV yawed hard to the left, just before the turn in the trail. The leading side passenger's side tires dug into the soft soil, and the UTV overturned for three-quarters of a revolution. The belted driver was partially ejected during the overturn and fatally pinned underneath the vehicle's tubular rollover protective structure. After the event, the vehicle could not be driven as the left rear axle was fractured nearest the inner race of the outboard constant velocity (CV) joint, and the wheel hub and disc brake system were damaged. The investigation answered the question: "Did the overturn cause the axle fracture, or did the axle fracture cause a braking action and initiate the overturn?"

Keywords

Utility vehicle, UTV, rollover, fatigue, axle, CV joint, forensic engineering

Accident Details and the Tentative Overturn Mechanism

The incident vehicle, a single-row utility vehicle (UTV) in lightly used condition, was four years old at the time of the incident with a recorded engine time of approximately 350 hours and an odometer reading of approximately 2,000 miles (3,500 km). The vehicle was being driven by two minors, which was against the recommendations of the manufacturer as printed in the owner's manual and displayed with on-vehicle stickers, but in accordance with state law, given the fact that the vehicle was on private property.

The cattle ranch trail on which the UTV was being driven was familiar to the occupants — flat, dry, and well-traveled. The investigating officers measured and documented the final vehicle position and photographed the tire marks that ended at 4-wheel lift and vehicle overturn. A short debris field further indicated the overturning path. The reconstruction of the overturn provided an overturn velocity estimate of approximately 20 mph (~30 kph) at initiation, with the UTV rolling right-side leading for something more than ¾ of a revolution due to final rocking motion. The vehicle travelled between 25 to 30 ft (~8 to 10 m) after 4-wheel lift. The driver was asphyxiated following the overturn due to partial ejection and entrapment underneath the rollover protection system (ROPS). The UTV was not equipped with an electronic event recorder to measure and save data, such as engine rpm, throttle %, steering angle input, or brake application.

The UTV's owner attempted to move the vehicle into storage after the overturn but was unable to do so due to what he believed was drivetrain damage. A joint site and vehicle inspection was then conducted by engineering experts representing the driver's family and the manufacturer. This examination occurred less than two months after the fatal overturn. It was determined that the left rear axle at the constant velocity (CV) joint was broken, which caused a braking action at the left rear wheel position. **Figure 1** shows the right axle with a normal CV boot at the outboard position; a green arrow highlights the axle main shaft. In the **Figure 1** detail at left, a white arrow highlights the undamaged outer CV joint boot, while a blue arrow highlights the bearing carrier, which mounts the axle bearing and disk brake assembly.

Figure 2 shows the damaged left axle with a distorted CV boot at the outboard position. The twisted outboard CV boot, indicative of an axle fracture and the axle shaft rotating independently of the CV joint, is highlighted with a white arrow.

Stephen A. Batzer, PhD, PE, 8383 M-113 E, Fife Lake MI, (479) 466-7435, batzer@batzerengineering.com

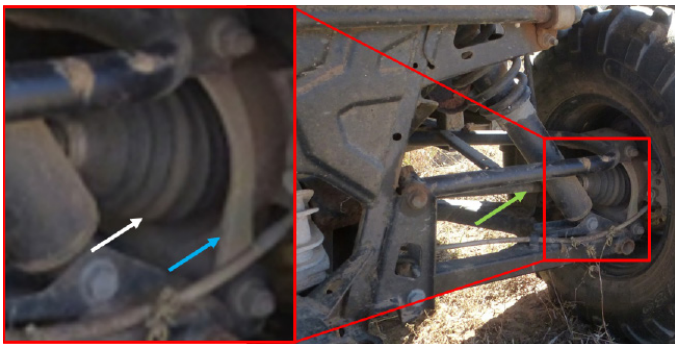

Figure 1
Right rear wheel assembly showing drive axle with normal CV boot indicative of axle shaft and joint rotating in tandem. Green arrow = axle main shaft; white arrow = right axle; and blue arrow = bearing carrier.

Figure 2
Left rear wheel assembly showing twisted CV boot indicative of axle shaft and joint turning independently. White arrow = twisted CV joint boot.

Figure 3 shows an overhead view of the left rear drive assembly, with the wheel and tire removed. From outboard to inboard is the grease cap (white arrow), which covers the cotter pin, castellated nut, washer, and threaded outboard end of the driving axle assembly. Next is the aluminum hub (black arrow), which has been painted black and contains four threaded studs to mount the wheel and the brake disc at the inboard side, which is secured by four low-profile hex head screws. The wheel hub is mounted against the bearing carrier (yellow arrow), a cast aluminum part that mounts the wheel bearing internally and the brake pad and shoe assembly externally (blue arrow). The

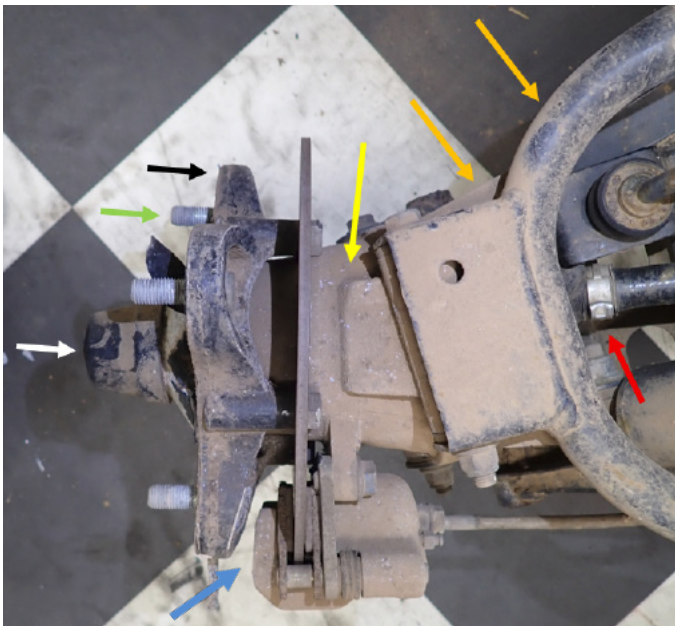

Figure 3
Left rear drive assembly, overhead view, tire and wheel dismounted. White arrow = grease cap; green arrow = lug stud; black arrow = hub; yellow arrow = bearing carrier; blue arrow = brake shoe assembly; orange arrows = A-arms; and red arrow = half shaft showing black axle, CV joint polymer boot, and mounting clip.

bearing carrier, along with all associated parts, moves up and down relative to the vehicle by the pivoting A-arms, which are mounted to the top and bottom (orange arrows). At the right of **Figure 3** is the drive axle, which mounts the outer CV joint rubber boot with a steel circumferential clip (red arrow).

The two rear independent drive axles were of conventional construction. Each axle assembly, also known as a half shaft, consisted of (from outboard at the wheel to inboard at the transaxle) a driving spline for torque transmission that mated to the wheel hub, a CV joint that allowed angular compliance of the axle shaft to the wheel, the main axle shaft, the dual offset joint (DOJ) that allowed both angular and axial position compliance of the axle shaft to the transaxle, and, finally, a driven spline mating to the transaxle (**Figure 4**). Both the DOJ and CV were protected

Figure 4
Exemplar half-shaft assembly for the incident UTV oriented with the outboard driving splined end at left and inboard driven splined end at right.

by flexible rubber boots, which rotated along with the axle, retained lubricating grease, and kept the bearings clean.

In addition to the CV boot, other relevant external damage at the left rear wheel position of the incident vehicle included a circumferentially fractured cast aluminum wheel hub, as shown in **Figures 5** and **6**. In **Figure 6**, note the chipped edges of the central fragment as indicated by red arrows. This chipping was consistent with damage after the circumferential crack separated the central and outer hub segments, during relative movement between the fractured segments.

Figure 5
Left rear wheel and tire showing paint spalling at the cast aluminum center hub.

Figure 6
Close-up of left rear wheel assembly showing the black painted steel wheel (blue arrow) that is secured by four threaded lugs and nuts (orange arrow), aluminum wheel hub (green arrow), spalling black factory paint to include a detached large flake at left (yellow arrows), and the circumferential hub crack with edge chipping (red arrows).

During forward travel of a UTV, a left rear axle failure would apply some level of differential braking to the vehicle, inducing counter-clockwise vehicle yaw. If this yaw commenced without warning and with sufficient severity, the vehicle would be misoriented compared to the travel direction and could overturn at normal travel speed due to side loading of the tires. As the UTV was rapidly approaching a left turn at the time of initiation of yaw marks by the tires (~25 mph = 40 kph), an overly aggressive steering input could also have presumably caused the overturn. It was the manufacturer's position throughout the investigation that driver input caused the overturn — and that a severe wheel strike during the overturn caused the left rear wheel and axle fractures.

Forensic Analysis

The UTV was transported to a local laboratory for disassembly and initial inspection as the basis of a formal forensic investigation[1]. The first action was removal of the outer plastic wheel cap to expose the castle nut and the cotter pin. The removal was done for both the right and left rear wheels to facilitate comparison. As shown in **Figure 7**, there is a patina of corrosion on the unpainted left threaded axle stub that is not present on the right stub. This is consistent with more moisture intrusion through the left grease cap when compared with the right but is otherwise inconsequential. The right rear cotter pin was unremarkable, but the left rear cotter pin was damaged inside the cap. The damage was evident after the ends were folded back from the position they were in after insertion and folding over the axle terminus. After photo documentation, the left rear cotter pin had to be further bent and hammered to remove it.

Notice how the right rear cotter pin through-hole in the threaded axle stub aligns with the castellated nut slot, while the left rear transverse axle stub cotter pin hole does not align properly with the cotter pin recess. The left rear

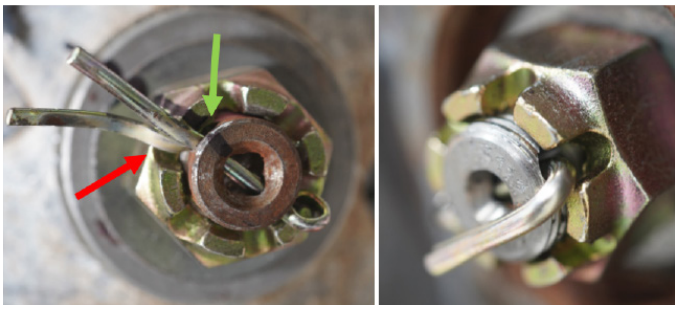

Figure 7
Left rear axle cotter pin showing post-installation misalignment of the axle cross hole and castellated nut slot (left). Right rear axle cotter pin showing undisturbed factory-installed alignment (right).

cotter pin segment in the foreground aligns with the axle transverse hole (green arrow), while the cotter pin segment in the background aligns with the castellated nut slot (red arrow); the head of the left cotter pin is also deformed. This is consistent with the threaded driving axle stub turning ~10° clockwise relative to the castellated nut after the cotter pin had been installed. Like the chipped wheel fracture surface shown in **Figure 6**, this is an indication that the axle and wheel damage occurred while the vehicle was in motion.

The circumferential crack of the left rear aluminum wheel hub disabled the rigid drive axle assembly at the wheel such that the wheel had some limited freedom of movement independent of the axle. Thus, the tire and wheel had to be ratchet-strapped to a fixed rigid frame to remove the wheel's lug nuts without causing further wheel hub damage. The CV joint boot was removed, and, as expected, the end of the main shaft that originally was attached to the CV joint inner race was fractured. There was also superficial post-fracture damage to the aluminum wheel fracture surface in the form of burnishing. After removal of the cotter pin, castellated nut, brake assembly, and wheel, several components were reassembled for visual clarity (**Figure 8**).

The burnished regions on both sides of the mating conical cast aluminum wheel hub fracture surfaces are from high points rubbing against each other (see **Figures 8** and **9**, red arrows). Also shown with a yellow arrow in **Figure 9** is the polished precision cylindrical interface surface for the wheel bearing; the blue arrow shows the splined internal recess for interaction with the driving end of the axle assembly, which is the outer race "bell housing" of the CV joint.

The physical evidence of burnishing is consistent with the fracture occurring during travel of the vehicle. There was also major abrasion damage to the disc brake assembly, consistent with the left rear wheel hub wobbling as it rotated. The largely axially symmetric conical wheel hub fracture surface is consistent with a centered inboard to outboard axial force being applied to the wheel hub, rather than a bending moment being applied by a local rim strike. Other than shape and post-fracture damage observations, no detailed fractography was performed on the cast aluminum wheel hub, since there was no macro evidence of a fatigue break at the aluminum hub. The wheel bearing at the center of **Figure 8** between the CV joint outer race at right and the fractured wheel hub at left spun freely. Consequently, it was not further examined.

Figure 8
Left rear-threaded axle stub, aluminum wheel hub fragment, bearing, CV joint outer bell. Red arrows indicate representative burnished surfaces; blue arrow shows the installation point of the fractured main axle shaft.

The left rear CV joint, detached from the wheel assembly and with the damaged flexible rubber boot removed, is shown from the inboard side in **Figure 10** (left). Although covered with grease, many details are apparent. From exterior to interior is the bell housing (outer race), the cage, the inner race with six cavities for hardened steel ball bearings with the balls removed, the retaining circlip near the bottom, and the fractured stub of the left rear drive axle in the center. **Figure 10** (right) shows the degreased inner race from the outboard side and the axle stub in the splined inner recess, which is not properly positioned fully outboard.

The splined male end of the axle main shaft contains

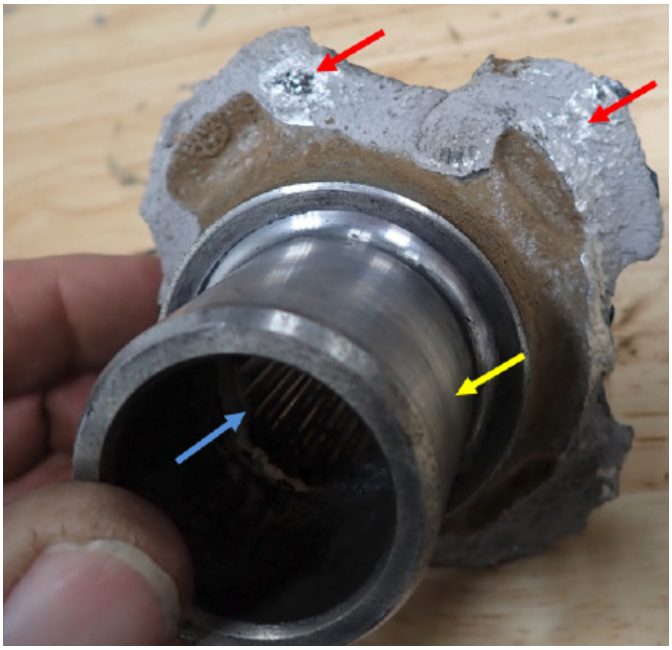

Figure 9
Central detached fragment of aluminum wheel hub, shown from inboard side.

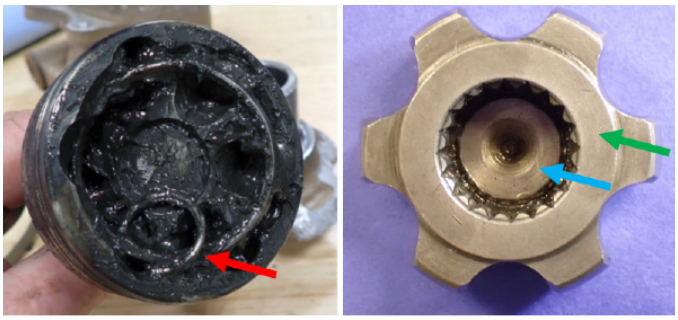

Figure 10
Left: Inboard view of CV joint bell housing showing fractured end of the main axle shaft and retaining circlip (red arrow). Right: Outboard view of degreased inner race; the stub end of the main axle is inappropriately inboard as the outboard face of the axle shaft (blue arrow) should be above flush of the outboard face of the inner race (green arrow).

a groove that accepts a retaining circlip. During assembly, the shaft end with circlip is pressed into the mating female splines of the inner race. This lightly compresses the circlip flush within the recess during installation. At full shaft insertion, the circlip then expands to provide axial fixation for the shaft to prevent the axle main shaft from displacing back inboard. However, that fixation either never occurred as the shaft was not inserted sufficiently or was otherwise unsuccessful, as **Figure 10** shows in the right photo. The circlip was marked with circumferential witness marks consistent with hard loading against the spline surfaces, suggesting that it was loaded coming back out of the subject inner race.

Figure 11 shows that the fatigue break occurred at the end of the main axle shaft at the outboard side of the circlip groove nearest the inner race. The fracture surface developed at the region of greatest axle bending moment and minimum cross section. The entire axial width of the circlip groove was present on the longer inboard axle shaft fragment (**Figure 11**, right). As a rotating cylindrical member, the fatigue crack progressed semi-uniformly planar to the shaft axis from outside to inside. This also ensured rotary compressive loading of the circlip as the axle shaft and the end past the groove became misaligned; a light in color witness mark of this compression is visible in **Figure 11** (left) — see green arrows.

The arc-like impressions on the main face of the outboard main shaft fragment are consistent with the interfacing rim of the detached inboard axle shaft pressing against the outboard stub during rotation, producing the fracture of the aluminum wheel hub with an inboard to outboard force. The light-colored groove end perimeter in **Figure 11** (right, red arrows) is no longer sharp but presents an

Figure 11
Left: Inboard end of CV inner race and fractured axle end showing a circlip compression mark and multiple arc-shaped impressions from the detached axle main shaft. Right: Outboard side of fractured axle shaft showing classic topographic macro features of fatigue fracture.

irregular beveled interface of the groove wall at the fracture surface. This was caused by cold work compression of this inboard edge against the outboard axle stub center segment during vehicle travel. The fracture surface on the inboard axle shaft fragment is better preserved for macro features of fatigue (**Figure 11**, right). Notable features include[3-5]:

A. The overall planar fracture surface that is perpendicular to the shaft axis.

B. The ratchet marks that initiated the planar crack perpendicular to the shaft axis once the axle shaft had backed off sufficiently for the circlip groove to be exposed past the splined region;

C. Radial spaced arc-like markings of crack progression from exterior to interior; and

D. An identifiable point of final fracture near the shaft centerline. These macro features were plainly visible with low power optical microscopy and did not require scanning electron microscope (SEM) examination.

Witness marks about the circlip were consistent with the axle main shaft having been inserted some distance into the inner race, but these marks could not confirm that the main shaft had been fully inserted with circlip expansion at the factory during half shaft assembly. On the main splined surface of the axle were circumferential compression marks documenting bending loading on the axle as the end moved incrementally inboard relative to the CV joint inner race (**Figure 12**). These marks strongly indicate that the shaft was, at least, nearly fully inserted — though perhaps not fully inserted — which would be one potential failure mode mechanism of the shaft backing out. The axle

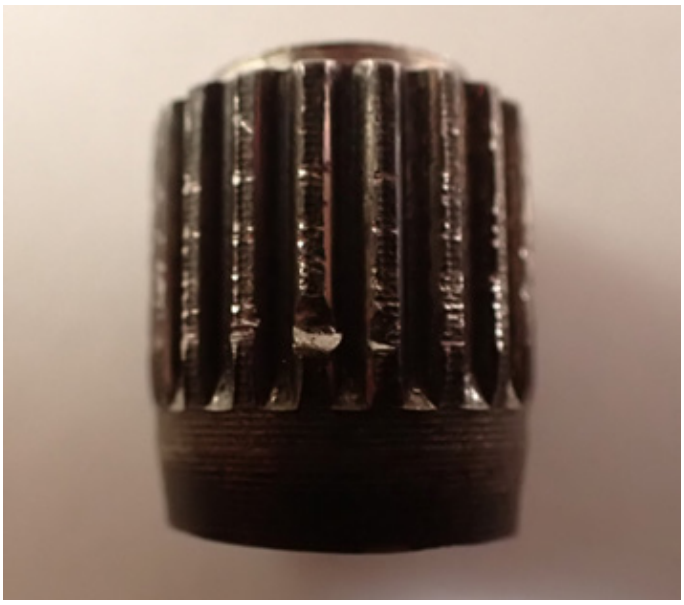

Figure 12
Sawn-off end of main axle stub, which fractured at circlip groove (top), showing circumferential compression marks developed while it backed out of the mating splines of the inner race.

fragment shown in **Figure 12** is the profile view of the segment shown in **Figure 11** at right.

Wheel Hub Demonstrative Testing

In any engineering investigation, it is critical to guard against confirmation bias — the processing of new information solely using an established paradigm[6]. The competing paradigms in this instance are either that the operator error caused the overturn and drive train damage or that the drive train damage self-manifested and initiated the loss of control, overturn, and resulting fatality. In this instance, the lead investigator (author) had personally inspected and analyzed hundreds of overturned vehicles that collectively have not presented an instance, much less a pattern, of a "severe wheel strike" in a barrel rollover causing an axle shaft failure in single overload or, more importantly, in fatigue loading, which is itself conceptually implausible as shaft fatigue failures require thousands to millions of shaft revolutions to manifest fracture.

Although the physical evidence strongly indicated that the fatigue failure preceded the overturn — and that the detached fractured axle shaft pressed against the displaced mating stub CV inner race and caused the wheel hub fracture in an outboard direction — demonstrative destructive testing was performed to investigate how a cast aluminum wheel hub fracture would present geometrically in both posited loading directions. Two aluminum rear wheel hubs of the type that were used on the incident UTV design were purchased from an on-line salvage retailer and axially loaded using a manual arbor press to develop a concentrated active load on one side and a diffuse reactive load on the other, thus producing outside-in and inside-out loading fracture (**Figure 13**). Note the wheel studs and brake disc attached to the black aluminum wheel hub.

The general shape of the fracture surface from the inboard-to-outboard loading produced an angular wheel hub fracture surface, reasonably matching the incident wheel hub (**Figure 14**). While the incident hub was rotating at least 5 revolutions per second at the initiation of yaw and of loss of control, the fracture is a form of "Hertzian cone" in which the principal tensile stresses within the brittle material subjected to focal compressive loading ensures an angular, conical crack progression[7]. As an analogy to the instant fracture, a lead pellet that is discharged from an air rifle into common annealed window glass will produce an entry hole the same diameter as the pellet, a conical fracture downstream of impact through the glass thickness, and, finally, a larger damage diameter hole at the exit plane.

Figure 13
Exemplar wheel hub and arbor press used to apply a concentrated inboard force against the wheel hub.

Figure 14
Incident wheel hub (left); Tested wheel hub given inside-to-outside loading (right).

The inboard concentrated load produced a conical fracture surface that diverged from inboard to outboard. The outboard concentrated load produced a conical fracture surface that diverged angularly from outboard to inboard.

The outcome of these rudimentary demonstrations was unsurprising for several reasons. First, an inboard-directed wheel impact force is not resisted by the axle, but rather by the suspension A-arms shown in **Figures 1** through **3**. That is, hard cornering action by any UTV or passenger vehicle pushing a tire/wheel/wheel hub assembly toward or away from the vehicle centerline direction will be resisted inboard of the wheels by the suspension (not the drive axle), which "floats" axially as enabled by the DOJ joint.

Pushing on a UTV tire or wheel inboard produces no compressive or tensile stress on the drive axle. This is easily seen when comparing two-wheel drive and four-wheel drive vehicles — in that the deletion of a drive axle does not require a change to the suspension, as the suspension resists the loading in all directions. Second, as a counterfactual thought experiment, suppose excessive slop existed in the mounts of the incident UTV A-arms that allowed the tires and wheels to objectionably move inboard and/or outboard. The half shaft could, in this hypothetical case, be loaded axially by a wheel strike. However, a wheel strike during barrel rollover would displace the wheel assembly inboard against the half shaft (**Figure 15**).

In this diagram, the components mating to the CV joint end of the half shaft are not shown. What is shown is the driving outer race "bell" end, the ball bearings as brown spheres, the inner race in yellow, the main axle in blue, the retaining circlip in red, the flexible rubber boot in green, and the boot clips in gray. The red arrows show the impact force that could potentially be transmitted to the axle, which is resisted by the black arrow that is traceable to the inboard mounting end of the axle assembly at the transaxle. The combined impact force (red) will tend to move the inner race (yellow) toward the right, while the resisting force will tend to move the axle and circlip to the left. This would act to seat the outboard end of the main axle shaft to the CV joint inner race — not to overcome the fixation of the circlip and move the main axle shaft inboard. Thus, a conceptual free body diagram of an inboard directed wheel strike loading path further indicates that a substantial wheel strike would not cause the damage observed in the incident overturned UTV.

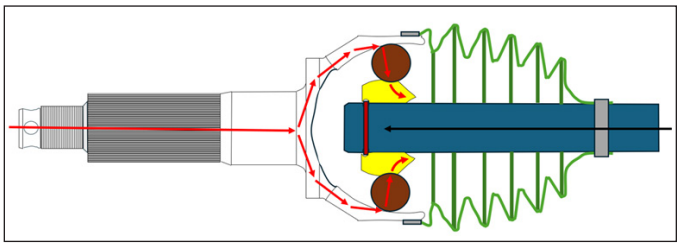

Figure 15
Free body diagram of wheel force from outboard to inboard against the axle.

Summary and Conclusions

The failure at this UTV's left rear wheel assembly initiated with a progressive axial inboard repositioning of the main axle shaft with respect to the CV joint inner race over time during vehicle travel. The inboard positioning is physically documented by damage to the retaining circlip and circumferential witness marks, which plastically indented the splined surface of the outboard end of the main axle shaft. After the circlip groove became fully exposed inboard of the CV joint inner race, the maximum bending moment and minimum area were at the outboard face of the axle shaft's circlip groove. This groove also contained a sharp stress-enhancing inner edge that ordinarily would be unproblematic, since that groove was never designed to receive bending stresses. Fatigue cracks initiated as documented by circumferential ratchet marks. The crack progression was from exterior to interior as is universal in rotating shafts with bending loading.

Once fractured, the axle and wheel spun independently, as documented by the damaged flexible CV joint boot. During travel, the loose main axle shaft fracture surface edge pressed against its mating outboard fracture surface and pushed the outboard drive components outboard against the cast aluminum wheel hub. The brittle aluminum wheel fractured due to a concentrated inboard-to-outboard loading, producing a Hertzian cone fracture surface. The tire/wheel/hub component was then only lightly attached to the suspension and brake assembly. The brake disc, including its mounting bolts, continued to rotate and impacted on the mating brake components that were still properly affixed to the bearing carrier, causing scouring and torque about the rear wheel. This braking action at the left rear wheel initiated suddenly and without warning. It induced the counterclockwise vehicle yaw and overturn.

The subject half shaft, with approximately 2,000 miles of usage, was original to the vehicle. Upon leaving the factory, the left rear axle shaft may not have been fully seated within its mating CV joint inner race, but this was not revealed by the inspections. It could also be that, for some other undetermined reason, the main axle shaft backed out

of its properly seated initial position as the retaining circlip was unable to prevent the displacement. No definitive cause of the initial displacement of the axle shaft in the inboard direction was determined. Still, as the half shaft was not a component that was intended to be adjusted, maintained, repaired, or even inspected by the vehicle owner (beyond visual inspection the flexible joint boots for damage or grease leaks), user error could reliably be ruled out. The fact that the two occupants of the incident UTV were approaching a left-hand turn at the time of overturn was merely a remarkable coincidence.

References

1. D. P. Dennies, How to Organize and Run a Failure Investigation. Materials Park, OH, USA: ASM International, 2005.

2. F. L. Singer and A. Pytel, Strength of Materials, 3rd ed. Reading, MA, USA: Addison-Wesley, 1980, p. 285.

3. W. Hertzberg, Deformation and Fracture Mechanics of Engineering Materials. New York, NY, USA: John Wiley & Sons, 1996.

4. N. W. Sachs, Practical Plant Failure Analysis. Boca Raton, FL, USA: CRC Press, 2007.

5. D. J. Wulpi, Understanding How Components Fail. Materials Park, OH, USA: ASM International, 1999.

6. T. Gilovich, How We Know What Isn't So: the Fallibility of Human Reason in Everyday Life. Vancouver: Langara College, 2007.

7. A. C. Fischer-Cripps, Introduction to Contact Mechanics. New York, NY, USA: Springer, 2007.

8. S. A. Batzer, "Forensic Engineering Analysis of Roof Failure in Rollovers," Journal of the National Academy of Forensic Engineers, vol. 27, no. 1, Jan. 2013.

9. O. Jacobson, S. A. Batzer, M. Kittel, J. A. Grantham, G. J. Barbera, and A. Molitoris, "Forensic Engineering Analysis of Failed UTV Roll Cages," Journal of the National Academy of Forensic Engineers, vol. 33, no. 1, Jan. 2016.

10. S. A. Batzer, "Forensic Engineering Analysis of Side Glazing Failure in Rollover Collisions," Journal of the National Academy of Forensic Engineers, vol. 26, no. 2, Jul. 2012.

Forensic Analysis of Construction Variances Associated with Cement Plaster (Stucco) Veneer Installed Over Wood Framing

By Brian C. Eubanks, PE, DFE (NAFE #962S), Garrett T. Ryan, PE, DFE (NAFE #1125M), and Derek T. Patoskie, PE (NAFE #1312A)

Abstract

The International Residential Code (IRC) provides prescriptive specifications for the installation of cement plaster (stucco) veneer on wood framing. Since 2006, the IRC has also referenced ASTM C926 (Standard Specification for Application of Portland Cement-Based Plaster) *and ASTM C1063* (Standard Specification for Installation of Lathing and Furring to Receive Interior and Exterior Portland Cement-Based Plaster) *as applicable standards that provide additional specifications associated with the installation of cement plaster veneer. The IRC and the applicable code-referenced standards do not consider all available materials, designs, and/or methods of construction — nor do they consider possible alternatives or construction variances. Since there is more than one way to accomplish a goal, a forensic investigation should consider the intent and purpose of a specification (i.e., the desired performance) to determine whether an as-built alternative or construction variance is capable of accomplishing the same without adversely affecting a structure. This paper explores common construction alternatives and variances associated with the installation of cement plaster veneer (including control joints, attachment, thickness, and clearance) using methodologies for evaluating whether an alternative or variance can still achieve the intent and purpose of the specifications provided in the IRC and/or applicable code-referenced standards.*

Keywords

Alternative, analysis, ASTM, attachment, cement plaster, clearance, control joints, evaluation, international residential code, performance, stucco, specification, thickness, variances, veneer, wood framing, forensic engineering

Introduction and Background

Cement plaster veneer, often referred to as "stucco," is a common exterior cladding material used in residential and commercial construction worldwide. The International Residential Code (IRC)[1] provides prescriptive specifications for the installation of cement plaster (stucco) veneer for residential construction, and it references ASTM C926 (*Standard Specification for Application of Portland Cement-Based Plaster*)[2] and ASTM C1063 (*Standard Specification for Installation of Lathing and Furring to Receive Interior and Exterior Portland Cement-Based Plaster*)[3] as additional code-referenced standards for the installation of cement plaster veneer and associated accessories.

The authors of this paper find that cement plaster veneer is often installed with alternative means/methods and/or variances from the specifications of the applicable building code and/or code-referenced standards, and some frequently consider such alternatives and variances to be construction deficiencies. One should endeavor to perform construction services in accordance with the applicable building code and/or code-referenced standards; however, meeting prescriptive code specifications after the fact is primarily academic. A forensic approach to alleged

Brian C. Eubanks, PE, 6275 W. Plano Parkway, Suite 140, Plano, Texas 75093, (469) 892-7520, info@pseglobal.com

deficiencies should not blindly follow prescriptive specifications; instead, it should employ engineering analysis to consider the performance aspects of the construction variances before concluding that such variances are construction defects[4]. Construction alternatives and variances are commonly encountered in cement plaster veneer; such alternatives/variances require a forensic evaluation to determine if they are adequate to perform their intended function.

According to Section R104.2.2 and Section R104.2.2.3 of the 2024 IRC (similar verbiage is also presented in all preceding versions of the IRC)[1]:

> ***R104.2.2 Alternative materials, design and methods of construction and equipment.***
>
> *The provisions of this code are not intended to prevent the installation of any material or to prohibit any design or method of construction not specifically prescribed by this code, provided that any such alternative has been approved.*
>
> ***R104.2.2.3 Compliance with code intent.***
>
> *An alternative material, design or method of construction shall comply with the intent of the provisions of this code.*

Based upon the preceding, the IRC acknowledges its prescriptive limitations. As such, it permits the use of alternative materials, designs, and construction techniques when an alternative is deemed to "comply with the intent" of the code's provisions.

In this paper, the authors explore a practical, objective forensic methodology for evaluating construction alternatives and variances in various components of cement plaster veneer to determine whether an alternative or variance can still achieve the intent and purpose of the specifications provided in the IRC and/or applicable code-referenced standards.

Drainage Mechanisms at Transitions Between Vertical and Horizontal Surfaces

Section A2.2.2 of ASTM C926-21 states the following regarding transitions between vertical and horizontal surfaces clad with cement plaster veneer (similar verbiage is also presented in all preceding versions of ASTM C926)[2]:

> ***ASTM C926-21***
>
> *A2.2.2 Where vertical and horizontal exterior plaster surfaces meet, both surfaces shall be terminated with casing beads with the vertical surface extending at least ¼ in. (6 mm) below the intersecting horizontal plastered surface, thus providing a drip edge. The casing bead for the horizontal surface shall be terminated not less than ¼ in. (6 mm) from the back of the vertical surface to provide drainage.*

According to ASTM C926-21, a functional drainage mechanism at vertical-to-horizontal transitions in the cement plaster veneer (as shown in **Figure 1**) is required to provide a means of draining water from the underlying drainage plane to the exterior[2].

Although the omission of a drainage mechanism at a vertical-to-horizontal transition in cement plaster veneer may be a consistent industry practice in some locales, it may result in staining, potential biological growth, and/or other signs of distress due to water accumulation/entrapment, as shown in **Figure 2**.

If cement plaster veneer is installed without a functional drainage mechanism at a vertical-to-horizontal transition, the as-built condition should be further evaluated to determine whether it is susceptible to damage.

A forensic investigation should consider other factors such as roof cover and/or weather exposure. For example, if the roof projects beyond the exterior wall/header plane for a horizontal distance greater than the vertical height of the wall/header area above the vertical-to-horizontal transition in the veneer (as shown in **Figure 3**), the investigator

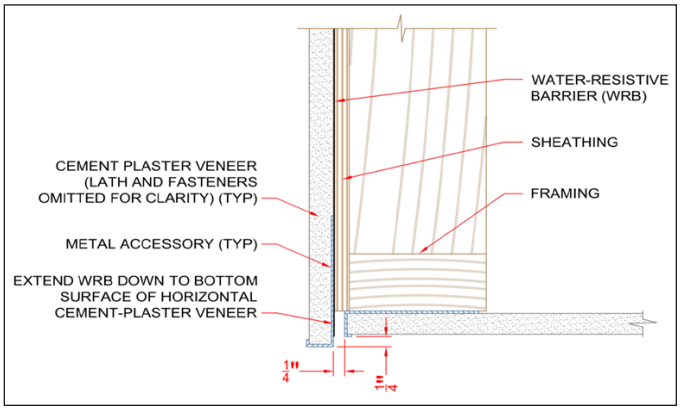

Figure 1
Example of vertical-to-horizontal transition in general compliance with ASTM C926-21.

Figure 2
Example of deteriorated wood framing at vertical-to-horizontal transition without a drainage mechanism.

Figure 3
Example of a vertical-to-horizontal transition at a covered location.

may be justified in concluding that the as-built omission of a drainage mechanism at the vertical-to-horizontal transition is not susceptible to damage because the roof overhang would serve to mitigate any potential water contact with the upper portion of the wall above the transition and significantly decrease the volume of water to be evacuated from the drainage plane underlying the veneer above the transition, if any.

In addition, a forensic investigation should consider the past performance of the cement plaster veneer at the location in question. The investigator should inspect for any salient signs of distress consistent with an accumulation of water underlying the veneer at a vertical-to-horizontal transition at a covered location. If there are no salient signs of damage consistent with water accumulation/entrapment at a location of a protected vertical-to-horizontal transition, the investigator may be justified in concluding that the as-built omission of a drainage mechanism at the vertical-to-horizontal transition is not a construction deficiency, and no remediation is necessary.

In the event that cement plaster veneer is installed without a functional drainage mechanism at a vertical-to-horizontal transition as a means of providing drainage for the wall assembly in accordance with ASTM C926-21, the as-built condition should be further evaluated to determine whether it would yield an accumulation of water behind the veneer. If the vertical-to-horizontal transition in the cement plaster veneer occurs at a location that is protected by roof cover (where water is not likely to pass behind the veneer) and the cement plaster veneer does not exhibit any salient signs of excessive cracking and/or staining associated with an accumulation of water behind the veneer (with no reason to suspect that such distress may manifest in the future), the investigator would be justified in concluding that the as-built condition is "satisfactory," as the prescribed drainage mechanism is not necessary.

On the contrary, if the vertical-to-horizontal transition in the cement plaster veneer is exposed to the elements, where water is likely to pass behind the veneer and require subsequent drainage, and/or the veneer exhibits signs of distress consistent with an accumulation of water behind the veneer (or such distress is likely to manifest in the future under typical service conditions), the investigator would be justified in concluding that the as-built condition is not capable of performing its intended function. Therefore, the construction variance is a deficiency.

Locations/Spacing of Control Joints

ASTM C1063-21 states the following regarding control joints in cement plaster veneer (similar verbiage is also presented in preceding versions of ASTM C1063)[3]:

> ***ASTM C1063-21***
>
> *7.4.10.2 Install control joint lathing accessories at locations to delineate cement plaster panel areas of 144 ft² (13 m²) maximum for walls and 100 ft² (9 m²) maximum for horizontal installations, that is, ceilings, curves, or angle type structures.*

ASTM C1063-21

7.4.10.3 Install control joint lathing accessories at locations to delineate cement plaster panel areas of 18 ft (5 m) maximum dimension, in either direction, or a maximum length-to-width ratio of 2½ to 1.

ASTM C1063-21

7.4.10.4 Install a control joint lathing accessory at locations where the ceiling framing or furring changes direction.

ASTM C1063-21

7.3.1.5 Lath shall not be continuous through control joints, but shall be stopped and tied at each side.

During a forensic investigation, the investigator should document the as-built location/spacing of control joints in the cement plaster veneer around the structure. In addition, the investigator should document the locations of distress in the cement plaster veneer and the size of substantial cracks to evaluate whether the observed cracks may be related to the placement and/or installation of control joints.

Depending upon the nature of the architecture, in conjunction with the location, orientation, and magnitude of distress, the investigator could then make a reasonable determination whether the existing control joints installed in the cement plaster veneer met the intent of ASTM C1063-21.

It should be noted that the continuity/discontinuity of metal lath behind control joint accessories in cement plaster veneer has been debated for many years, and the subject is currently up for discussion among the ASTM C1063 committee. In the past, ASTM C1063 was a voluntary standard, and its practices were not mandated by any building codes. When the 2006 IRC was released, ASTM C1063 became a referenced standard for the first time, so what was once offered as a "best practice" became a mandated practice.

Mark Fowler, the executive vice president of the Western Wall and Ceiling Contractors Association (WWCCA), and Frank Nunes, a former committee chairman of ASTM C926, co-authored an article addressing control joint installation and the need to allow for other acceptable practices[5]. In addition, the Association of the Wall and Ceiling Industry (AWCI) has issued the following statement[6]:

AWCI agrees that ASTM C1063 should be modified so that it allows and presents alternate methods for such things as installing control joints without cutting the lath. This modification will allow design professionals and contractors to include methods they know to work and avoid being penalized for not complying with the letter of the law.

In addition, Technical Bulletin 6.003 (April 2014) from the Wall & Ceiling Conference (WCC) states the following regarding the continuity/discontinuity of metal lath behind control joint accessories[7]:

The ASTM C1063 compliant method for installing control joints is to do so prior to the lath installation, thereby providing discontinuous lath terminating into the joint. ASTM C1063 does not, however, explain that to do so, you must have backing at either side of the vertical joint to properly secure the discontinuous ends of the lath and the flanges of the accessory…

…Where backing is not provided for and cannot be added for scheduling or other issues, vertical control joints are surface-applied to the face of continuous lath with tie wire. Not only has this proven method been practiced for decades, The Wall and Ceiling Bureau, Northwest Wall and Ceiling Bureau and The Technical Services Information Bureau endorse this installation…

In fact, an independent study performed in Galveston, Texas by an architecture/engineering consulting firm concluded that cement plaster veneer exhibited relatively similar performance regardless of the continuity/discontinuity of metal lath behind control joint accessories[8].

Cement plaster veneer is relatively brittle and can crack when subjected to stresses exceeding its tensile strength. Cracks in cement plaster veneer are a form of stress relief resulting from internal or external stresses. Due to the water-based nature of the material, cement plaster shrinks as it cures, which may result in hairline shrinkage cracks from internal stresses during the natural curing and drying process. In addition, expansion and contraction of cement plaster with thermal variances are also internal

stresses that can result in cracks. External stresses can be caused by any transfer of force to the cement plaster assembly, including, but not limited to, differential movement of a structural supporting element and/or deflection of a structural supporting element. Although steps can be taken to minimize cracks, there is no guarantee of eliminating them.

"Technical Bulletin 4" from the Plaster Council states the following regarding cracks in cement plaster veneer[9]:

> *... The building owner should expect hairline cracks and diagonal cracks emanating from the corners of windows and doors.*
>
> *By following industry best practices, the potential for cracking can be reduced (but not eliminated)...*
>
> *... Industry practice is to repair any cracks that exceed $^{1}/_{16}$" in width, although jobsite circumstances may suggest deviations from this normal practice.*

In addition, the "Three-Coat Stucco Maintenance Guidelines" published by the Stucco Manufacturers Association (SMA) states the following regarding cracks in cement plaster veneer[10]:

> *Cracking will occur on most residential homes finished with exterior cement based plaster. Cracking is typical in cement based plaster systems and in most cases is not considered a defect... It is important to note that these cracks do not jeopardize the water resistant properties of your stucco system. The weather resistive barrier is located beneath the cement coating. This is the component that protects your home from moisture intrusion.*

A forensic investigation should consider the architecture of the structure and the locations of existing control joints (in conjunction with the location, orientation, and magnitude of distress) to determine if the observed distress is causally related to the placement/construction of control joints. In addition, an investigator should consider and rule out other potential mechanisms that may yield similar distress (e.g., differential foundation movement, integration of roofing components, etc.) before concluding that the observed distress is causally related to the placement/construction of control joints.

In the event that cement plaster veneer is installed with placement/construction of control joints that do not meet the specifications of ASTM C1063-21, the as-built condition should be further evaluated to determine whether it is capable of performing the intended function. If the cement plaster veneer is installed with control joints sufficient to accommodate expansion/contraction of the veneer, thus limiting distress to the veneer — and the veneer does not exhibit any salient signs of systematic cracking associated with inadequate placement/construction of control joints — the investigator would be justified in concluding that the as-built placement/construction of control joints is "satisfactory" and "complies with the intent" of the provisions of the IRC. Therefore, the construction variance is not a construction deficiency.

On the contrary, if the cement plaster veneer is installed with control joints that do not meet the specifications of ASTM C1063-21 — and the veneer exhibits signs of systematic distress consistent with the omission and/or improper construction of control joints — the investigator would be justified in concluding that the as-built placement/construction of control joints is not capable of performing its intended function. Therefore, the construction variance is a construction deficiency.

Thickness of Cement Plaster Veneer

Table 4 of ASTM C926-21 provides specifications regarding the thickness of cement plaster veneer (a similar table is also presented in preceding versions of ASTM C926)[2].

According to Section 7.3.1 of ASTM C926-21[2]:

> ***ASTM C926-21***
>
> *7.3.1 Portland cement plaster shall be applied by hand trowel or machine to the nominal thickness specified in Table 4. The nominal values expressed in Table 4 represent neither a maximum nor minimum value. They consider the inherent variation of thickness due to the nature of the application process, and the allowable variation of the substrate and the finished plane of the plaster.*

While the total nominal specified thickness for cement plaster veneer applied over a metal plaster base ($^{7}/_{8}$ of an inch or 0.875 inches) has remained unchanged throughout the history of ASTM C926, it has clarified that the nominal value specified represents neither a maximum

nor minimum value[2].

During a forensic investigation, an investigator may evaluate the thickness of the cement plaster veneer around the perimeter of a structure. An evaluation of cement plaster thickness may be performed either by visual, non-intrusive measurements at exposed edges of panels, or it may be performed through intrusive methods.

Suppose an investigator elects to evaluate the thickness of the cement plaster veneer via non-intrusive measurements at exposed edges of panels. In that case, the investigator should consider the space between the wall framing and the edge casing accessory, the thickness of the edge casing accessory, and/or the protrusion of the textured finish. The investigator should measure the thickness of the cement plaster veneer from the back edge of the edge casing accessory, rather than the face of the exterior wall framing, to obtain an accurate measurement of the cement plaster thickness. In addition, measurements should be obtained at various locations around the perimeter of the structure, as shown in **Figure 4**. The investigator should attempt to place the vertical measuring tool on edge or at a slight back-sloping angle to account for the protruding texture. By taking measurements at multiple locations, any measurement influenced by the textured finish may be mitigated.

Suppose an investigator elects to evaluate the thickness of the cement plaster veneer via intrusive methods. In that case, the investigator should consider the necessary measures to properly remediate the underlying water-resistive barrier potentially damaged during the intrusive investigation process, as shown in **Figure 4**. Similar to non-intrusive methods, measurements should be obtained at various locations around the perimeter of the structure to mitigate any influence from the textured finish and/or isolated outliers.

When reviewing the results of the thickness measurements obtained (intrusive and/or non-intrusive), the investigator should consider that ASTM C 926-21 clarifies that the nominal values specified for the total thickness of cement plaster veneer represent neither a maximum nor minimum value[2]. In addition, the investigator should consider that ASTM's use of the word "nominal" to describe the total thickness suggests that some variation is to be expected.

Based on the evaluation of the thickness of the cement plaster veneer, the investigator may determine that the average thickness of the cement plaster veneer is generally in compliance with (or within an allowable tolerance of) the nominal value for total thickness specified by ASTM C926, despite the fact that the specified nominal value is not a minimum threshold.

A forensic investigation should consider the thickness of the cement plaster veneer, in conjunction with the location and magnitude of distress, to determine if the observed distress is systematic and causally related to the thickness of the plaster.

If cement plaster veneer is installed with a total thickness that is not generally compliant with (or within an allowable tolerance of) the nominal value for total thickness specified by ASTM C926, the as-built condition should be further evaluated to determine whether the as-built condition is capable of performing the intended function. If the cement plaster veneer does not exhibit any salient signs of systemic cracking within the area in question associated with the thickness of the veneer — and the veneer has been in place for a period of time sufficient to reasonably forecast its future performance — the investigator would

Figure 4
Example of non-intrusive (left) and intrusive (center and right) cement plaster veneer thickness measurements.

be justified in concluding that the as-built thickness of the cement plaster veneer is "satisfactory" and "complies with the intent" of the provisions of the IRC. Therefore, the construction variance is not a construction deficiency. On the contrary, if the cement plaster veneer exhibits signs of systematic distress related to the thickness of the veneer, the investigator would be justified in concluding that the as-built thickness of the cement plaster veneer is not capable of performing its intended function. Therefore, the construction variance is a deficiency.

Clearance Between Cement Plaster Veneer and Underlying Concrete Surfaces

Section R703.7.2.1 of the 2024 IRC states the following regarding the clearance between cement plaster veneer and underlying surfaces (similar verbiage is also presented in all preceding versions of the IRC)[1]:

> ***R703.7.2.1 Weep screeds***
>
> *A minimum 0.019-inch (0.5 mm) (No. 26 galvanized sheet gage), corrosion-resistant weep screed or plastic weep screed, with a minimum vertical attachment flange of 3½ inches x(89 mm), shall be provided at or below the foundation plate line on exterior stud walls in accordance with ASTM C926. The weep screed shall be placed not less than 4 inches (102 mm) above the earth or 2 inches (51 mm) above paved areas and shall be of a type that will allow trapped water to drain to the exterior of the building…*

Section R703.7.2.1 of the 2024 IRC specifies that weep screeds along the bottom edges of cement plaster veneer shall be placed not less than 4 inches above the earth or 2 inches above paved areas[1]. The 2024 IRC does not explicitly include any specifications for a minimum clearance between cement plaster veneer and an underlying horizontal foundation surface (e.g., porch, patio). Still, it is often asserted in forensic investigations that such surfaces should be considered "paved surfaces," thus requiring not less than 2 inches of clearance between the horizontal foundation surface and the veneer.

It should be noted that cement plaster veneer and adhered masonry veneer are similar cladding systems, as both systems maintain the same requirements for underlying moisture management systems, and both require base coats of cement plaster installed with the same accessories (e.g., lath, edge casing accessories, corner accessories, weep screeds, etc.), where applicable. In fact, both cladding systems can be installed identically until the surface finish is applied. While cement plaster veneer is completed with an application of a finish/color coat over the cement plaster base, adhered masonry veneer is finished with an application of brick, stone, or tile adhered to the cement plaster base. The only material difference between cement plaster veneer and adhered masonry veneer is the finished surface.

With respect to residential structures governed by the IRC, required clearances between adhered masonry veneer and underlying horizontal surfaces are addressed in Section R703.12.1 of the 2024 IRC[1]:

> ***R703.12.1 Clearances***
>
> *On exterior stud walls, adhered masonry veneer shall be installed with one of the following:*
>
> *Not less than 4 inches (102 mm) above the earth.*
>
> *Not less than 2 inches (51 mm) above paved areas.*
>
> *Not less than ½ inch (12.7 mm) above exterior walking surfaces that are supported by the same foundation that supports the exterior wall.*

Section R703.12.1 of the 2024 IRC specifies that adhered masonry veneer shall be installed a minimum of 4 inches above the earth and a minimum of 2 inches above paved areas — similar to the aforementioned prescriptive specifications for cement plaster veneer. However, unlike the prescriptive specifications for cement plaster veneer, Section R703.12.1 of the 2024 IRC also explicitly specifies that adhered masonry veneer shall be installed a minimum of ½ of an inch above exterior walking surfaces that are supported by the same foundation as the exterior wall (e.g., porch, patio), as illustrated in **Figure 5**.

The 2024 IRC permits the installation of adhered masonry veneer within a distance of ½ of an inch above a monolithic porch/patio surface, apparently acknowledging that ½ of an inch of clearance at such locations is sufficient to provide adequate drainage for a cladding system comprised of cement plaster (adhered masonry veneer and/or stucco). The intent of specifications associated with

Figure 5
Adhered masonry veneer installed with not less than ½ of an inch of clearance to the foundation.

clearances between cement plaster veneer and underlying horizontal surfaces is to ensure that the moisture management system can evacuate water at the base of the wall and protect the veneer/wall assembly from contact with surficial water and/or ground movement.

In the event that cement plaster veneer is installed with a clearance of less than 2 inches to an underlying monolithic foundation surface (e.g., porch, patio), the as-built condition should be further evaluated to determine whether the as-built condition is capable of performing the intended function. If the cement plaster veneer is installed with sufficient clearance to provide adequate drainage for the moisture management system and protect the veneer/wall assembly from contact by surficial water and/or ground movement (½ of an inch is considered sufficient for similar cladding systems), and the veneer does not exhibit any salient signs of excessive cracking and/or staining associated with an accumulation of water behind the veneer (with no reason to suspect that such distress may manifest in the future), the investigator would be justified in concluding that the as-built clearance of the cement plaster veneer is "satisfactory" and "complies with the intent" of the provisions of the IRC. Therefore, the construction variance is not a construction deficiency.

On the contrary, if the cement plaster veneer is installed with less than ½ of an inch of clearance and/or the veneer exhibits signs of distress consistent with an accumulation of water behind the veneer (or such distress is likely to manifest in the future under typical usage conditions), the investigator would be justified in concluding that the as-built clearance of the cement plaster veneer is not capable of performing its intended function. Therefore, the construction variance is a deficiency. Other factors, such as roof cover, weather exposure, and grading/drainage conditions, may also be considered in the evaluation of this construction variance.

Attachment of Cement Plaster Veneer

Section R703.7.1 of the 2024 IRC and Section 7.10.2.2 of ASTM C1063-21 state the following regarding the attachment of metal lath for cement plaster veneer (similar verbiage is also presented in all preceding versions of the IRC and ASTM C1063)[1,3]:

2024 IRC

R703.7.1 Lath

Lath and lath attachments shall be of corrosion-resistant materials in accordance with ASTM C1063. Expanded metal, welded wire, or woven wire lath shall be attached to wood framing members or furring... The lath shall be attached with 1½-inch-long (38 mm), 0.120-inch-diameter (3mm), 11 gage nails having a 7/16-inch (11.1 mm) head, or $^{7}/_{8}$-inch-long (22.2 mm), 16 gage staples, spaced not more than 7 inches (178 mm) on center along framing members or furring and not more than 24 inches (610 mm) on center between framing members or furring, or as otherwise approved. Additional fastening between wood framing members shall not be prohibited…

ASTM C 1063-21

7.3.3.1 Diamond-mesh expanded metal lath, flat-rib expanded metal lath, and wire lath shall be attached to… vertical wood framing members with 6d common nails… or 1-in. (25 mm) wire staples driven flush with the plaster base. Staples shall engage not less than three strands of diamond mesh and flat rib expanded metal lath or not less than two strands of wire lath and penetrate the wood framing not less than ¾ in. (19 mm). When metal lath is installed over sheathing, use fasteners that will penetrate the framing members not less than ¾ in. (19 mm).

It should be noted that Section 7.3.3.1 of ASTM C1063-21 is not directly aligned with Section R703.7.1

of the 2024 IRC with respect to lath fasteners. Section 7.3.3.1 of ASTM C1063-21 specifies that lath fasteners shall penetrate wood framing members not less than 3/4 of an inch; however, Section R703.7.1 of the 2024 IRC only prescribes that fasteners align with wood framing members (or furring); it does not specify a minimum penetration depth into the wood framing members[1,3].

In fact, the 2024 IRC prescribes the use of $^{7}/_{8}$-inch-long staples to attach the lath, which is not consistent with the penetration depth suggested by Section 7.3.3.1 of ASTM C1063-21 when lath is applied over exterior sheathing materials. According to Section R102.4.1 of the 2024 IRC, where conflicts occur between the provisions of the IRC and referenced standards, the provisions of the IRC shall apply[1]. As a result, it is debatable whether the specifications of ASTM C1063-21 even apply to metal lath fasteners because the IRC provides its own specifications for lath attachment that take precedence over those provided elsewhere. The installation of metal lath utilizing fasteners that align with wood framing members (wall studs) is illustrated in **Figure 6**.

In some parts of the United States, it is a standard construction practice to attach the metal lath directly to wood structural sheathing panels, such as plywood or oriented strand board (OSB), with staples spaced at approximately 6 to 7 inches on center each way without any regard for the alignment of fasteners with underlying wood framing members (wall studs) as illustrated in **Figure 6**. Without any analysis, the aforementioned practice is often asserted to be a construction deficiency by some simply because the placement of fasteners does not strictly comply with the exact prescriptive specifications of the IRC; however, it should be noted that Section R703.7.1 of the 2024 IRC also provides an option to attach the metal lath "as otherwise approved"[1].

In consideration of metal lath installed over an exterior wall sheathed with $^{7}/_{16}$-inch-thick OSB panels, a staple fastener $^{7}/_{8}$ of an inch in length would penetrate the full depth of the sheathing panel regardless of whether the staples were aligned with framing members. According to the International Staple, Nail and Tool Association (ISANTA), the withdrawal capacity of a staple fastener in a wood substrate is a function of the staple leg diameter, the staple leg penetration depth, and the specific gravity of the wood substrate[11]. According to the National Design Specification (NDS) for Wood Construction, the specific gravity of Spruce-Pine-Fir is 0.42 (a common lumber species for wall studs in the authors' part of the country)[12]. According to the NDS, the specific gravity of OSB sheathing is 0.50[12]. Assuming the same staple gauge (leg diameter) for both substrates, a nominal increase in the specified quantity of staples would be required to penetrate $^{7}/_{16}$ of an inch into OSB sheathing with a specific gravity of 0.50 in order to yield an equivalent withdrawal capacity as the minimum quantity of staples specified in Section 7.3.3.1 of ASTM C1063-21 (¾ of an inch of penetration into a wall stud with a specific gravity of 0.42).

Assuming the presence of additional fasteners to transfer forces from the OSB sheathing to the wall studs, an equivalent withdrawal capacity that meets the intent of ASTM C1063 can be achieved by utilizing a nominal increase in the minimum quantity of specified fasteners when installed through $^{7}/_{16}$-inch thick OSB sheathing by itself. In addition, installing $^{7}/_{8}$-inch staples at approximately

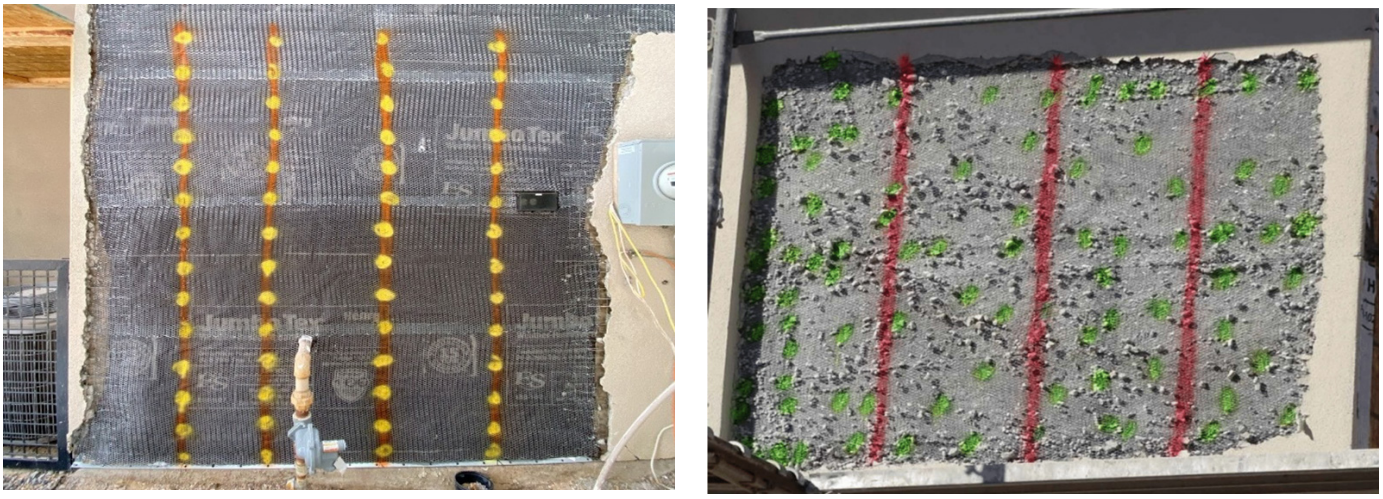

Figure 6
Installation of lath fasteners with (left) and without (right) regard to alignment with underlying framing members.

6 to 7 inches on center each way would provide more than three times the total quantity specified in Section 7.3.3.1 of ASTM C1063-21 when exterior wall studs are spaced at 16 inches on center. As a result, metal lath installed with staple fasteners spaced at approximately 6 to 7 inches on center each way would actually exhibit a higher withdrawal capacity than metal lath installed in compliance with ASTM C1063-21. Although the installation of metal lath with staples spaced at 6 to 7 inches on center each way requires the use of more fasteners, it should be noted that Section R703.7.1 of the 2024 IRC explicitly states that additional fastening between wood framing members shall not be prohibited.

In a white paper titled "Questioning the Stucco Lath Fastening Requirements of ASTM C1063," which was published in the *Journal of Architectural Engineering* (March 2010), Brett D. Newkirk, P.E. of Alta Engineering The company reached a similar conclusion regarding the attachment of cement plaster veneer to an underlying wood substrate[14]:

> *In fact, the analysis shows that when consideration is given to the greater frequency of fasteners naturally occurring through implementation of the hand rule, the attachment to the sheathing alone is superior to the attachment to the framing members alone.*

The intent of specifications associated with the attachment of metal lath in cement plaster veneer is to ensure that the cement plaster veneer is adequately attached to the structure for safety and durability. As previously discussed, it is possible to attach metal lath to a wood structural sheathing panel in a manner that provides an equivalent (or greater) withdrawal capacity than the prescriptive specifications of 2024 IRC without meeting the exact prescriptive specifications of the 2024 IRC (i.e., without aligning the fasteners with framing members).

In the event that metal lath for cement plaster veneer is attached to the substrate in a manner that does not meet the exact prescriptive specifications of the building code, the as-built condition should be further evaluated to determine whether the as-built condition is capable of performing the intended function. If the metal lath is attached to the substrate in a manner to provide a withdrawal capacity equivalent to (or better than) the withdrawal capacity provided by the prescriptive specifications of the IRC, and there are no salient signs of excessive cracking, out-of-plane cracking, and/or detachment from the substrate (with no reason to suspect that such distress may manifest in the future), the investigator would be justified in concluding that the as-built attachment of the cement plaster veneer is "satisfactory" and "complies with the intent" of the provisions of the IRC. Therefore, the construction variance is not a construction deficiency. On the contrary, if the metal lath is attached to the substrate in a manner that yields associated distress in the veneer (or such distress is likely to manifest in the future under typical usage conditions), the investigator would be justified in concluding that the as-built attachment of the cement plaster veneer is not capable of performing its intended function. Therefore, the construction variance is a deficiency.

Sheathing Gap Behind Cement Plaster Veneer

Section 6.1.4 of ASTM C1063-21 states the following regarding the installation of structural sheathing panels underlying cement plaster veneer with respect to the potential for future expansion of the panels[3]:

> ***ASTM C 1063-21***
>
> *6.1.4 Plywood and oriented strand board sheathing panels shall be installed with $^1/_8$ in. (3 mm) minimum panel edge gaps, and panel edges shall be offset 4 in. (10 cm) minimum from wall opening reentrant corners…*
>
> *NOTE 2 – This $^1/_8$-in. (3 mm) gap is intended to accommodate expansion. Linear expansion that is not accommodated by an expansion gap can cause stress on the stucco membrane resulting in stucco cracks.*

Plywood and oriented strand board (OSB) are wood structural panels that will expand and contract slightly with variations in moisture content. If the wood structural panels are tightly butted during installation, there is no room available to accommodate subsequent panel expansion. Any subsequent expansion of a tightly butted panel will yield an internal compressive stress within the panel, which may result in the panel bowing or buckling between supports in an attempt to relieve the stress.

As stated in Note 2 of Section 6.1.4 of ASTM C1063-21, the $^1/_8$-inch separation between adjoining sheathing panels is intended to accommodate potential expansion of the panels without bowing or buckling. APA - The Engineered Wood Association (APA) provides a similar recommendation to implement a $^1/_8$-inch spacing between panel ends and edges during the installation of wall, floor, and

roof sheathing panels; however, the APA's recommendation is accompanied by the following note [bold emphasis provided by the authors of this paper][14]:

> *Panel spacing is an **APA RECOMMENDATION**, to provide installers with a means of minimizing the potential for panel buckling; however, it is not a requirement… Panel buckling may be an aesthetic or serviceability issue but is not a structural deficiency. **There is no reason to expect this recommended space to be maintained when the panel becomes acclimated.** Gaps that were initially present may have closed due to normal moisture-related expansion…*

During a post-construction forensic evaluation, an investigator should understand that the referenced 1/8-inch spacing between adjacent sheathing panels applies to the installation of sheathing at the time of original construction, and it is not intended to be utilized as a standard for the evaluation of the sheathing years following construction of the structure. As acknowledged by the APA, there is no reason to expect the recommended space to be maintained when the panel becomes acclimated, and gaps that were initially present may have closed due to normal moisture-related expansion.

A forensic investigation should consider the spacing between sheathing panels, in conjunction with the location and magnitude of distress, to determine if the observed distress is systematic and causally related to the joints between sheathing panels.

In the event that a post-construction investigation of cement plaster veneer uncovers joints between underlying wood structural sheathing panels that are less than $^1/_8$ of an inch in width, the observed condition should be further evaluated to determine whether the as-built spacing of sheathing panels actually caused and/or contributed to distress in the veneer. If the spacing of sheathing panels is less than $^1/_8$ of an inch — yet the cement plaster veneer does not exhibit any salient signs of systematic cracking corresponding with the joints of sheathing panels — the investigator would be justified in concluding that the as-built spacing of sheathing panels was originally adequate to accommodate expansion/contraction of the panels. This is because there is no reason to expect an original as-built spacing to be maintained once the panel becomes acclimated, and the current condition is not a construction deficiency. On the contrary, if the spacing of sheathing panels is less than $^1/_8$ of an inch, and the cement plaster veneer exhibits signs of systematic distress corresponding with the joints of panels, the investigator would be justified in concluding that the as-built joint spacing between sheathing panels is causally related to the observed distress. Therefore, the current condition is a deficiency.

Repairs to Cement Plaster Veneer

ASTM C926-21 states the following regarding the installation of cement plaster veneer[2]:

> ***ASTM C926-21***
>
> *7.3.5 Each plaster coat shall be applied to an entire wall or ceiling panel without interruption to avoid cold joints and abrupt changes in the uniform appearance of succeeding coats. Wet plaster shall abut set plaster at naturally occurring interruptions in the plane of the plaster, such as corner angles, rustications, openings, expansion joints, and control joints where this is possible. Joinings, where necessary, shall be cut square and straight and not less than 6 in. (152 mm) away from a joining in the preceding coat.*

The following specification/definition is applicable to Section 7.3.5 of ASTM C926-21[2]:

> ***ASTM C926-21***
>
> *3.2.12 cold joint ("joining" or "jointing"), n – the juncture of fresh plaster application adjacent to set plaster, in the same plane.*

Following a forensic investigation, an investigator may recommend repairs and/or removal/replacement of portions of the cement plaster veneer. The authors of this paper have encountered some investigators who claim that localized repairs to cement plaster veneer is "not allowed," and they claim it is a "requirement" for the cement plaster veneer to be replaced in full panels (i.e., between control joints, from a corner to a control joint, from edge to edge of a continuous panel, etc.). When considering remedial recommendations, the investigator should be aware that ASTM C926 is a code-referenced standard for applying new cement plaster veneer, and it does not explicitly address repairs to existing cement plaster veneer. Nevertheless, ASTM C926 acknowledges "joinings" or "cold joints" in the same plane as the veneer, and it provides specifications for implementing "joinings" where necessary.

The Portland Cement Plaster/Stucco Manual by the Portland Cement Association (PCA) provides the following guidance for performing repairs to existing cement plaster veneer[15]:

> *Apply patching materials in thin consecutive layers, troweling each layer until firm, and continue applying thin layers until the base-coat plaster has been replaced (Figure 27). The finish-coat plaster then can be applied and textured to match the surrounding plaster.*

Figure 27 from the aforementioned document is shown as **Figure 7**, which depicts the recommended preparation of existing cement plaster veneer to receive a new patch[15].

Based upon the preceding, in conjunction with the authors' experience in the design, construction, and forensic investigation of cement plaster veneer construction, it has been found that patching cement plaster veneer is an accepted industry practice, and replacement of entire panels from corner-to-corner is not typically warranted for localized repairs. Although it is not a "requirement" for cement plaster veneer to be repaired/replaced in full panels, it may be necessary to do so in some climate zones to avoid hairline cracks between the original cement plaster and the newer cement plaster due to differential expansion/contraction associated with freeze-thaw cycles. As a result, the investigator should consider the geographic location of a project when determining an appropriate scope of remediation.

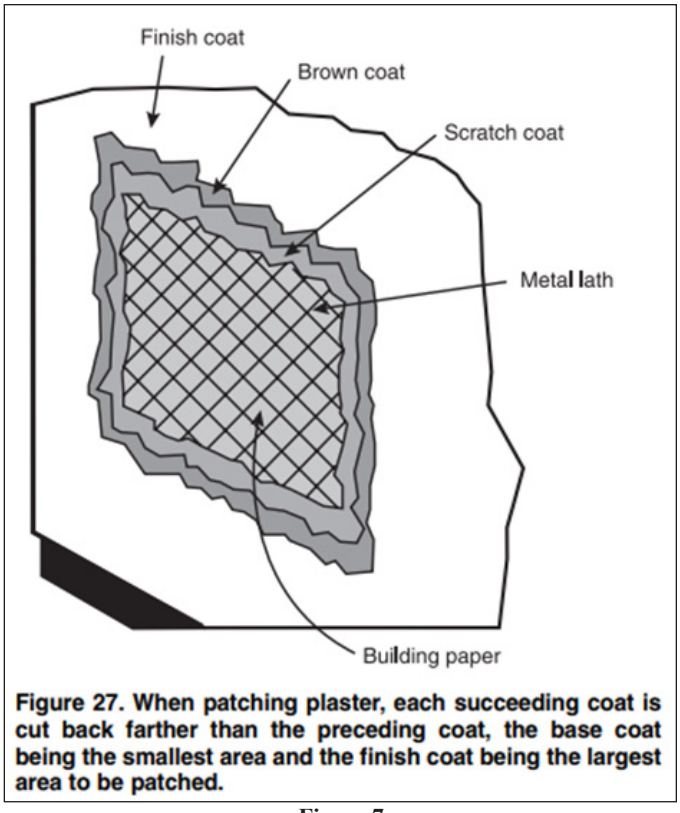

Figure 27. When patching plaster, each succeeding coat is cut back farther than the preceding coat, the base coat being the smallest area and the finish coat being the largest area to be patched.

Figure 7
Figure 27 from the Portland Cement Plaster/Stucco Manual by the PCA[15].

Summary and Conclusions

Cement plaster veneer is regularly installed with alternatives or variances with respect to the prescriptive specifications of the applicable building code and/or applicable code-referenced standards. A forensic evaluation should consider the intent and purpose of a specific construction specification, in conjunction with the as-built construction and resultant conditions, to provide a thorough evaluation for determination of whether an alternative or variance constitutes a construction deficiency. Depending upon the evaluation results, a reasonable and economical scope of remedial measures should be proposed to address alternatives and variances that are determined to be unable to perform their intended function.

As demonstrated by various aspects of cement plaster veneer construction, a construction alternative or variance requires a thorough forensic investigation to determine whether it constitutes a construction deficiency. An investigator should consider the as-built condition, the presence of distress, and the likelihood for distress to manifest in the future prior to opining whether remediation is necessary.

References

1. International Residential Code, IRC 2024, International Code Council, Falls Church, VA, 2024.

2. Standard Specification for Application of Portland Cement-Based Plaster, C926-21, ASTM International, West Conshohocken, PA, 2021.

3. Standard Specification for Installation of Lathing and Furring to Receive Interior and Exterior Portland Cement-Based Plaster, C1063-25a, ASTM International, West Conshohocken, PA, 2025.

4. B. Eubanks, D. Patoskie, and G. Ryan, "Beyond the Building Code: A Forensic Approach to Construction Defect Evaluation Utilizing the Construction Variance Evaluation Methodology," JotNAFE, vol. 41, no. 2, Jan. 2025.

5. Mark Fowler, Frank Nunes, “Stress Relief for Portland Cement Plaster (Stucco),” Walls & Ceilings, June 9, 2009. [Online]. Available: https://www.wconline.com/articles/86283-stress-relief-for-portland-cement-plaster-stucco.

6. Association of the Wall and Ceiling Industry, “Control Joints in Stucco,” AWCI, May 2015. [Online]. Available: https://www.awci.org/media/codes-standards/control-joints-in-stucco/

7. Wall & Ceiling Conference, “Lath & Plaster Control Joints over Continuous Lath,” WCC, Technical Bulletin 6.003, April 2014. [Online]. Available: https://www.wccinfo.org/Files/Tech%20Documents/new%20updated%20all/6.003%20-%20Continuous%20Lath%204-25-14%20-%20Final.pdf

8. J. Bishop, B. Coltzer Jr., T. LeCompte, A. Price, N. Roque, “Cement Plaster Control Joint Movement Study 2017,” Z6 Commissioning, LLC, Houston Lath & Plaster, Galveston, TX, USA.

9. Plaster Council, “Crack Policy,” Plaster Council, Technical Bulletin 4, Laguna Woods, CA, USA, May 2008. [Online]. Available: https://www.stuccomfgassoc.com/wp-content/uploads/2014/06/plastercouncil_tech4_crackr14.pdf

10. Stucco Manufacturers Association, “Three-Coat Stucco Maintenance Guidelines,” SMA, Laguna Woods, CA, USA, 2014. [Online]. Available: https://www.stuccomfgassoc.com/wp-content/uploads/2014/06/technicalpapers_maintenancer14.pdf

11. “ICC-ES Evaluation Report ESR-1539”, ICC Evaluation Service, LLC, Oct. 2023. [Online]. Available: https://icc-es.org/report-listing/esr-1539/

12. National Design Specification (NDS) Supplement: Design Values for Wood Construction, 2015 ed. Leesburg, VA, USA: American Wood Council, 2015.

13. Brett D. Newkirk, P.E., “Questioning the Stucco Lath Fastening Requirements of ASTM C1063,” Journal of Architectural Engineering ASCE, Mar. 2010, Volume 15, Issue 1.

14. APA, “Prevent Buckling with Proper Spacing,” APA, Form No. M300S, Tacoma, WA, USA, May 2013. [Online]. Available: https://www.apawood.org/buildertips/pdfs/M300.pdf

15. J. Melander, J. Farny, and A. Isberner, Portland Cement Plaster/Stucco Manual, 5th Ed. Skokie, IL, USA: Portland Cement Association, 2003.

Unreliable at the Boundary: Analysis of Two Sub-Optimum Crossbow Trigger Designs

By Stephen A. Batzer, PhD, PE (NAFE #677F)

Abstract

It is a fundamental principle that any weapon activated by a trigger — whether a crossbow, pistol, rifle, or shotgun — should only fire when the safety is set to the FIRE position, and the trigger is pulled. This study examines two distinct crossbow trigger designs associated with injuries. In the first crossbow, the trigger safety can be unintentionally or intentionally moved to an "intermediate" position (a point on the edge between SAFE and FIRE). This setting creates uncertainty, leading to instances where the crossbow discharges unexpectedly, either during arrow handling or even after sitting idle with no user action. In the second crossbow design, if the bowstring is not drawn with enough force, the safety fails to fully lock in place, resulting in the sear providing inadequate support to the corresponding release component. This creates a hazardous situation, observed to cause unintended discharge and injury to the user without any trigger activation. In both cases, the injuries did not stem from deliberate misuse; instead, the archer was operating the crossbow in a reasonable way that slightly deviated from the manufacturer's intent.

Keywords

Anti-dry fire, crossbow, failure analysis, false safety, inadvertent discharge, trigger, forensic engineering

Introduction and Historical Background

The crossbow, an ancient weapon, continues to hold significant value in contemporary applications for hunting and recreational shooting. Unlike vertically oriented compound bows, crossbows are typically fired from the shoulder in a manner akin to rifles, offering superior accuracy at extended ranges. The predominant design of modern commercially successful crossbows features a traditional layout, comprising an axial stock (or barrel) with limbs positioned laterally, constructed from advanced metal alloys and synthetic composites. Most modern crossbows incorporate eccentric cams, utilizing a bowstring and multiple power cables to enhance performance. Domestic manufacturers have largely adopted the term "arrows" for crossbow projectiles, phasing out the historical terms "bolts" and "quarrels." While contemporary crossbow designs remain unmistakably recognizable, they differ markedly from their traditional counterparts, as illustrated in **Figure 1**, which depicts a modern narrow, high-velocity crossbow.

With the relaxation of crossbow hunting prohibitions in multiple states, there has been a market-driven increase in crossbow performance. There appears to be a goal of allowing crossbows to compete with rifles for mid-sized game such as white-tailed deer, and at least one manufacturer has rather optimistically advertised its latest model with the tagline "Meet your next rifle[2]." However, compared to even muzzle-loading rifles, crossbows are short-range weapons.

Figure 1
Modern narrow compound crossbow as of 2025, which is capable of 410 fps arrow speed[1].

Stephen A. Batzer, PhD, PE, 8383 M-113 E, Fife Lake MI, (479) 466-7435, batzer@batzerengineering.com

The newest crossbows, which launch 400-grain arrows at 500 feet per second, develop approximately 220 ft-lbs of kinetic energy. This is approximately 10% of the kinetic energy at the muzzle of a 30-30 Winchester cartridge, which discharges a 150-grain bullet at 2,390 feet per second, producing ~1,900 ft-lbs of kinetic energy with a much flatter trajectory. In addition to new patents, innovations by crossbow designers have produced dedicated tooling and machines for parts production and assembly, telescopic sights, composite stocks, sophisticated fiberglass construction for the limbs, increased-strength synthetic filament flexible cables and bowstrings, and carbon-fiber shafted arrows. Important patented innovations include the reverse limb layout[3], complex trigger systems including mechanical arrow presence sensors[4], discharge noise attenuation accessories[5], flight rail finger guards[6], reverse draw cam bowstring layout[7], helical power cables[8], narrower limbs[9], and innovative power cable anchoring[10].

It has been the goal of designers to increase arrow velocity and kinetic energy, improve accuracy, reduce vibration, suppress cocking and discharge sounds, and diminish weight and size, all while maintaining durability and affordability. As an example of how advanced the trigger mechanism is in at least one modern crossbow design, see the X-ray in **Figure 2**, which details the significant number of interconnecting components. At the lower right of the image is the polymer pistol grip with the trigger shoe just visible. This trigger interface pivots about an axle, moving an actuating bar backward to trip the clasp through intervening linkages.

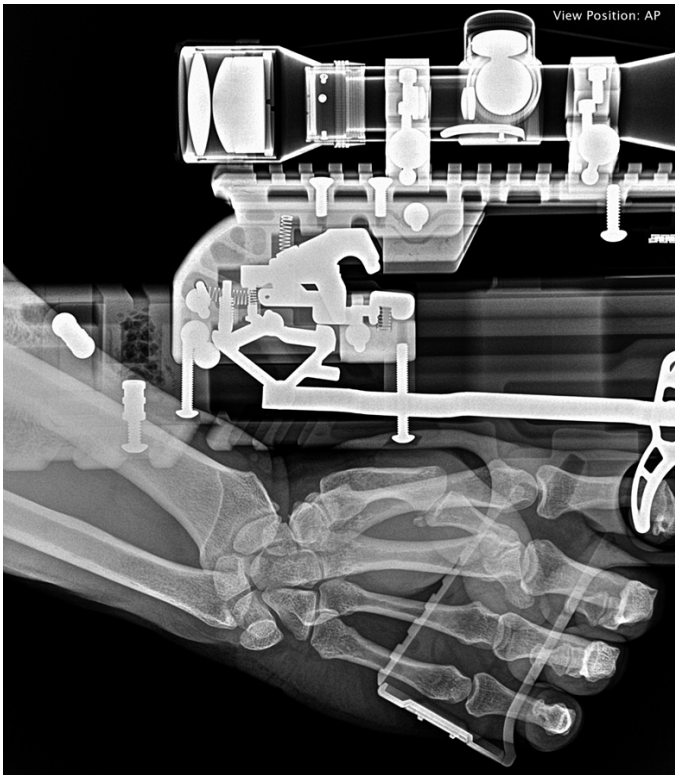

Figure 2
Modern crossbow trigger mechanism, safety off, trigger drawn, and bowstring clasp up.

The design, manufacture, and sale of crossbows in the United States remain largely unregulated at the federal level. Notably, crossbows are exempt from the provisions of the National Firearms Act of 1968[11] and are not subject to federal age restrictions for purchase or possession. The Archery Trade Association (ATA) [https://archerytrade.org/] provides a limited set of voluntary guidelines[12], which outline standardized measurements for archery equipment specifications, such as force-draw and let-down curves for recurve and compound bows. However, these guidelines, first issued in 2009 and most recently revised in 2021, were not developed in accordance with American National Standards Institute (ANSI) protocols. They are adopted solely voluntarily by ATA member companies and do not address safety standards, even indirectly.

At the state level, regulations primarily focus on the use of archery equipment, including crossbows, in hunting and public activities. No federal or state regulations specifically govern crossbow safety or design standards, leaving a significant gap in oversight for these devices.

This paper examines two forensic case studies involving crossbows that inadvertently discharged, resulting in injuries to their users. Both incidents were investigated using a standardized protocol to identify or confirm the mechanism of bowstring release without trigger activation. The analysis highlights that an unreliable crossbow may discharge unexpectedly without exhibiting mechanical failure or visible damage.

General Protocol for Studying an Inadvertent Crossbow Discharge

1. Read the owner's manual. Identify any omitted, unclear, or ambiguous instructions. Understand the mechanism as described in the manual.

2. Acquire and read promotional written materials; watch user instructional videos.

3. Inspect the incident crossbow visually. Read the warning stickers, and document the model and the serial number (if present). Look for cracks in the limbs and other structural components, the

condition of the bowstring and cables, evidence of impact damage to the cams, gap size between the limbs and risers (if any), loose fasteners, evidence of contamination, missing parts, and wear. Do not proceed with cocking, loading, and discharging this crossbow if it is unsafe to do so. Look for evidence that the crossbow was dropped. Look for evidence of cam and/or limb impact. Consider using personal protective equipment (PPE), such as latex gloves and impact-resistant eyewear, and look for blood or other potential biohazards.

4. Inspect the arrows, including the nocks, and any associated material included with the incident crossbow.

5. Conduct a preliminary functions test of the crossbow without cocking or shooting it. A shortened arrow stub can be used to actuate the arrow presence sensor, and a lightly stretched elastic band or taut, loose bowstring can substitute for a bowstring drawn tightly by the limbs. Test the safety, trigger, and clasp — and the arrow presence mechanism.

6. Conduct a functions test of the crossbow by shooting it in accordance with the owner's manual instructions. Draw, load, and discharge properly weighted arrows numerous times for function familiarity. Examine the behavior of the safety when it is engaged, ensuring that the trigger does not release the internal sear. Verify the average measured trigger pull weight, compare the average with the published value, and determine any trigger pull-to-pull force variance. Evaluate the grouping of arrow shots as an indicator of a possible mechanical issue.

7. Examine, if available, blueprints and patent documents. Note that a patent typically visually describes the preferred instantiation of the invention at the time of submission, and the commercialized version may have differences — even substantial details — compared to the patented design.

8. Acquire an exemplar crossbow for disassembly. Determine if any design changes have been made. A comparison with earlier and/or later models may be necessary to determine whether any functional parts have been revised by the designer or manufacturer.

9. Use X-ray or CT [computed tomography] scanning to examine the internal trigger parts and/or other visually inaccessible parts. Compare to a scan of an exemplar as necessary.

10. Conduct a rubber mallet test, inputting a reasonable acceleration to the crossbow from a variety of vectors to see if an acceleration impulse will prompt the sear to disengage the bowstring clasp [see, i.a.,[13]]. Do this testing both with the safety engaged and with the safety disengaged. It is essential to keep safety in mind during this testing as the crossbow may unexpectedly release the drawn bowstring.

Thoroughly and formally document all observations and findings to ensure precision and traceability. The inspection checklist provided earlier constitutes a preliminary assessment. Once the incident mechanism is sufficiently understood, it is prudent to pause for reflection prior to further analysis[14]. This strategic pause facilitates careful planning and enhances the rigor of the investigation. Address the following key considerations:

- What potential factors could lead to an unintended outcome?

- Can the conditions causing an inadvertent discharge be intentionally reproduced for controlled analysis?

For a more comprehensive analysis, consult the following sources:

- Online archery forums for accounts of comparable incidents.

- The Consumer Product Safety Commission (CPSC) database for relevant product recalls.

- Manufacturer websites, which typically publish recall notices.

- Customer reviews to identify recurring issues or patterns associated with the incident crossbow model.

- Surveillance footage of the inadvertent discharge, if it exists.

This methodical approach ensures a comprehensive

and systematic investigation, which will support reliable forensic engineering conclusions.

A primary cause of inadvertent discharges in crossbows, as with firearms, is deviations by the user from the intended use envisioned by the designers. Such deviations may not constitute abuse, but could be classified as misuse from the designers' perspective. It is a well-established principle that user behavior varies significantly, encapsulated in the adage "results vary." Each operator interacts with the weapon in a manner that is subtly or markedly distinct from others. This variability underscores the importance of analyzing the mechanism and exploring how different inputs can alter its function.

To thoroughly investigate potential misuse, consider how each operator action could be performed differently or incorrectly. For every intended function, evaluate the following:

- How might the action be executed incrementally differently from the prescribed method?
- Could the action be deliberately performed incorrectly, and what would be the outcome?

A non-exhaustive list of user input variables includes:

- The arrow may not be inserted as far axially rearward onto the bowstring as possible.
- The safety switch may not be moved fully from SAFE to FIRE, or vice-versa.
- The trigger may be pulled partially (but not fully), and the crossbow trigger safety is not then returned to the SAFE position.
- The trigger may be pushed forward, rather than pulled backward.
- The arrow's cocking vane may be inverted, making the arrow 180° out of rotational position.
- The bowstring may be worn beyond its need for replacement, diminishing the center diameter.
- The bowstring may not have been pulled fully backward during the cocking cycle.
- The crossbow may have been dropped.
- For a pristine new crossbow, a user may "baby" the mechanism in an unintentional attempt to ensure the crossbow isn't damaged. This is a mistake, but it occurs. For weapons, authoritative positive inputs are best.

Case Study 1

In the initial unintended discharge incident, the owner acquired the crossbow in new but non-standard condition, as depicted in **Figure 3**. The crossbow, which was assembled from factory components, lacked a serial number sticker, indicating that it was neither sold through wholesale nor retail channels. Instead, it was privately sold by an employee of the local crossbow factory to an acquaintance. This modern crossbow, constructed from synthetic materials, belongs to an earlier design generation compared to the model shown in **Figure 1**. It was assembled circa 2017 and features an optical sight, a rudimentary anti-dry fire (ADF) mechanism (components that prevent cocked bowstring discharge in the absence of an arrow), cams (rotating wheels at the outboard position of the limbs), and power cables crossing beneath the barrel (the axial "flight rail" of the crossbow).

According to the user's testimony, he had taken his crossbow hunting for the first time, and he was hunting deer from elevation. The crossbow was cocked but not loaded with an arrow, with the safety at least partially engaged. He rested his right hand on the crossbow flight rail, and no part of his body was touching the trigger. The crossbow discharged, and the bowstring sliced through his hand, severing his middle finger. Subsequent investigation showed that there had been multiple reported OSIs (other similar incidents) of this crossbow inadvertently discharging and causing user injury. These reports were found in warranty claims, internet archery discussion forums, and litigation.

An inspection of the crossbow was performed, including removal of the trigger mechanism, as shown in **Figure 4**. Similar to the crossbow trigger mechanism previously

Figure 3
Case Study 1 incident crossbow assembled circa 2017.

Figure 4
Incident crossbow showing removal of trigger mechanism and scope mount with draw bar leading to trigger shoe.

x-rayed (**Figure 2**), the bowstring center is anchored by the clasp, substantially behind the trigger shoe user interface, to produce a shorter overall length. Note: The "trigger shoe" is the typically curved, vertically disposed lever that the archer pulls with his release trigger finger. Movement of the trigger shoe – typically through intermediary components – causes bowstring release.

The trigger shoe pivots on an axle and pulls an internal trigger draw bar forward, which is mechanistically opposite that of the crossbow previously shown as **Figure 2**, for which the trigger shoe pushes a transfer bar backward.

Figure 5 shows the trigger mechanism removed from the crossbow stock with the trigger draw bar rotated backward. The basically rectangular stamped steel housing is perforated to mount transverse pins that act as axles, torsional spring posts, and component stops. An internal-stamped steel leaf spring near the top of the housing is indicated with a white arrow in **Figure 5**. Recesses in the spring act as detents to keep the pivoting safety lever either fully forward or backward.

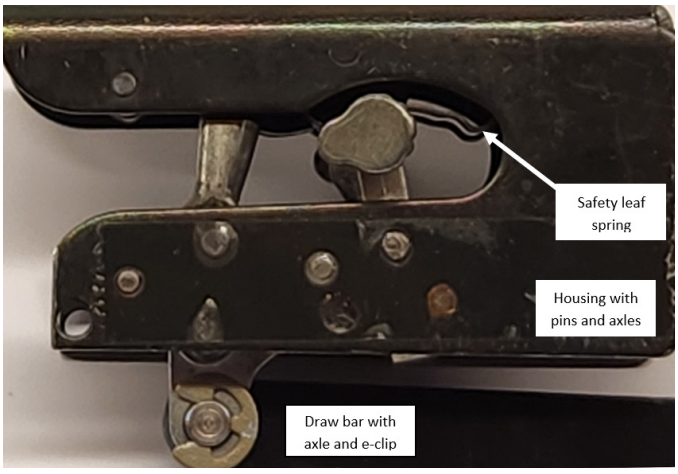

Figure 5
Incident crossbow trigger mechanism, ready, with the safety in the FIRE position with trigger draw bar folded ~180° rearward.

The trigger mechanism components and their axles were removed from the stamped steel box housing, and longer gage pins were inserted into the component axle holes from the left side to facilitate a positional layout of the major moving components, as shown in **Figure 6**. The multiple torsion springs, which bias individual component motion, are not shown. The biasing springs rotate the anti-dry fire (ADF) lever DOWN, the clasp VERTICAL, the tumbler ENGAGED (as shown, fully counter-clockwise), and the safety fixed either fully forward or backward as a detent. In **Figure 6**, the sear surface of the tumbler is in the engaged position — such that the clasp cannot rotate forward counter-clockwise into its released position.

To cock this model of crossbow, a rope cocking device with two hooks is attached to the bowstring on either side of the barrel. The user places his foot in the stirrup at the discharge end of the crossbow and pulls the two handles of the rope cocking device upward toward his shoulders. See **Figure 7** for an explanatory image of the cocking of the incident crossbow. The two hooks ensure that the center portion of the drawn bowstring is locally flat and perpendicular to the flight rail, and the bowstring itself (blue arrow) glides over the clasp and causes it to rotate out of the way (white arrow). At full draw, the safety rotates clockwise, and its bottom U-shaped cavity engages against the mating surface of the tumbler (yellow arrow), restraining

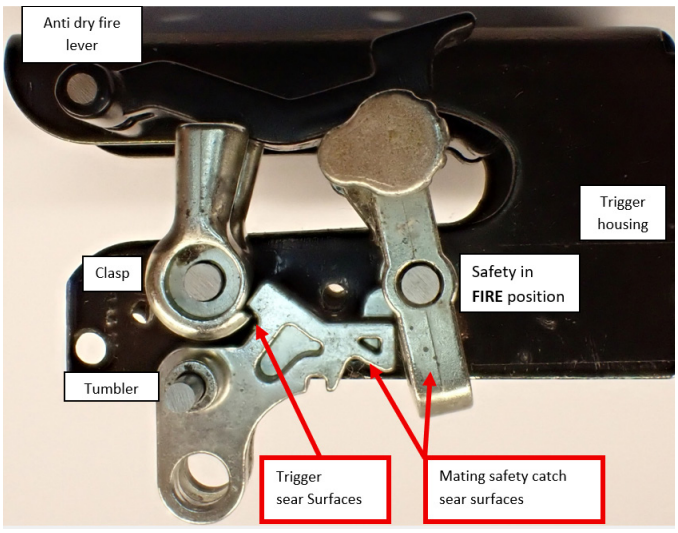

Figure 6
Incident crossbow trigger mechanism with internal components and axles removed with the four major components affixed to the left exterior side of the housing and the trigger bar removed from the sear.

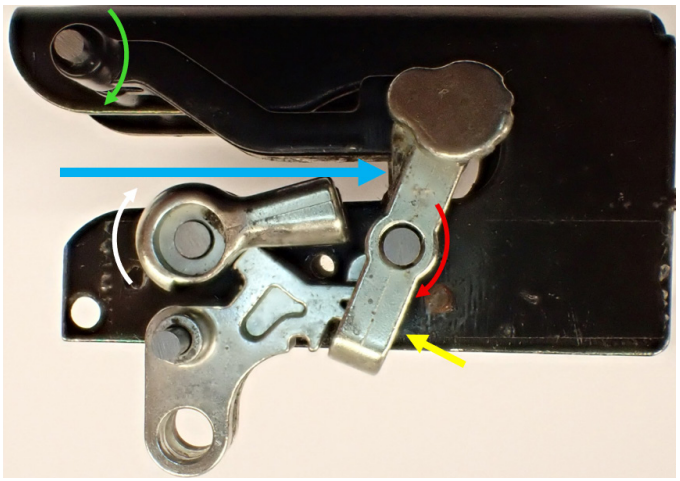

Figure 7
Incident crossbow trigger mechanism showing full draw position of bowstring represented by a blue arrow.

it from rotational motion. Also at full draw, the ADF rotates downward (green arrow). It will prevent the safety from rotating back to the FIRE position until the ADF is rotated back upward by the insertion of an arrow and nock onto the bowstring.

Figure 8 shows the trigger mechanism components as they are positioned at the moment of firing. The ADF lever had been moved up by the presence of the arrow. The safety was then moved forward to the FIRE position. The draw bar pulled the tumbler such that it rotated clockwise, disengaging the tumbler's sear surface from the mating surface of the clasp. The unconstrained clasp rotated ~90° counter-clockwise and released the bowstring and arrow, which rapidly moved forward (left) as represented by the blue arrow.

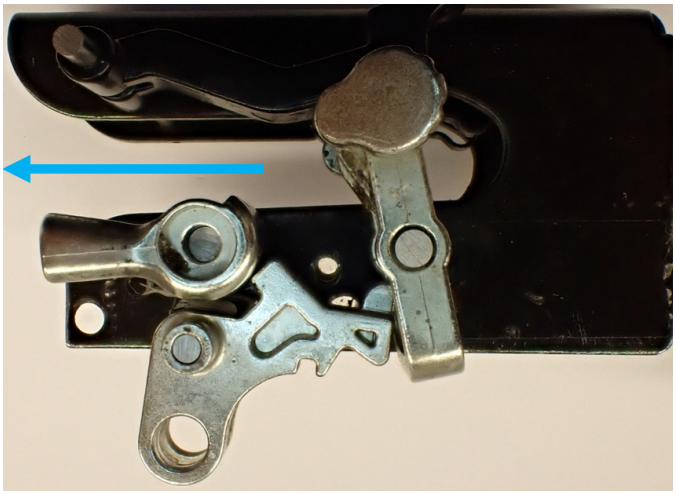

Figure 8
Incident crossbow trigger mechanism showing discharge position.

Analysis and physical testing of the incident mechanism revealed that the most likely situation was consistent with the testimony of the crossbow owner and other users who complained of inadvertent discharge. By pulling the rope cocking mechanism backwards incompletely, the clasp would index and accept the bowstring while not fully pushing the safety to its full SAFE position. This is illustrated in **Figure 9**. As is shown with the dismounted components, the tumbler and safety can each be in the partially engaged position if the crossbow is not vigorously cocked by the rope cocking device.

This is also shown with the components properly assembled in the crossbow. The top image of **Figure 10** shows the safety in the fully SAFE position without the bowstring present. Note that the ADF lever has moved downward, blocking forward motion of the safety if no arrow is loaded. The lower image of **Figure 10** shows the cocked crossbow with the bowstring and clasp in the proper position, but the ADF and the safety are not in the proper position. This miscocked condition was deliberately produced by a minimal rope cocking device pull for which the bowstring would index the clasp but not move the top of the safety lever fully rearward.

Based upon analysis and investigation of the incident crossbow, it was determined that this trigger design was sub-optimal. It was found that the ADF lever, while somewhat valuable, was not "active" in that the safety could be moved to FIRE after an arrow was loaded. Then if the arrow were removed, the safety would not automatically return to SAFE. In addition, the geometry of this mechanism was such that the bowstring could be deliberately or

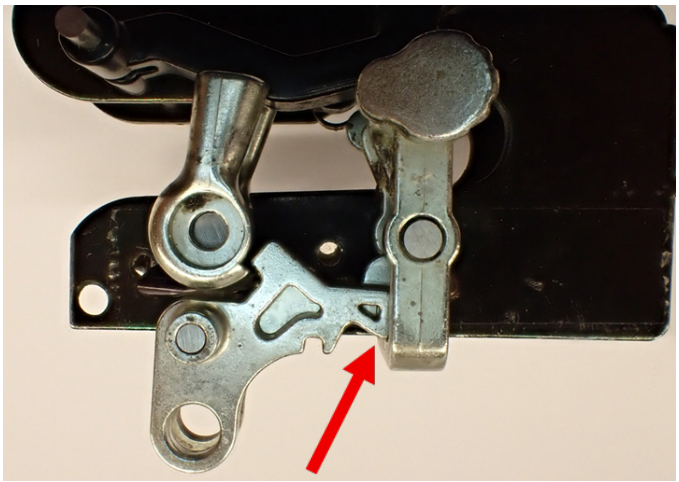

Figure 9
Incident crossbow trigger mechanism showing position in which the tumbler is barely constrained by the mating ledge of the safety (see red arrow).

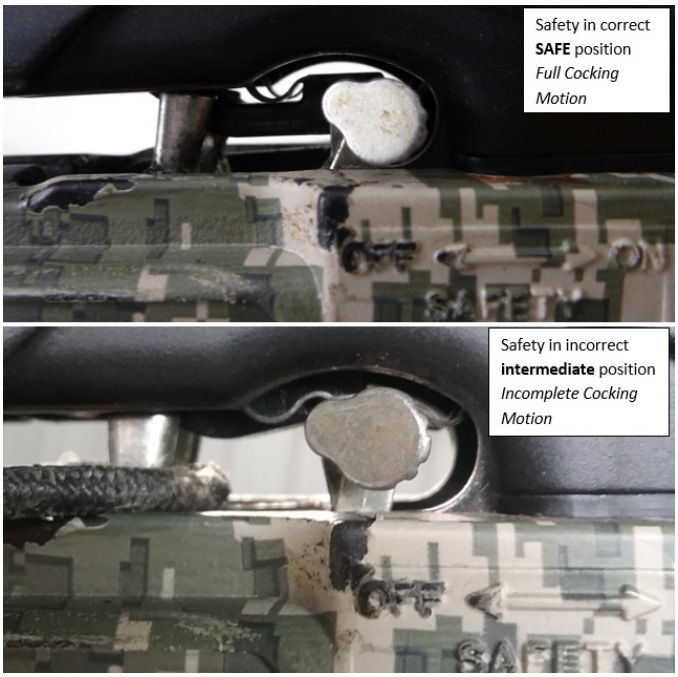

Figure 10
Incident crossbow safety and ADF lever showing the proper position when drawn at top (bowstring not shown), and an incorrect intermediate position at bottom with the ADF not actuated and the tumbler not fully constrained, if at all.

unintentionally cocked with the clasp in the proper position without the safety being moved to the full SAFE position to engage the tumbler completely. This design is no longer in production and has been replaced by more sophisticated and ostensibly more reliable designs.

Case Study 2

The second crossbow design evaluated in this study represents a significant technological advancement over the "value" crossbow model described in Case Study 1, despite their brief concurrent market presence. Introduced in 2016 by Ravin, a startup company founded to develop and market this design, this premium model features composite construction materials, relatively short power cables that do not cross under the barrel, and helical power cable journals facilitating a compact limb arrangement. Unlike many designs (e.g., Case Study 1 crossbow), this crossbow omits a foot stirrup as it incorporates an integrated crank cocking mechanism to draw the bowstring. This design also features an internal ADF trigger mechanism intended to allow the crossbow to only fire when an arrow nock is fully engaged to the center of the bowstring (**Figure 11**).

Despite its commercial success, the model faced significant safety challenges. Reports of unintended discharges led to a prompt recall in collaboration with the Consumer Product Safety Commission[15]. While the recall officially targeted the proprietary clip-on arrow nocks, the primary defect lay in the internal trigger components, which permitted hang fire (a hazardous unpredictable delayed discharge after trigger pull) and subsequent accidental discharge, even with replacement nocks. To address this, Ravin redesigned several trigger components, integrating them into later production runs and offering one-to-one parts replacement as a silent recall measure for customers returning early R9 and R15 models for repair. The R15, an enhanced version of the R9, features stronger limbs and increased arrow velocity but shares the same foundational design.

Figure 11
Photograph of the crossbow design of Case Study 2, Ravin R9 / R15 at top, along with a close-up of the trigger shoe and trigger pack at bottom.

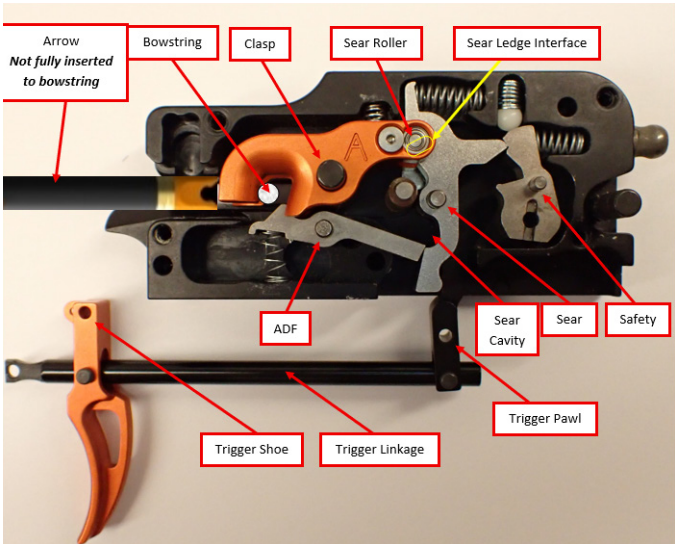

Figure 12
Photograph of the generation 1 trigger mechanism in the cocked but unloaded position.

Figure 12 illustrates the dismounted and partially disassembled "generation 1" (that is, originally marketed) trigger mechanism of the Ravin R9 and R15 crossbows, which are detailed in the associated patent[16]. To enhance visibility of key components, the left cover of the trigger housing has been removed. For clarity, a digital representation of an arrow stub equipped with an orange post-recall nock and a circular depiction of the bowstring cross-section, held by the clasp, have been superimposed. Red arrows, used to label component nomenclature, indicate the rotational axes of the respective parts where applicable. A yellow rectangle highlights the concealed sear ledge interface, which must disengage to enable crossbow discharge. The arrow retention actuator and its forward coil spring (located ahead of the clasp) have been omitted, as has the trigger shoe return spring, typically anchored at the forward holes of the trigger shoe and trigger linkage.

When the crossbow is cocked, the clasp is in the down position, and it retains the tensioned bowstring until the sear disengages, releasing the clasp, bowstring, and arrow. As depicted in **Figure 12**, the clasp is prevented from rotating to the open position by the sear's interfacing sear ledge surface. The clasp's sear roller, a cylindrical hardened steel pin, is transversely mounted within the clasp and supported by sealed ball bearings on both sides. The trigger mechanism of **Figure 12** is shown with the safety in the SAFE position, locking the sear against clockwise rotation. Additionally, the ADF lever blocks sear rotation in this illustration, as the digitally inserted arrow has not been fully inserted rearward to push down the ADF lever's leading nose (see green arrow in **Figure 13**, which shows the trigger mechanism in the discharged configuration). For the sear to release the clasp, two conditions must be met: the user must rotate the safety to the FIRE position, and the ADF lever must be rotated counterclockwise by the full insertion of an arrow. After firing, the clasp moves to the upward position, the ADF endform rests within the sear cavity, and the safety automatically returns to the SAFE position.

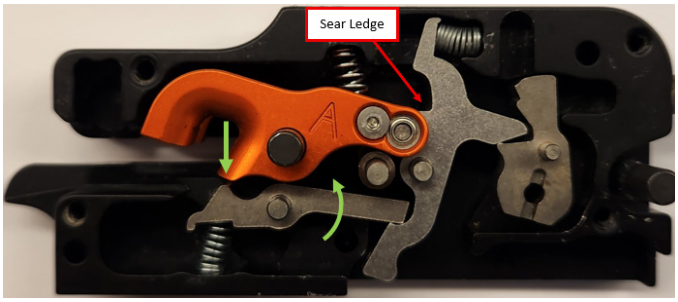

Figure 13
Photograph of the generation 1 trigger mechanism in the discharged position with the ADF lever inside of the sear cavity and the green arrows indicating the direction of ADF travel to disengage the ADF and allow sear rotation.

The typical loading and discharge cycle of the Ravin R9 and R15 crossbows operate as follows. The trigger pack is released from its rearward-firing position and advanced to engage the bowstring. The clasp descends to capture the bowstring, and the safety remains in the SAFE position. Using the integrated ratcheted cranking mechanism, a fabric belt pulls the trigger pack and bowstring rearward, cocking the bowstring. Once fully retracted, an arrow is inserted into the front of the trigger pack, and the polymer arrow nock securely clips onto the bowstring serving (transverse filament windings) at the bowstring's midpoint. This action depresses the ADF lever nose, pushing the rear endform upward to align it with the sear cavity to enable discharge. The user then pushes the safety tactile (button) forward to disengage the safety's internal blocking surface away from the sear, switching to the FIRE position. To discharge, the trigger shoe is pulled rearward, driving the trigger linkage backward. This linkage motion causes the top of the trigger pawl to move forward, contacting the bottom rear face of the sear. The sear rotates clockwise, disengaging the sear ledge from the sear roller, allowing the clasp to release the bowstring and propel the arrow.

The sequence of user crossbow actions that produced inadvertent crossbow discharge multiple finger injuries followed a regularly described pattern:

1. The archer cocks the crossbow using the integral crank mechanism, which automatically engages the physical blocking safety against the sear. The user interface button is below the safety rotation axle, so that the button moves backward to the SAFE position and displays a white dot, while the internal ledge, which is above the axis of rotation, moves forward and supports the sear.

2. The archer loads a factory arrow with its clip-on nock. The nock clicks and vibrates upon interaction with the bowstring, giving the user both tactile and audible feedback of success. The bottom surface of the arrow nock rotates the ADF lever from its fully engaged at-rest position, but not completely, putting it in a position that will prevent it from entering the sear cavity upon trigger pull. That is, the ADF is rotated into an intermediate position (**Figure 14**), with a prominent

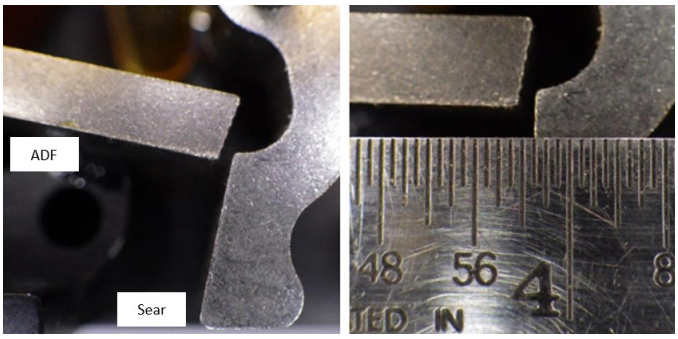

Figure 14
Photographs of the generation 1 ADF and sear in the intermediate position with the ADF trailing edge not completely clearing the entrance to the sear cavity.

gap between the ADF endform and the sear. This gap is objectionable; it allows the sear to rotate enough to assume an unsafe and unstable position.

3. The crossbow's safety button is pushed forward, concealing the white SAFE dot and revealing the red FIRE dot. This motion rotates the internal safety ledge rearward to the FIRE position, disengaging it from the mating surface of the sear.

4. The archer's trigger finger pulls the trigger shoe, causing the front surface of the trigger pawl to press against the back surface of the sear and rotate it slightly, taking up the gap between the sear and the ADF lever. As the ADF lever is only partially aligned with the sear cavity's entrance, it prevents the sear from fully rotating. As a result, the sear roller shifts beyond the supporting point on the sear ledge (**Figure 15**), exerting considerable force and prying the sear toward the discharged position. The red arrows in **Figure 15** highlight the insufficient support of the clasp's sear roller by the sear ledge, indicating a design error.

5. The actions of the sear, ADF, and clasp have placed the crossbow's trigger into a semi-stable, dangerous configuration. The sear roller teeters on the radiused end of the sear ledge, while the sear is prevented from fully disengaging due to the blocking ADF.

6. The user, informed by the Ravin R9 / R15 crossbow manual and instructional videos that the crossbow cannot fire with a partially engaged arrow, attempts to re-engage the safety by pushing

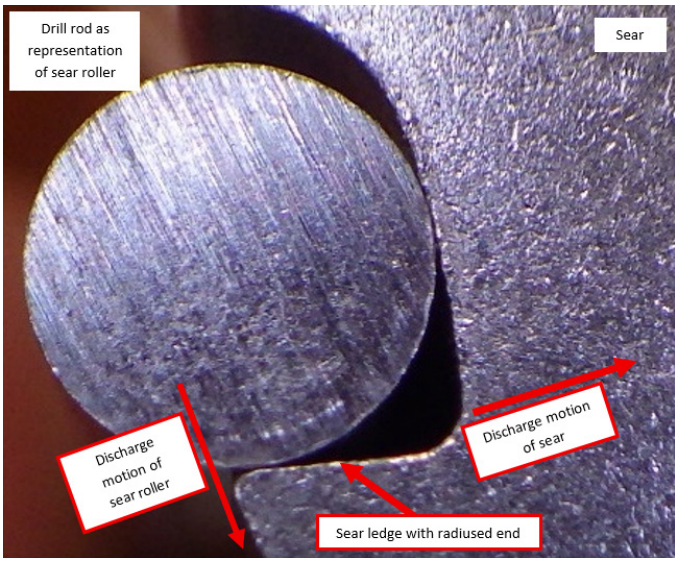

Figure 15
Drill rod in the same diameter as the sear roller resting on the sear ledge, showing that the contacting point of the cylinder is incrementally past the point of edge radius initiation with red arrows representing discharge motion direction.

the safety button rearward (away from the discharge end). However, the internal safety mechanism only partially moves and becomes fixed in an unstable intermediate position — unable to fully engage beneath the sear's horn (**Figure 16**). The sear obstructs the safety's path, preventing proper engagement.

7. The archer, confident that the manual safety has fully engaged due to the familiar actuation resistance and audible click, observes the external safety button's window indicator displaying half of the white SAFE dot and half of the red FIRE dot. Unaware of the crossbow's internal mechanics, the novice user does not realize that the Anti-Dry Fire (ADF) mechanism, sear, clasp, and safety are all in unstable intermediate positions,

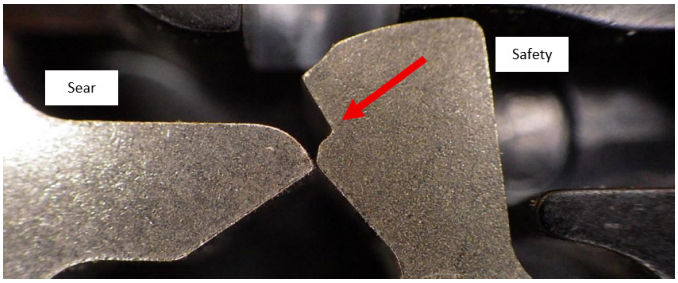

Figure 16
Generation 1 sear in the intermediate position at left and the safety at right in the FALSE SAFE position, with the red arrow showing both the direction of motion of the safety against the sear and the unengaged safety ledge.

precariously holding the immense tension of the drawn crossbow limbs.

8. The archer, having unsuccessfully attempted to engage the safety and with no finger on the trigger, firmly grasps the arrow shaft and forcefully inserts it into the trigger pack to re-seat the nock. This backward force on the arrow causes the ADF lever to rotate, disengaging from contact with the sear and entering the sear cavity. Although the safety was moved toward the SAFE position, it failed to engage properly; the sear roller pushed past the sear ledge, causing the clasp to release and the arrow to discharge. This sudden release invariably resulted in injury to the archer from the arrow's vanes or the bowstring. Some archers, trusting the crossbow's reliability, attempt to re-seat the arrow with their fingers in the bowstring's path, mistakenly believing that the crossbow could not fire since no finger was actuating the trigger, and the safety appeared to be engaged.

To validate the mechanistic feasibility of the incident sequence, crossbows involved in user injuries were individually tested using modified arrow nocks. These modifications enabled a cock/load/trigger pull sequence with the ADF lever positioned at various angles. Specifically, the bottom surfaces of polymer nocks were incrementally filed to reduce the ADF lever's rotation when an arrow was fully inserted. Minimal filing had a negligible impact on the ADF lever's rotation, whereas extensive filing prevented arrow discharge by entirely restricting the sear's rotation. The objective was to identify an "intermediate" degree of filing that replicated the conditions leading to user injuries and to document the crossbow's characteristics when this intermediate condition manifested, as shown in **Figure 17**.

As anticipated, the intermediate position was reliably replicated by iterative nock filing. When the ADF lever was rotated incompletely and into the intermediate position, the cocked and loaded crossbow would make a subtle clicking sound when the trigger shoe was pulled, signifying the internal unstable re-arrangement of components, but no arrow discharge. This indicating sound was not recognized by unsophisticated archers who had no knowledge of trigger mechanism defect. When the safety button was pushed forward during filed nock testing, the safety position indicator window reliably indicated that the crossbow was neither set to SAFE nor to FIRE (**Figure 18**). This subtle indicator of the crossbow's intermediate position was also not recognized by the users.

All crossbows tested in the intermediate position, with the safety mechanism set to the FALSE SAFE state, underwent further evaluation by re-seating the arrow shaft and nock into the trigger pack using a shaft-gripping implement. In every instance, this action resulted in immediate crossbow discharge (**Figure 19**).

To document the extent of the issue, photographs were taken of multiple Ravin R9 and R15 Generation 1 trigger design crossbows with their safety mechanisms in the FALSE SAFE position, confirming a systemic design flaw rather than isolated incidents. Additional tests were conducted to evaluate crossbow performance, including:

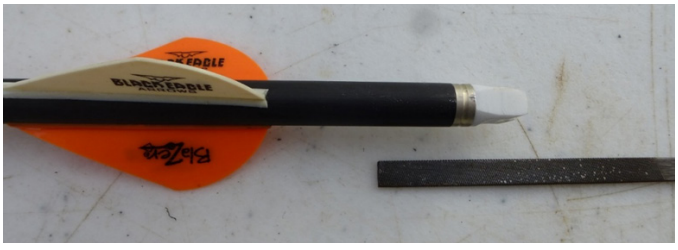

Figure 17
Jeweler's file and Ravin crossbow filed nock on the side with the index vane — the bottom surface of the arrow when inserted into the trigger pack.

Figure 18
Ravin R9 crossbow safety showing the intermediate FALSE SAFE position with half of the SAFE white dot showing and half of the red FIRE dot showing.

Figure 19
Author deliberate re-seating of an arrow in an incident crossbow using an implement causing discharge without a finger on the trigger — notice the arrow vane which has dislodged as a result of the discharge.

- Force testing of the safety button motion when engaged into the normal SAFE position and into the FALSE SAFE position when the internal components were in the intermediate misfire position.

- Sound testing of safety button when engaged in the normal SAFE position and into the FALSE SAFE position.

- Analysis and testing of the redesigned trigger mechanism, as shown in **Figure 20**. The same filed nock testing was performed on this trigger, and this mechanism demonstrated superior performance when compared to the generation 1 trigger. Pull testing of both the generation 1 and generation 2 triggers was performed. Based upon the testing, it required more force to discharge the generation 2 trigger-equipped crossbows, as expected, due at least in part to an increased engagement of the sear roller to the sear ledge surface of the sear.

Figure 20
Photograph of the generation 2 trigger mechanism documenting geometric changes at ADF / sear interface amongst other improvements.

Laboratory testing of the incident crossbow trigger design substantiated the eyewitness accounts of the multiple injured users, confirming that their crossbows discharged unexpectedly during arrow reseating. These incidents occurred under the following conditions: (A) after a misfire; (B) following re-engagement of the safety mechanism as outlined in the user manual; (C) without subsequent trigger activation; and (D) during the manual reseating of the factory-supplied arrow. Changes were made to the ADF lever, sear, sear roller, and other components of the generation 1 trigger mechanism as a comprehensive upgrade, making the generation 2 trigger that has shown to be substantially more reliable.

Summary and Conclusions

In forensic investigations of manufactured products, the terms “abuse” (typically meaning intentional wrongdoing) and “misuse” (typically meaning error in use) are often conflated. However, using a consumer product in a manner slightly deviating from the owner's manual does not necessarily constitute an “abuse.” This analysis examined two case studies involving distinct crossbow designs, highlighting failures at critical operational boundaries.

In the first case study, the bowstring was drawn with less force than anticipated by the designers, resulting in a failure to fully cock the crossbow leaving the automatic safety disengaged. This issue delineates the boundary between the completely cocked and uncocked states. In the second case study, a boundary was identified between a fully inserted arrow, which enabled expected performance and an incompletely inserted arrow that prevented the sear from releasing the clasp, revealing a latent defective intermediate position. Variations in the anti-dry fire (ADF) lever rotation were attributed to differences in bowstring serving diameter, the force applied by users during arrow insertion, and standard manufacturing tolerances.

References

1. TenPoint Crossbow Technologies, “TX 28 Crossbow,” TenPoint Crossbows, 2024. [Online]. Available: https://www.tenpointcrossbows.com/product/tx-28/. Accessed: Jul. 4, 2025.

2. Ravin Crossbows, “Meet Your Next Rifle: Ravin Crossbows,” ravincrossbows.com, 2021. [Online]. Available: https://ravincrossbows.com/pages/meet-your-next-rifle. Accessed: Jul. 3, 2025.

3. J. Nishioka, “Shooting Bow,” U.S. Patent 4,879,987 A, Nov. 14, 1989.

4. B. Horton-Corcoran and N. Rowlandson, "Self-Actuating, Dry-Fire Prevention Safety Device for a Crossbow," U.S. Patent 5,085,200, Feb. 4, 1992.

5. W. Bednar, "Crossbow Vibration Damping Device," U.S. Patent 5,553,596, Sep. 10, 1996.

6. R. Bednar and M. Shaffer, "Crossbow GripGguard," U.S. Patent 7,661,418 B2, Feb. 16, 2010.

7. J. Kempf, "Powerstroke Crossbow," U.S. Patent 7,836,871 B2, Nov. 23, 2010.

8. P. Stanziale, "Device for Firing a Projectile or Another Object to Be Fired," U.S. Patent Application US2012/0125302 A1, May 24, 2012.

9. M. Shaffer and R. Bednar, "Narrow Crossbow with Large Power Stroke," U.S. Patent 8,439,025 B2, May 14, 2013.

10. J. Islas, "Bowstring Cam Arrangement for Compound Crossbow," U.S. Patent 8,651,095 B2, Feb. 18, 2014.

11. U.S. Congress, Gun Control Act of 1968, Pub. L. No. 90–618, 82 Stat. 1213, Oct. 22, 1968.

12. Archery Trade Association, ATA Technical Guidelines. [Online]. Available: https://archerytrade.org. Accessed: (add access date if required).

13. B. Heard, Forensic Ballistics in Court. Chichester, West Sussex, UK: Wiley-Blackwell, 2013, pp. 198–202.

14. D. Aliya, Constructing Competence in Failure Analysis: A Technical and Human Factors Guide, 1st ed. Clackamas, OR, USA: Koho Pono, LLC, 2024, p. 226.

15. U.S. Consumer Product Safety Commission, "Ravin Crossbows Reannounces Recall of White Arrow Nocks Due to Injury Hazard and Additional Incidents; Nearly Two Dozen Serious Injuries Reported," CPSC.gov, Aug. 17, 2021. [Online]. Available: https://www.cpsc.gov/Recalls/2021/Ravin-Crossbows-Reannounces-Recall-of-White-Arrow-Nocks-Due-to-Injury-Hazard-and-Additional-Incidents-Nearly-Two-Dozen-Serious-Injuries-Reported. Accessed.

16. C. Yehle, "String Control System for a Crossbow," U.S. Patent 9,494,380 B1, Nov. 15, 2016.

Beyond the Building Code: Expansive Soils

By Rebecca A. Bowman, Esq., PE, DFE (NAFE 1153M), Brian C. Eubanks, PE, DFE (NAFE 962S), Lauren E. Kelley, PE (NAFE 1358A), and Joseph P. Roberts, PE (NAFE 1354A)

Abstract

As defined by ASTM, soils that are susceptible to significant volumetric changes from the addition and/or removal of external elements are deemed "expansive." Expansive soils associated with clay soil compositions are predominantly encountered throughout the central portion of the United States as well as portions of the southeast and west regions. Although it is not well documented, expansive soils are also encountered adjacent to coal deposits throughout the Appalachian coal region in the eastern United States. Depending on the mineralogy, clay soils comprised of expansive minerals can bond with moisture, causing the volume of the soil to increase with the addition of moisture and decrease with the withdrawal of moisture. This paper will explore tools for identifying expansive soils and factors to consider in the design and construction of ground-supported structures to mitigate the risk of post-construction differential foundation movement caused by expansive soils. It will also explore consequences to ground-supported structures not adequately designed and/or constructed for expansive soils as well as potential remedial measures to address adverse foundation performance.

Keywords

Active zone, chemical injection, deep foundations, expansive clay soils, expansive index (EI), expansive pyritic soils, expansive soil, foundations, geotechnical testing, moisture conditioning, montmorillonite, plasticity index (PI), potential vertical movement (PVM), potential vertical rise (PVR), slab-on-grade, soil survey, swelling capacity, water injection, forensic engineering

Introduction and Background

Susceptible to significant volumetric changes from the addition and/or removal of external elements, expansive soils are prevalent throughout the central portion of the United States as well as portions of the southeast and west regions. Although not well documented, expansive soils are also encountered adjacent to coal deposits throughout the Appalachian coal region in the United States. When expansive soils are identified through site-specific geotechnical tests or regional soil surveys, certain design and construction considerations should be used for ground-supported structures with foundations placed on or within the active zone of expansive soils to ensure that the structures will perform. Without using those design and construction considerations, ground-supported structures on expansive soils are subject to differential movement outside of specified performance standards and may require remediation to perform acceptably. Four case studies are presented to illustrate the effects of expansive soils on ground-supported structures as well as to illustrate performance evaluations and remediation options of ground-supported structures on expansive soils.

Three types of expansive soils will be discussed in this paper, including expansive clay soils, expansive carbonaceous soils, and expansive pyritic soils.

Definition of Expansive Soils

Expansive soils often contain minerals that easily mix and dissolve into water, such as montmorillonite and illite[1], and are susceptible to significant volumetric changes from the addition and/or removal of external elements, such as water. When introduced to moisture, expansive soils comprised of clay are susceptible to swell, whereas

Rebecca A. Bowman, Esq., PE, DFE, 114 Aston Court, McMurray, PA 15317, (724) 941-1532, RBowmanEsq@aol.com

the removal of moisture causes expansive soils to shrink. Certain volumetric changes exceeding specified performance standards by a structural and/or geotechnical engineer can interfere with the usability and/or serviceability of a ground-supported structure, and, in some cases, cause structural damage and failure.

Expansive clay soils are often rich in montmorillonite (commonly referred to interchangeably as bentonite and smectite) and illite. Montmorillonite has a crystalline structure that is not tightly bound and allows for the intervention of water. Montmorillonite has a greater expansion capacity than other clays, including illite, due to its ability to allow water to penetrate the interlayer molecular spaces[2]. Illite minerals are contained in cyclical alumina and silica layers and have high absorption capacity. Montmorillonite has a similar molecular arrangement to illite[3].

The plasticity index (PI) of soil is defined as the difference between the liquid limit and the plastic limit during which the soil is in a semi-solid state. As documented by Fredlund and Rahardjo (1993)[4], as well as Lytton (1994)[5], the volume of a soil can increase with the addition of moisture and decrease with its withdrawal. A relationship between the PI of a soil and its inherent swelling capacity was documented and qualitatively categorized by Terzaghi, Peck, and Mesri (1996)[6], which is shown in **Figure 1**.

ASTM D4829-21 "Standard Test Method for Expansion Index of Soils" provides a standardized test method to compute the expansion index (EI), an indicator of a soil's swell capacity, of a soil sample[7].

According to ASTM D4829-21:

> *5.1 The expansion index, EI, value is used by engineers and other professionals as an indicator of the soil's swelling potential. It may also be used to determine the suitability of a soil to satisfy requirements set by specifying agencies.*

Plasticity Index (PI) Percent	Inherent Swelling Capacity
0-10	Low
10-20	Medium
20-35	High
35 and greater	Very high

Figure 1
Approximate relationship between plasticity index (PI) and inherent swelling capacity.

ASTM D4829-21 classifies a soil with EI ranging from 0-20, 21-50, 51-90, 91-130, and greater than 130 to have potential expansion of very low, low, medium, high, and very high, respectively.

Geographic Prevalence

Expansive soils are prevalent in the central portion of the United States as well as portions of the southeast and west regions. A map of the United States showing the distribution of soils based on their swelling potential is provided in **Figure 2**.

Other types of expansive soils are also encountered adjacent to coal deposits throughout the Appalachian coal region in the eastern United States, although their prevalence is not well documented. Two main types of coal-adjacent soils are expansive: carbonaceous and pyritic. Carbonaceous expansive soils are rich in organic matter, particularly carbon, and are often found in shales. Not only does the organic material characteristic of carbonaceous expansive soils increase the volume and duration of water retention, but it also resists compaction[9]. The upper limit of expansion for pyritic soils relies upon the depletion of the soil components[10]. Pyritic expansive soils contain large amounts of pyrite, which is reactive with both water and oxygen, resulting in the production of sulfuric acid. The

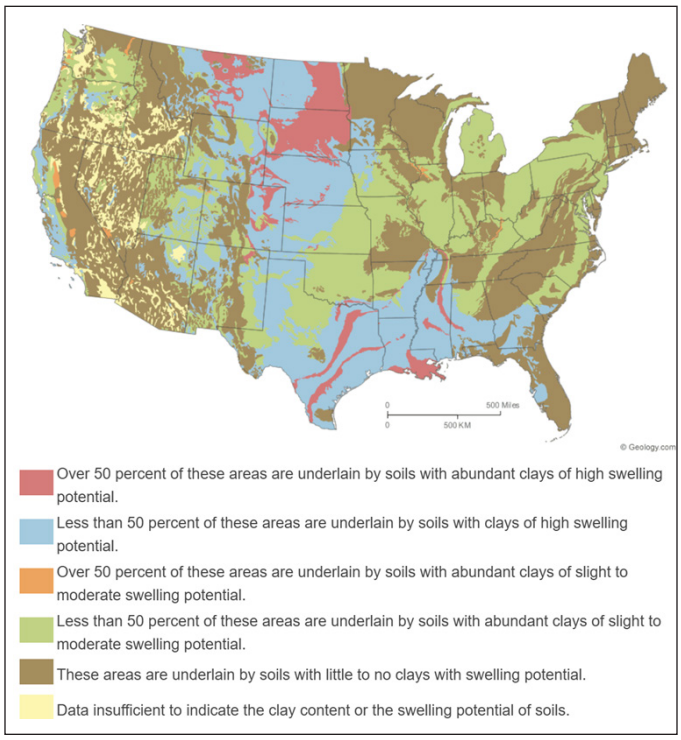

Figure 2
Distribution of soils in the United States based upon their swelling potential[8].

sulfuric acid can then react with minerals in the soil, causing swelling and shrinking; therefore, the expansion-contraction manifestation is a two-step process. Although it is outside the scope of this paper, it should be noted that the presence of sulfuric acid in soils supporting a structure can actually lead to deterioration of the structural materials, such as wood, concrete, and steel, over time. Furthermore, while other forms of expansive soils have a practical upper limit on their expansion capacity, the only upper limit on pyritic decay is depletion of components. Although the USGS map in **Figure 2** does not reflect coal-adjacent expansive soils, the coal deposit map in **Figure 3** and **Figure 4**[11] can serve as a predictor for the presence of both carbonaceous and pyritic expansive soils.

There are adopted standards that define expansive soils based upon various size and expansion parameters. For example, the International Building Code (IBC), which is the building code standard that is widely adopted in the United States, specifies that soil materials shall be classified in accordance with ASTM D2487, provides additional requirements for areas that are likely to have expansive soil, and offers guidelines on how to classify a soil as expansive.

According to Section 1803.5.3 of the 2024 IBC[12]:

1803.5.3 Expansive soil.

... Soils meeting all four of the following provisions shall be considered to be expansive, except that tests to show compliance with Items 1, 2 and 3 shall not be required if the test prescribed in Item 4 is conducted:

1. Plasticity Index (PI) of 15 or greater, determined in accordance with ASTM D4318.

2. More than 10 percent of the soil particles pass a No.200 sieve (75 µm), determined in accordance with ASTM D6913.

3. More than 10 percent of the soil particles are less than 5 micrometers in size, determined in accordance with ASTM D6913.

4. Expansion index greater than 20, determine in accordance with ASTM D4829.

Section R403.1.8.1 of the 2024 International Residential Code (IRC) includes a similar definition for expansive

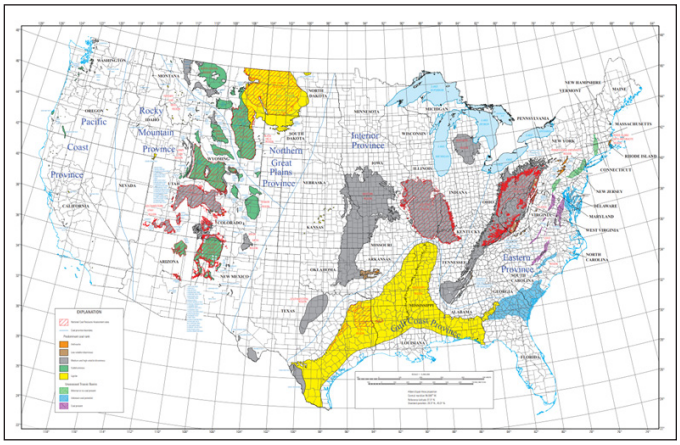

Figure 3
Map showing coal field of the conterminous United States (2013)[11].

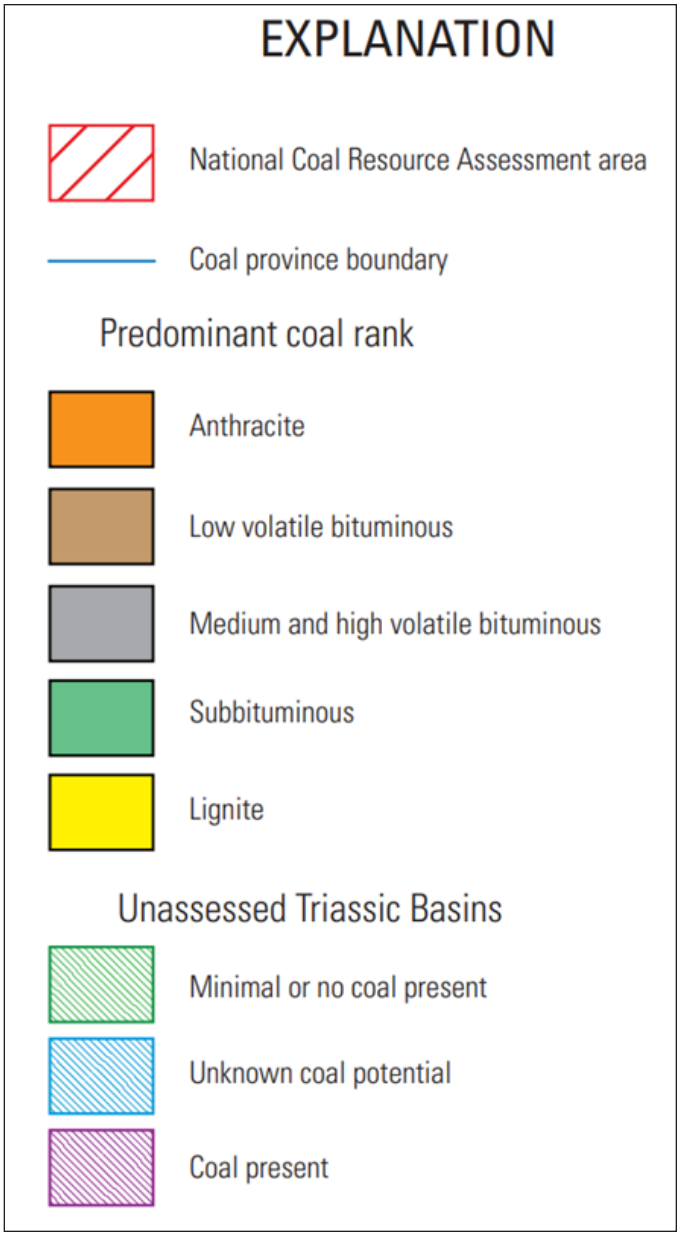

Figure 4
Enlarged "explanation" from Figure 3[11].

soils as the 2024 IBC; however, items 2 and 3 refer to ASTM D422 rather than ASTM D6913[13].

In addition, the National Building Code of Canada (NBCC), which is the building code standard that is widely adopted in Canada, provides guidelines for identifying expansive soils.

According to Section 4.2.4.11 of the 2020 NBCC, Volume 1[14]:

> ***4.2.4.11 Swelling and Shrinking Soils***
>
> *1) Where swelling or shrinking soils, in which movements resulting from moisture content changes may be sufficient to cause damage to a structure, are encountered or known to exist, such a condition shall be fully investigated and provided for in the design.*

For the purposes of this paper, soils that meet the requirements of 1803.5.3 of the 2024 IBC will be considered "expansive." To reiterate and summarize, according to the 2024 IBC, an expansive soil is defined as a soil that exhibits a PI of 15 percent or greater, where more than 10 percent of the soil particles pass a number 200 sieve, where more than 10 percent of the soil particles are less than 5 micrometers in size, and/or where the EI is greater than 20.

Identification Tools

There are various methods that can be used to identify expansive soils, including site-specific geotechnical testing and regional soil surveys. Site-specific geotechnical testing is not always required for construction at a subject site. The applicable building code specifies when site-specific geotechnical testing is required.

According to Section 1803.5.3 of the 2024 IBC[12]:

> ***1803.5.3 Expansive soil.*** *In areas likely to have expansive soils, the building official shall require soil tests to determine where such soils do exist…*

Similarly,

According to Section R401.4 of the 2024 IRC[13]:

> ***R401.4 Soil tests.*** *Where quantifiable data created by accepted soil science methodologies indicate expansive soils, compressible soils, shifting soils or other questionable soil characteristics are likely to be present, the building official shall determine whether to require a soil test to determine the soil's characteristics at a particular location. This test shall be done by an approved agency using an approved method…*

Site-specific geotechnical tests provide information regarding boring locations, boring logs, elevation of groundwater (if encountered in the borings), recommendations for foundation types, foundation design criteria, lateral pressures for below-grade structures, expected total and differential movements, and soil remediation recommendations (if warranted).

In Texas, the Texas Department of Transportation (TXDOT) established a test procedure to empirically estimate the swell potential for natural subgrade soils. According to TXDOT's "Test Procedure for Potential Vertical Rise of Natural Subgrade Soils" (TXDOT Designation: Tex-124-E)[15], the potential vertical rise (PVR) is defined as the "potential of soils to swell in the vertical direction at a given density, moisture, and loading condition when exposed to capillary ground or surface water, and thereby increases the elevation of its upper surface, along with anything resting on it." Another empirical estimate for soil swell capacity is potential vertical movement (PVM), which is often considered when evaluating the soil properties for construction sites in Texas; however, PVM may not have a published basis. Typically, geotechnical reports in Texas include an estimate for PVR or PVM that may occur in the subgrade soil.

There are also regional organizations that specify recommended practices depending on the location of a project site. For example, the Texas Section of the American Society of Civil Engineers (TXASCE) "Recommended Practice for the Design of Residential Foundations – Version 2" provides recommendations for site-specific geotechnical testing used for the design of residential foundations[16].

According to TXASCE "Recommended Practice for the Design of Residential Foundations – Version 2":

> ***3.1 Geotechnical Services***
>
> *Prior to foundation design, a geotechnical investigation and report shall be completed by a geotechnical engineer….*

The TXASCE document also provides recommendations for how a geotechnical investigation should be

conducted. For subdivisions, TXASCE recommends that borings be spaced at a maximum of 300 feet (91.44 meters) on center. For single lots, they recommend one to two borings. TXASCE recommends that borings shall be a minimum of 20 feet (6.10 meters) in depth, unless rock strata are encountered. In addition, TXASCE[16] recommends that borings shall extend through any known fill or potentially compressible materials.

Section 1803.6 of the 2024 IBC includes a list of information that shall be included in a geotechnical report. According to Section 1803.6 of the 2024 IBC, the information required to be included in a geotechnical report includes provisions to mitigate the effects of expansive soils as well as special design and construction provisions for foundations of structures founded on expansive soils.

According to Section 1803.6 of the 2024 IBC[12]:

1803.6 Reporting.

Where geotechnical investigations are required, a written report of the investigation shall be submitted to the building official by the permit applicant at the time of permit application. This geotechnical report shall include, but need not be limited to, the following information:

1. A plot showing the location of the soil investigations.

2. A complete record of the soil boring and penetration test logs and soil samples.

3. A record of the soil profile.

4. Elevation of the water table, if encountered.

5. Recommendations for foundation type and design criteria, including but not limited to: bearing capacity of natural or compacted soil; provisions to mitigate the effects of expansive soils; mitigation of the effects of liquefaction, differential settlement and varying soil strength; and the effects of adjacent loads.

6. Expected total and differential settlement.

7. Deep foundation information in accordance with Section 1803.5.5.

8. Special design and construction provisions for foundations of structures founded on expansive soils, as necessary.

9. Compacted fill material properties and testing in accordance with Section 1803.5.9.

10. Controlled low-strength material properties and testing in accordance with Section 1803.5.9.

In addition, TXASCE's "Recommended Practice for the Design of Residential Foundations – Version 2"[16] includes recommendations for information that should be included in a geotechnical report. At a minimum, TXASCE recommends that geotechnical reports include the following information:

a. Dry density

b. Moisture content

c. Atterberg limits

d. Pocket penetrometer estimates of cohesive strength

e. Torvane

f. Strengths tests

g. Swell and/or shrinkage tests

h. Hydrometer testing

i. Sieve size percentage

j. Soil suction

k. Consolidation

TXASCE recommends that all laboratory testing be performed in accordance with ASTM standards or other recognized standards.

Similarly, for Ontario, the Association of Professional Engineers of Ontario (APEO) published a guideline in 1993 titled Professional Engineers Providing Geotechnical Engineering Services, which outlines the extent of geotechnical services provided, the methodology to be followed, the reporting standards, and the normal range of

recommendations that may be included in the report[17].

According to APEO, normal standard sampling is done at 0.75-meter (2.46-feet) intervals initially and may be increased to 1.5 meters (4.92 feet) below the 4.5-meter (14.76-feet) or 6-meter (19.69-feet) depth, if warranted. In addition, APEO recommends that geotechnical reports include details of the field investigation, field testing results, records of groundwater observations (if encountered), laboratory test results, a site plan, infrared soil stratigraphy, and recommendations.

Particularly in residential construction, developers and/or general contractors opt out of site-specific geotechnical testing and rely instead on regional soil surveys. An example of a regional soil survey that is often referred to in residential construction in the United States is the United States Department of Agriculture (USDA) Natural Resources Conservation Service (NRCS) Web Soil Survey[18], which is an online service that provides general information about soil types and their characteristics depending on the geographical location of a site. Similarly, Canada has an online resource for soil surveys for many provinces and territories provided by the Canadian Soil Information Service (CanSIS)[19].

Design Considerations

Many design options can be implemented to reduce the potential vertical movement of soils on a site, which depend on a geotechnical investigation, existing site conditions, and the owner/developer's acceptable level of risk with respect to differential movement of a ground-supported structure.

It is worth noting that the IRC[13] refers to the IBC[12] for design methods for foundations on expansive soils.

According to Section R403.1.8 of the 2024 IRC[13]:

> ***R403.1.8 Foundations on expansive soils.***
>
> *Foundations and floor slabs for buildings located on expansive soils shall be designed in accordance with Section 1808.6 of the International Building Code.*

According to Section 1808.6.1 of the 2024 IBC[12]:

> ***1808.6.1 Foundations.***
>
> *Foundations placed on or within the active zone of expansive soils shall be designed to resist differential volume changes and to prevent structural damage to the supported structure. Deflection and racking of the supported structure shall be limited to that which will not interfere with the usability and serviceability of the structure…*

The depth in a soil to which periodic changes of moisture occur is usually referred to as the active zone[20].

According to the IBC[12], foundations placed on expansive soils are designed to prevent structural damage, usability, and serviceability of the structure. Therefore, foundations designed in accordance with the IBC are not designed to prevent cosmetic distress.

General consensus within the local industry (Texas) is that 4.5 inches is the maximum allowable PVR/PVM for a slab-on-grade foundation system. In general, if the PVR/PVM of the soils on a specific site exceeds 4.5 inches, the soil can be remediated to lower the PVR/PVM, or a different foundation type can be selected such that it is not supported by the expansive soils.

Frequent sub-slab plumbing failures in expansive soil conditions triggered a response from the International Code Council (ICC). The International Plumbing Code (IPC) was updated in 2024 to include new regulations regarding plumbing penetrations through foundations on expansive soils.

According to Section 305.8, Section 305.8.1, and Section 305.8.2 of the 2024 IPC[24]:

> ***305.8 Expansive soil.*** *Where expansive soil is identified under buildings in accordance with Section 1803.5.3 of the International Building Code, but not removed in accordance with Section 1808.6.3 of the International Building Code, plumbing shall be protected in accordance with Section 305.8.1 or 305.8.2.*
>
> ***305.8.1 Nonisolated foundations.*** *Under foundations with slabs that are structurally supported by a subgrade, buried plumbing shall be permitted.*
>
> ***305.8.2 Isolated foundations.*** *Under foundations with a slab or framing that structurally spans over an under-floor space that isolates*

the slab or framing from the effects of expansive soil swelling and shrinking in accordance with 1808.6.1 of the International Building Code, the plumbing shall be suspended so that plumbing, hangers and supports are isolated, by a void space, from the effects of expansive soil swelling and shrinking.

***Exception:** Plumbing shall be permitted to be buried where it provides drainage of an underfloor space.*

To protect the voidspace, soil shall be sloped, benched or retained in accordance with an approved design methodology. Plumbing, hangers and supports below the slab or framing shall not be permitted to be in contact with the soil or any assemblage of materials that is in contact with soil in the active zone. A slab and plumbing shall not be permitted to be lifted as an assembly to create a voidspace unless the under-floor space is a crawlspace with access to allow inspection of plumbing after lifting.

Organic materials subject to decay shall not be used for hangers, supports and soil retention systems. Materials subject to corrosion shall not be used for hangers, supports and soil retention systems unless protected in an approved manner. Where plumbing transitions to a buried condition beyond the perimeter of the foundation, an adequately flexible expansion joint shall be provided in the plumbing system to accommodate the effects of expansive soil swelling and shrinking.

Soil Remediation Methods

Expansive soil remediation options typically include water injection, chemical injection, moisture conditioning, and/or removal and replacement of the in-situ soils with select fill.

Water injection was developed in the Dallas/Fort Worth area of Texas in the 1950s and early 1960s and is a popular option to reduce the swell capacity of in-situ soils[21]. Water injection involves the controlled introduction of water into in-situ soils to increase the moisture content of the soil, which initially swells the soil and reduces the residual swell potential of the soil. Water injection is accomplished by pushing injection rods vertically downward into expansive soil strata, typically 10 to 15 feet deep from the ground surface, in stages that range from approximately 12 to 18 inches in depth. The injection rods have tips on the ends that allow water to be injected horizontally.

Water is typically injected until it is observed directly at the ground surface (referred to as refusal) or until a minimum time requirement is met. There are specialized injection rigs utilized for water injection, which typically have a maximum injection depth of 18 feet. The injection rods are typically spaced at 5 feet on center across the rig. Once the injection is complete, the rig will move 5 feet, resulting in a 5 foot by 5 foot grid. Most of the time, multiple passes are required, which are offset from the initial grid, resulting in tightening the grid across the site. Most of the time, the injection area is defined as the footprint of a structure plus a nominal distance beyond the footprint of the structure — commonly between 5 and 10 feet outside the footprint of the structure.

Chemical injection is similar to water injection, but rather than injecting water, a chemical solution (lime, bitumen, cement, oils, potassium, etc.) is injected into the soil[22]. The chemicals permeate into the soil and fill in cracks or fissures, which can help improve the volumetric stability of the in-situ expansive soils.

Moisture conditioning of in-situ expansive soils typically requires the removal and re-work of the in-situ soils such that a specified water content and density are achieved through the addition of water and placement of soil in prescribed, compressed lifts. The water content and density are determined by performing appropriate field density-moisture measurements based on a Proctor test for the soils. The resultant soil mixture will have reduced shrink-swell capacity if the design requirements are met.

Finally, a common soil remediation option is the removal and replacement of site soils with select fill materials. Select fill materials have parameters that are defined by the design professional in responsible charge. This option requires the removal of the site soils throughout the footprint of the structure to a specified depth (typically 5 to 10 feet beyond the foundation footprint). The removed soil is then replaced with new select fill materials that have a lesser degree of shrink-swell capacity than the removed soils.

While this is a commonly used method, it also poses a risk for a phenomenon known as the “bathtub effect.” This occurs when water is collected in the excavation zone

and highly permeable fill is utilized, which allows water to flow freely and create a reservoir within the fill material[23]. The water can then permeate into the surrounding in-situ expansive soils over time.

To avoid the bathtub effect, it is recommended to install a clay cap or moisture barrier, such as geomembrane, between the in-situ soils and the select fill material as well as between the finished grade surface and the select fill materials. If the bathtub effect occurs, post-construction measures may have to be implemented to restore the moisture content of the fill material and adjacent in-situ expansive soils to a more uniform composition, such as water and/or chemical injection, modified watering, installation of vertical/horizontal moisture barriers, and/or a sub-surface drainage system.

Foundation Types

If soil remediation is not preferred, other foundation types may be considered that reduce/eliminate the impact of shrink/swell of underlying expansive soils on the structure.

Slab-on-grade foundations with piers are commonly designed for areas where soil settlement is a concern. If properly designed and constructed, portions of a slab-on-grade foundation supported on deep foundation elements (i.e., piers/piles) will be prevented from downward movement; however, portions of a slab-on-grade foundation with deep foundation elements (i.e., piers/piles) are still susceptible to heave from the underlying expansive soils.

Sometimes slab-on-grade foundations are only partially supported on deep foundation elements (i.e., piers/piles), and, in such cases, portions of the slab-on-grade foundation that are not supported on deep foundation elements (i.e., piers/piles) are susceptible to both heave and settlement from underlying expansive soils. With any kind of ground-supported foundation, it is important to maintain uniform/consistent soil moisture content, typically achieved by irrigation around the perimeter of the foundation, as well as positive drainage grades to prevent the accumulation of moisture that creates uneven moisture conditions in the soil.

Elevated foundation systems (pier-and-beam, structural concrete slab on void cartons, and proprietary systems) can be used to create a void between the slab and expansive soils to prevent the slab from interacting directly with the underlying soils.

Pier-and-beam foundations are those where the piers (typically wood, concrete, and/or steel) are constructed, ideally, to a bearing stratum, and the grade beams and/or framing members (typically wood, steel, and/or wood/steel composites) are designed to span between the pier supports. If a pier is properly designed and constructed, it will not be susceptible to vertical displacement from the underlying soils. In addition, when concrete-grade beams are designed, a void form may be specified below the grade beams to prevent soil from having a direct impact on the concrete grade beams. The required design depth of piers in expansive soils is often controlled by the uplift force exerted on the pier by expansive soil in the active zone and the resultant required penetration depth into a deeper stratum to resist such uplift.

Structural concrete slabs on void cartons are comprised of piers and grade beams. Before the concrete is formed, void boxes, which are decomposable forms, are placed below the slab and the beams. Once the concrete is placed, it sits upon the void boxes, which decompose over time to ultimately provide a void between the supporting soil and the grade beams and slabs, which prevents the grade beams and slabs from being directly impacted by soil shrinkage and swell. Certain types of void boxes have been found to perform better than others.

It should be noted that trapezoidal void boxes have been found to be problematic as they allow concrete to flow down along the sides of the void boxes, which can result in a portion of the grade beam bearing on the expansive soil beneath the void forms. In addition, although counterintuitive, certain waterproofing methods do not work well with void boxes. In many cases, designers specify — or installers construct — moisture barriers around the void boxes in an effort to protect the void boxes during construction. However, by encapsulating the void box with a weather barrier, it is prevented from decomposing and will remain in place, transferring any pressure from the underlying shrinking and swelling soils below to the foundation structure above.

Finally, there are various proprietary elevated foundation systems that are commonly encountered. In some instances, proprietary systems may not account for all critical details of a foundation structure, including plumbing and gas penetrations. The performance evaluation of these proprietary foundation systems is considered outside the scope of this paper.

Site Conditions

Existing site conditions prior to construction may also

affect design considerations for a site and structure, including the presence of a body of water, large vegetation (trees), prior site use, site slopes, and fill depth. For the purposes of this paper, only filled-in bodies of water and vegetation will be discussed.

If a large body of water was previously filled in on a site prior to construction, the fill material installed may have been uncontrolled fill. Therefore, it may not be representative of the site soils outside the perimeter of the prior body of water. In this case, it is important to understand the history of the site and sample soils inside the prior body of water as well as outside the fill area. In addition, if the body of water was naturally occurring due to the location of the water table, ground water may still exist below the fill material, which could impact the performance of the ground-supported structure if not identified and mitigated.

Existing trees removed from a site can also trigger a soil-structure interaction mechanism through natural equilibration of soil moisture. Typically, geotechnical reports should include information about how to properly treat soil adjacent to removed trees to minimize the effect of natural equilibration of soil moisture. Trees possess root systems that withdraw moisture from the soil through the process of transpiration, and the moisture content of soil located near an area of mature vegetation is typically lower than the moisture content of soil not located in proximity to mature vegetation; therefore, previously removed trees at a site would have contributed to moisture withdrawal and relatively drier conditions in a bowl of soil material below and around the location of the trees' root systems for many years prior to construction of a structure.

Construction Considerations

There are construction considerations that can be implemented to ensure the performance of a ground-supported structure on expansive soils. Depending on the design recommendations for soil remediation, the geotechnical engineer and/or civil/structural engineer may specify construction material testing (CMT) methods and testing frequency to monitor the moisture content and/or densities of the soils. If directed to do so, it is the responsibility of the general contractor and their earthwork subcontractor to adhere to the requirements set forth in the geotechnical report and/or civil/structural engineering plans with respect to CMT for site soils.

For example, for re-working soil, a geotechnical engineering report will usually provide requirements for excavation depth, depths for soil lifts for the re-worked soils, compaction density requirements for each lift of soil, an acceptable range for moisture content of the re-worked soil, and a frequency for testing the density and moisture content of soil samples in each lift.

Certain regions and municipalities may require inspections to be conducted during the construction process for portions of ground-supported foundations, such as pier inspections to document the pier depth and bearing capacity for drilled piers, concrete sampling to ensure that the concrete strength meets the minimum requirements of the design, and visual inspections of post-tensioned cable reinforcing and conventional steel reinforcing to ensure proper spacing and cover. While these types of inspections may not be required, they are recommended to ensure that the ground-supported structure meets the minimum requirements of the design specifications.

Documentation of as-built relative elevations for a slab-on-grade foundation, or any type of concrete foundation, can be beneficial for future evaluation of the structure's performance over time. While not commonly documented, original construction elevations (OCEs) can be measured and documented soon after a foundation is constructed, and future relative elevation surveys can be compared with the OCE survey to evaluate potential impacts of the supporting expansive soils.

As previously discussed, the IBC[12] specifies that foundations on expansive soils be designed to prevent structural damage and negative impacts to the usability and serviceability of the structure; however, they are not designed to prevent cosmetic damage. "Slab-on-Ground Foundation Performance Evaluation"[25] by Brian Eubanks, Dean Reed, and Robert Pierry, Jr. discusses foundation performance evaluation methods in accordance with TXASCE "Guidelines for Evaluation and Repair of Residential Foundations"[26] and the Post-Tensioning Institute (PTI) DC10.8-18 "Guide for Performance Evaluation of Slab-on-Ground Foundations,"[27] which provide guidelines for the relative elevations of the foundation to be measured and analyzed for two criteria limits: tilt and deflection.

Tilt is defined as the planar variation from a level condition to one that slopes across the entire foundation[26]. Deflection is defined as the maximum deviation from a straight line between two points[26]. When deflection is referred to as "global" or "overall," the deflection profile is analyzed across the overall foundation dimension in a given direction; whereas "local" deflection is analyzed over a shortened length. Tilt and global deflection are analyzed

by taking elevation profiles edge-to-edge of the subject foundation and comparing the maximum values for tilt and deflection against limiting criteria. TXASCE and PTI also require local deflection profiles to be analyzed. In conjunction with tilt and deflection, TXASCE and PTI require distress to be evaluated to determine if the foundation has failed.

It is also recommended that general contractors clearly indicate in their contract documents and/or warranty documents what specific performance standards will be referred to if a structural claim is made regarding differential movement of a ground-supported structure. Some general contractors and owners purchase third-party warranties that may have different evaluation criteria. For example, in Texas, many residential construction contracts utilize the Texas Association of Builders (TAB)[28] templatized contracts, which typically reference the TXASCE "Guidelines for the Evaluation and Repair of Residential Foundations"[26] for performance guidelines for residential slab-on-grade foundations.

Some custom contracts limit the applicability of the TXASCE performance standards by not requiring the evaluation of local deflection profiles. In addition, many third-party warranty standards consider tilt and deflection of a foundation and have requirements for minimum occurrences of distress based upon their severity.

An in-depth discussion of the performance evaluation of ground-supported structures on expansive soils is beyond the scope of this paper; however, some performance evaluation concepts will be presented in the case studies herein.

Potential Remediation Options

It is worth noting that differential movement of ground-supported structures does not "settle out" over time without intervention. As previously discussed, the performance of a ground-supported structure is dependent on the relative moisture content of the supporting soils. Certain mechanisms, such as soil hysteresis and large vegetation, can worsen the performance of a foundation over time due to the lasting and worsening impacts on the soils supporting the structure.

Soil hysteresis is permanent deformation in the soils as a result of cycling of the moisture conditions of a soil over time, which can result in subsequent downward movement of the ground-supported structure. In addition, large vegetation has a lasting impact on soils. As the vegetation and root systems grow over time, more water is extracted by the vegetation, which causes shrinkage of the soils and subsequent downward movement of any ground-supported structure in proximity of, or above, the root system.

The TXASCE "Guidelines for Evaluation and Repair of Residential Foundations" includes various potential remediation options for foundations that exhibit differential movement causally related to expansive soils[26]. Remediation options for foundations exhibiting differential movement due to expansive soil include non-structural and structural measures. Non-structural remedial measures may include a conscientious irrigation regimen/program, vegetation alteration, root barriers, gutters and downspouts, surface grading, sub-surface drainage, and/or moisture barriers. Structural remedial measures may include underpinning, grouting, mudjacking, crack injection, and/or tendon stressing (if the foundation is post-tensioned). The repair of pier and beam foundations typically includes floor shimming, framing repairs, additional support, and/or crawl space moisture control.

Whenever a foundation is lifted or lowered as part of a structural foundation remediation plan, plumbing tests should be performed after completion of the lifting/lowering process to verify whether leaks are present, and any leaks should be repaired. Further, it is recommended to perform a baseline relative elevation survey shortly thereafter for future evaluation purposes if any additional signs of differential foundation movement arise.

Expansive Soils Case Studies

In the following sections, this paper will explore four case studies to illustrate the effects of expansive soils on ground-supported structures and the performance evaluations and remediation options of ground-supported structures on expansive soil. As previously noted, an in-depth discussion of the performance evaluation of ground-supported structures on expansive soils is beyond the scope of this paper.

Case Study #1: Negative Drainage Grades

The owners of a two-story, wood-framed, single-family residence reported distress throughout the interior and exterior of a residential structure. The residence was reportedly constructed circa 2005. An investigation was performed to evaluate the performance of the foundation and to determine the cause of the reported distress and movement. The residence was located in a suburb of Dallas, Texas, which is in the northeast portion of Texas in a region that is well known for exhibiting the presence of

expansive clay soils.

Prior to construction, a geotechnical engineer investigated the soil at the site to provide recommendations for the site preparation and foundation design. The geotechnical report indicated potential vertical movements in excess of 6 inches and soil with plasticity indices ranging approximately between 8 and 53. The geotechnical engineer recommended to excavate, moisture-condition, and replace the upper 9 feet of soil below the building pad in order to reduce the estimated potential vertical movement to 4.5 inches or less. The foundation engineer provided the design for a cast-in-place, concrete, slab-on-grade foundation system with auger-excavated cast-in-place concrete piers.

The geotechnical investigation report also provided recommendations for site grading and drainage conditions such that the lot drainage within 6 feet of the foundations should slope a minimum of 10 percent away from the foundations, and, beyond 6 feet, the lots should slope a minimum of 3 percent away from the foundation.

As previously discussed in the Design Considerations section, if properly designed and constructed, portions of a slab-on-grade foundation supported on deep foundation elements (i.e., piers/piles) will be prevented from downward movement (settlement); however, portions of a slab-on-grade foundation with deep foundation elements (i.e., piers/piles) are still susceptible to heave from underlying expansive soils.

Documentation during the construction of the subject residence indicated that the site soils were prepared in general accordance with the geotechnical report, and the foundation was constructed in general accordance with the engineered foundation plans.

On October 17, 2011, a relative elevation survey of the finished floor surfaces was conducted by an engineer utilizing a Zip-Level Pro-2000. According to the equipment manufacturer, the elevation measuring instrument has a tolerance of ±0.1 inch over a range of 200 feet.

The referenced surveying method is relative in that it does not reference a permanent benchmark. Adjustments for differences in floor covering thickness and built-in elevation changes (i.e., step ups/downs) were made for this relative elevation survey. Sloped areas, such as porches, patios, and garages, are typically excluded from the survey because they are typically constructed with built-in slopes to facilitate drainage. However, the garages were included due to the distress located in those areas and to compare with future elevation surveys, if needed. It is important to note that foundations are not constructed perfectly level; therefore, an elevation survey will reflect as-built variances in addition to any net post-construction movements of the foundation system. Furthermore, any zero-inch contour lines or elevations are not intended to indicate the foundation's original elevation, but are used as a reference to compare other relative elevation points. The location of the 0-inch reference point (datum) is generally arbitrary; however, experience and/or previous elevation information may assist in the selection of the reference datum location.

The survey datum was selected in the northwest corner of the living room. The highest relative elevation was +3.9 inches. Excluding the as-built slopes of the patio and garage, the lowest relative elevations were -0.6 inch. Subsequently, these relative elevations indicate a foundation levelness variance of approximately 4.5 inches (absolute difference between minimum and maximum elevation) across the interior portions of the foundation. In general, the foundation of the subject residence exhibited relatively higher elevations in the northeast portion of the structure and relatively lower elevations in the southwest and west portions of the structure.

At the time of the investigation, the site grading and drainage characteristics were documented. It was observed that the subject property exhibited adverse drainage conditions at the northeast corner of the site with water flow directed toward the foundation.

The relative elevation survey for the subject residence and a photograph of the negative drainage grades in the northeast portion of the property are included in **Figure 5** and **Figure 6**, respectively.

Although the site soils were reportedly remediated, the geotechnical report indicated that the subject residence could still be susceptible to potential movements up to 4.5 inches after soil remediation. The as-built site drainage conditions did not adhere to the recommendations of the geotechnical investigation report nor the provisions of the building code, and alternative approved drainage methods were not implemented at the northeast corner of the subject lot. As a result, surficial water was directed toward the northeast corner of the residence, which induced differential heave of the foundation at that location.

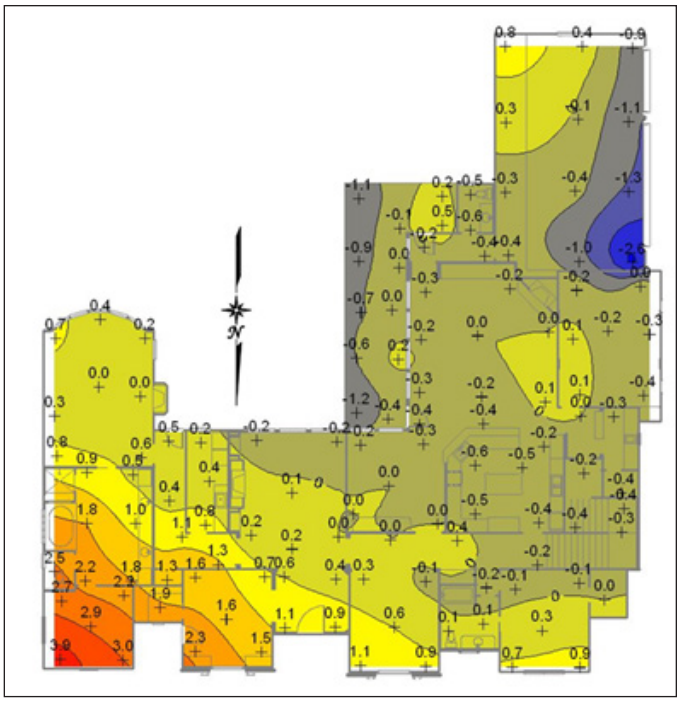

Figure 5
Relative elevation survey of subject residence (October 17, 2011).

Figure 6
Photograph of drainage grades in
northeast portion of the subject property.

Based upon the investigation, distress in the northeast portion of the subject residence was determined to be causally related to moisture-related soil heave under a portion of the foundation adjacent to negative drainage grades in the northeast portion of the subject property.

Case Study #2: Pre-Existing Vegetation

The owners of a two-story, wood-framed, single-family residence reported distress throughout the interior and exterior of the house. An investigation was conducted to evaluate the foundation's performance and determine the cause of the reported distress and movement. The residence was located in a suburb of Dallas, Texas, which is in an area in the northeast portion of Texas that is well known for its expansive clay soils.

Prior to construction, a geotechnical engineer investigated the soil at the site to provide recommendations for the site preparation and foundation design. The geotechnical report indicated potential vertical movements on the order of 1 to 3 inches and soil with plasticity indices ranging approximately between 20 and 39. The foundation engineer provided the design for a cast-in-place, concrete, slab-on-grade foundation system with auger-excavated cast-in-place concrete piers.

As a note in the foundation plans, the structural engineer of record provided specifications for tree removal, indicating that where trees are to be removed within the footprint and extending 10 feet away from the foundation, the area where the tree bulbs are removed should be continuously filled with water for five days before commencement of the foundation construction.

A relative elevation survey of the finished floor surfaces was conducted by an engineer utilizing a Zip-Level Pro-2000. Refer to Case Study #1 for additional information regarding how relative elevation surveys are performed and documented.

The survey datum was selected in the central portion of the foundation. The highest relative elevation was +1.0 inch, recorded in the south-central portion of the structure. Excluding the as-built slopes of the porch, patio, and garage, the lowest relative elevation was -3.2 inches, recorded along the west perimeter of the structure. Subsequently, these relative elevations indicate a foundation levelness variance on the order of 4.2 inches (absolute difference between minimum and maximum elevation) across the interior portions of the foundation. In general, the foundation of the subject residence exhibited a band of relatively higher elevations oriented in the northwest-southwest direction through the central portion of the structure, and it exhibited areas of relatively lower elevations near the interior east-central portion of the structure as well as toward the southwest portion of the structure.

Following the site investigation, historic aerial imagery was reviewed to determine the pre-development conditions of the site. The historic imagery revealed that various

trees were previously located within the footprint of the residence.

Trees possess root systems that withdraw moisture from the soil through the process of transpiration, and the moisture content of the soil located near an area of mature vegetation is typically lower than the moisture content of a soil not located in proximity to mature vegetation. Therefore, the previously removed trees at the site would have contributed to moisture withdrawal and relatively drier conditions in a bowl of soil material below and around the location of the tree's root system for many years prior to the construction of the relatively new residence.

When mature vegetation is removed, the soil moisture content of the affected soil is allowed to equilibrate with that of the surrounding soils. The equilibration process involves a natural migration of water or moisture from areas of higher moisture content to areas of lower moisture content. Desiccated root bowls can take several years to rehydrate. The volumetric changes that occur in soil during the equilibration process can cause differential movement in ground-supported foundation structures.

It was determined that a soil-structure interaction causally related to a majority of the differential foundation movement at the subject residence was due to natural soil equilibration in an area of removed trees. Based on the investigation, it was clear that the general contractor and/or their subcontractor associated with site grading had not properly wetted the soil in accordance with the foundation plans at the locations of the removed trees. Aerial imagery of the subject property/residence before and after development is included as **Figure 7**.

Based on the correlation of the location of previously removed mature trees and areas of relatively higher elevations along a northwest/southeast band across the central portion of the residence — and in the southwestern portion of the residence — it was concluded that the relatively higher foundation elevations were causally related to moisture-related soil heave from re-hydration of desiccated soil in proximity to the location of the removed trees.

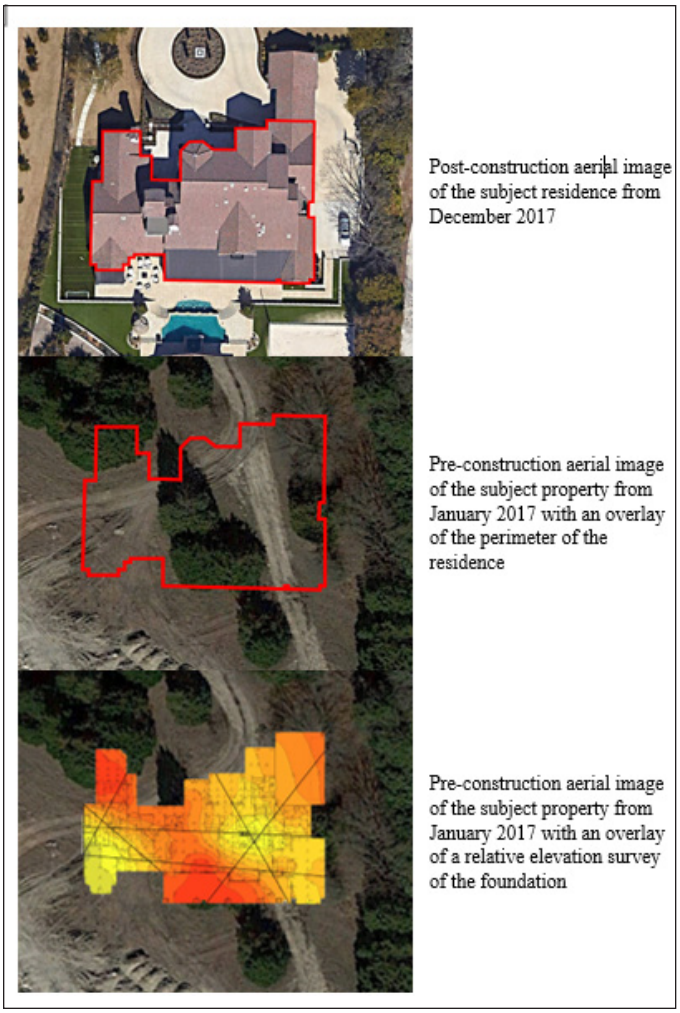

Figure 7
Pre-development and post-development aerial imagery with residence outline overlay and relative elevation survey overlay.

Figure 8
General view of subject site topography.

Case Study #3: Basement Wall Failure

Prior to the development of a complex of duplex carriage homes and single-family homes in McMurray, Pennsylvania, carbonaceous expansive soils were identified through geotechnical investigative testing directed by the developer. Development of the sites in the complex began in approximately 1999, and construction of residential structures began in 2001 (starting at the bottom of a steep hill and working up). A photograph of the site, illustrating the site topography, is included in **Figure 8**.

The owner of a residential unit of one of the duplex structures reported ongoing distress and rotation of a basement wall. According to the owner, the subject residential unit was purchased in 2009. At the time of purchase, there

was no visible distress and/or rotation to the basement wall. According to county records, the residential structure in question was among the first to be built in the development. The subject residence has a front-entrance garage, with the dwelling area to the side and rear. A photograph of the subject unit is included in **Figure 9**.

The basement of the subject residence was contained within the footprint of the living area of the main level, and it did not extend below the garage. Schematics illustrating the general layouts of the main and basement levels are included in **Figure 10**.

During construction, carbonaceous expansive soils encountered during excavation of the basement were reportedly removed; however, based on the investigation, the builder did not excavate or remove the corresponding carbonaceous expansive soils beneath the garage or driveway. As those soils expanded, pressure was exerted along the 21-foot-long, front load-bearing wall of the basement and along the 11-foot projecting, load-bearing wall of the basement.

Figure 9
Front elevation of the subject unit.

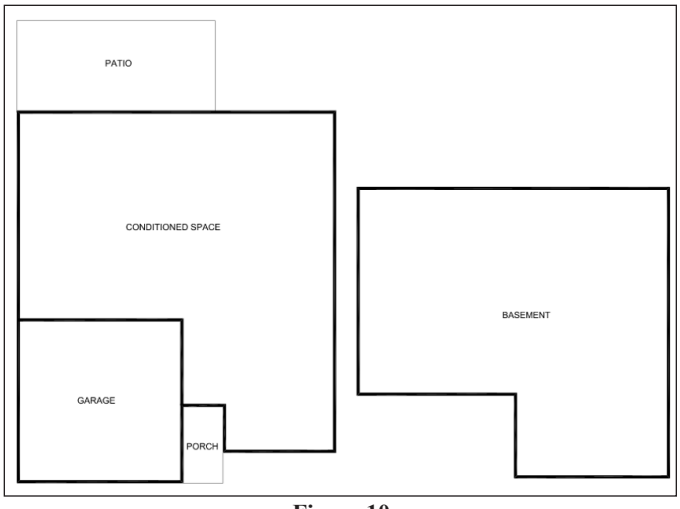

Figure 10
Schematic of the main level (left) and the basement level (right).

The 11-foot wall appeared to be relatively unaffected by the pressure of the expansive soil due to the short span and additional stiffness from the adjacent wall structures; however, the 21-foot, front load-bearing wall was not as stiff and experienced distress due to the expansive soil pressure. The pressure was highest at the interior corner, and the 21-foot wall broke free from the 11-foot wall and began to rotate, reaching a maximum displacement of 14 inches. **Figure 11** illustrates the movement of the basement wall.

The developer initially denied liability; however, immediately upon filing a writ of summons (initiating litigation), the developer agreed to install temporary jacks, to excavate the expansive soils beneath the garage and driveway and replace them with clean, non-expansive, compacted fill, to re-build the displaced 21-foot wall and the damaged corner formed by the 21-foot and the 11-foot walls — all under the supervision of a 3rd-party inspector — and to provide an assignable extended structural warranty.

Although the reported damage was extensive, the subject residential unit suffered less damage than some other units in the same development due to improperly mitigated carbonaceous expansive soils. Another single-family residential unit in the development experienced such extensive damage that the entire residential structure was rendered unsafe and had to be demolished. The owners

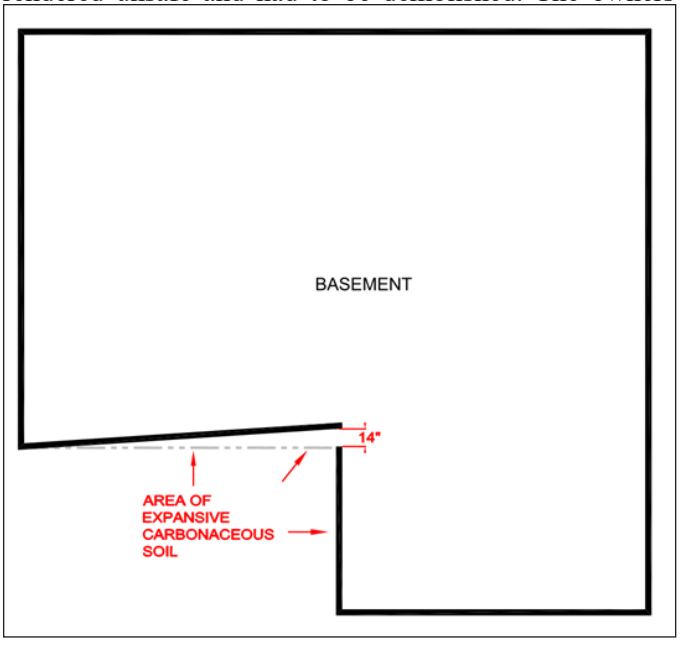

Figure 11
Schematic of the resultant movement to the basement wall.

of the demolished residence were temporarily relocated and subsequently provided with a completely different unit, and the design of the residence was strengthened and rebuilt, according to more robust design and construction methods. However, the carbonaceous expansive soils were not removed. Over time, the previously demolished and rebuilt residential structure experienced distress and structural damage considered severe enough to warrant a second demolition. To the best of the authors' knowledge, the lot remains green space in the development.

Case Study #4: School on Pyritic Soil

The authors were informed that an elementary school structure in southwestern Pennsylvania had experienced differential vertical movement, which had reportedly been ongoing since 2010. The authors were able to access the most recent monitoring report as well as several of the background source documents.

Prior to construction, a geotechnical investigation was completed in 1992. According to the geotechnical investigation report, the existing soils at the site contained expansive pyritic soils. The geotechnical engineering report recommended that pyritic soils be "sealed" when encountered. In the construction and design documents, no reports related to construction material testing of the site soils were identified; therefore, it is unknown whether the general contractor followed the specifications and recommendations outlined in the geotechnical report.

Based upon the reviewed documentation, the construction of the subject school commenced in 1995 and was completed in 1996. The foundation of the subject school is comprised of shallow spread footers with a 4.5-inch concrete slab-on-grade over a 6-inch gravel subbase. Based upon the as-built elevations, the overall slab had moved upward between 1.250 and 2.625 inches since original construction. The as-built drawings included a detail requiring a 1-inch compressible filler to be installed between the non-load bearing CMU masonry walls and steel floor structure above. The inspecting engineer believed this measure was sufficient to prevent some or all of the vertical movement from being transmitted to the floors above.

It was reported that adjustments had been made to the entry doors in order to remain functional. Based on measurements of modifications to the front entry doors, the center of the vestibule floor appeared to have moved upward approximately 2 inches since original construction (**Figure 12**).

Floor cracking and unlevel floor surfaces could be observed throughout the subject school. There was no apparent movement of the columns themselves; however, the surrounding slab-on-grade appeared to have heaved up to 0.5 inches.

Distress to the walls, in the form of cracking and displacement, was observed in some masonry walls of the building, primarily within the electrical room (**Figure 13**). At the northernmost portion of the west masonry wall, a level-line was drawn across a vertical expansion joint on November 20, 2009. The masonry wall to the north is an exterior wall on a shallow spread footer, and the western wall is an interior, non-load-bearing CMU wall on the slab-on-grade. Since that level-line was drawn in 2009, the southern portion of the non-load bearing western wall has risen approximately 0.5 inch. Nearby stairstep cracking was later observed, and follow-up survey data gathered in this area indicated that the southern (interior) wall was rising at a greater rate than the eastern (interior) wall.

The footers, coupled with the weight of the exterior wall loads, appeared to be sufficient to resist expansive forces. Heaving was isolated to the slab-on-grade and non-load-bearing masonry walls, which suggested that expansive pyritic soils remained beneath many portions of

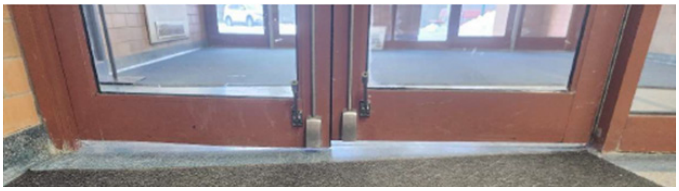

Figure 12
Photograph of the front entry doors.

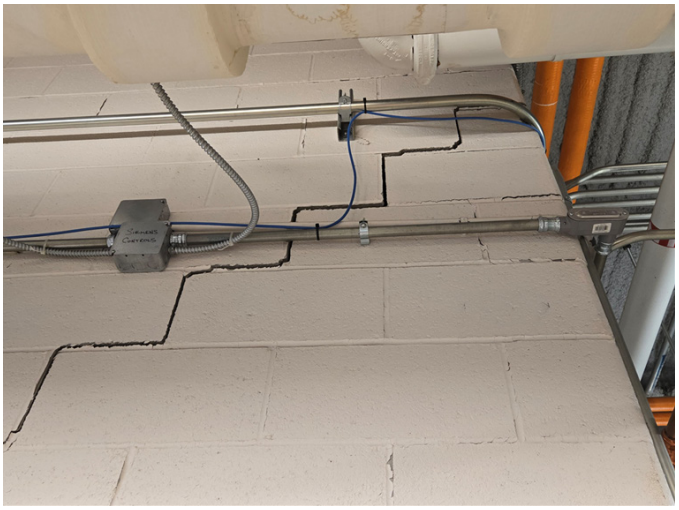

Figure 13
Photograph of cracking in masonry wall.

the slab on grade and were not remediated by removal or "sealing."

The inspecting engineer recommended interior test borings to verify the depth of the suspected expansive materials beneath the slab on grade, enabling a more accurate prediction of potential future performance. Furthermore, it was recommended to install access ports in the architectural finishes to facilitate expansion joints inspections over time.

Summary

Understanding the prevalence and implications of expansive soils in development and construction is paramount for providing proper design and construction methodologies to mitigate the movement potential of expansive soils to an acceptable level. ASTM standards as well as adopted building codes offer guidance for how to define the expansiveness of a soil. Site-specific geotechnical testing can be performed to classify the in-situ soils at a site, determine the potential movements of the soils, and provide recommendations for soil remediation (if needed) and foundation design options.

Engineered foundation designs may consider the recommendations of a geotechnical report, if available, or, if not, may rely on regional soil surveys. Performing different tests and quality control/assurance measures can ensure that the subject site and structure are prepared in accordance with the engineered plans. After original construction, the performance of ground-supported structures can be evaluated. When not performing as intended, various remediation options, both structural and non-structural, can be implemented to restore the structure's intended functionality.

Conclusion

Identifying the presence of expansive soils on a construction site prior to design and construction is critical to minimize the risks associated with potential soil movement and the resultant damages to ground-supported structures. Various cases have been presented that illustrate the potential damages that can occur when expansive soils are encountered and not properly planned for in design, construction, and site maintenance phases.

While these studies focus on the impacts of expansive soils on foundations and basement walls, the same principles can be applied to other ground-supported structures, including, but not limited to, in-ground swimming pools, retaining walls, tunnel structures, and trenches. Failure to identify and mitigate the risks associated with the construction of ground-supported structures on expansive soils can not only pose a risk to the appearance and serviceability of a structure, but may also pose a life-safety risk when the movement potential is substantial enough.

References

1. D. Li and S. Zhang, "The Influences of Sand Content and Particle Size on Desiccation Cracks of Compacted Expansive Soil," Advances in Materials Science and Engineering, vol. 2021, Art. No. 7752352, Jan. 2021.

2. G. A. Borchardt, Montmorillonite and Other Smectite Minerals, Soil Society of America, Inc., 1977.

3. B. Zamin, H. Nasir, K. Mehmood, Q. Iqbal, A. Farooq, and M. Tufail, "An Experimental Study on the Geotechnical, Mineralogical, and Swelling Behavior of KPK Expansive Soils," Advances in Civil Engineering, Jul. 8, 2021.

4. D. G. Fredlund and H. Rahardjo, Soil Mechanics for Unsaturated Soils, John Wiley & Sons, Inc., 1993.

5. R. L. Lytton, "Prediction of Movement in Expansive Clays," in Vertical and Horizontal Deformation of Foundation and Embankments, GSP No. 40, A. T. Yeung and G. Y. Felio, Eds., vol. 2, ASCE, New York, 1994.

6. K. Terzaghi, R. B. Peck, and G. Mesri, Soil Mechanics in Engineering Practice, 3rd ed., John Wiley & Sons, Inc., 1996.

7. ASTM International, ASTM D4829-21: Standard Test Method for Expansion Index of Soils, 2021.

8. W. W. Olive, A. F. Chleborad, C. W. Frahme, J. Schlocker, R. R. Schneider, and R. L. Schuster, Swelling Clays Map of the Conterminous United States, U.S. Geological Survey, Misc. Investigations Series Map I-1940, 1989.

9. K. N. Suravi et al., "The Effect of Organic Carbon Content on Soil Compression Characteristics," Soil and Tillage Research, vol. 209, May 2021.

10. L. Bryant, M. Mauldon, and J. K. Mitchell, Geotechnical Problems with Pyritic Soil and Rock, Virginia Polytechnic Institute and State University, Center for Geotechnical Practice and Research, Jan. 2003.

11. U.S. Geological Survey, Coal Fields of the Conterminous United States – National Coal Resource Assessment, updated version, Jan. 1, 2023.

12. International Code Council, International Building Code (IBC) 2024, Falls Church, VA, 2024.

13. International Code Council, International Residential Code (IRC) 2024, Falls Church, VA, 2024.

14. National Research Council of Canada, National Building Code of Canada, vol. 1, 2020.

15. Texas Department of Transportation, Tex-124-E: Test Procedure for Vertical Rise of Natural Subgrade Soils, Jan. 2017.

16. Texas Section of the American Society of Civil Engineers, Recommended Practice for the Design of Residential Foundations, ver. 2, Oct. 4, 2007.

17. Association of Professional Engineers of Ontario, Professional Engineers Providing Geotechnical Engineering Services, originally published 1993, revised Nov. 1998.

18. United States Department of Agriculture, Natural Resources Conservation Service, Web Soil Survey. [Online]. Available: https://websoilsurvey.nrcs.usda.gov/app/

19. Canadian Soil Information Service. [Online]. Available: https://sis.agr.gc.ca/cansis

20. B. M. Das, Principles of Foundation Engineering, 6th ed., 2007.

21. P. Gallet and N. Aro, "Water Injection: 20+ Years of Injecting Expansive and Collapsible Soils in the Front Range," Rocky Mountain Geo-Conference 2024, 2024.

22. S. Kazemain and B. B. K. Huat, "Assessment and Comparison of Grouting and Injection Methods in Geotechnical Engineering," European Journal of Scientific Research, vol. 27, no. 2, 2009.

23. U. Obinna, "Overexcavation and replacement of expansive soils," Structville Integrated Services. [Online]. Available: https://structville.com/2022/03/overexcavation-and-replacement-of-expansive-soils.html. Mar. 18, 2022.

24. International Code Council, International Plumbing Code (IPC) 2024, Falls Church, VA, 2024.

25. B. C. Eubanks, D. R. Read, and R. F. Pierry Jr., "Slab-on-Ground Foundation Performance Evaluation," in ASCE 10th Congress on Forensic Engineering, 2024.

26. Texas Section of the American Society of Civil Engineers, Guidelines for the Evaluation and Repair of Residential Foundations, ver. 3, Apr. 1, 2022.

27. Post-Tensioning Institute, DC10.8-18 Guide for Performance Evaluation of Slab-on-Ground Foundation, Farmington Hills, MI, 2018.

28. Texas Association of Builders. [Online]. Available: https://www.texasbuilders.org/.